STUDIES ON NUCLEAR EQUATION OF STATE, PROPERTIES OF NUCLEAR MATTER AND PHASE TRANSITION IN NUCLEI

THESIS SUBMITTED TO

SAMBALPUR UNIVERSITY

FOR THE DEGREE OF

DOCTOR OF PHILOSOPHY

IN

SCIENCE

2010

By

Aliva Pradhan

Supervisors:

Dr. Tushar Ranjan Routray & *Dr. Basudeb Behera*

POST GRADUATE DEPARTMENT OF PHYSICS

SAMBALPUR UNIVERSITY

JYOTI VIHAR

ALIVA PRADHAN
Dept. of Physics,
Sambalpur University,
Jyoti Vihar, Burla.

Dated: 9.9.2010

DECLARATION

I do hereby declare that the work embodied in the thesis entitled **"Studies on Nuclear Equation of State, Properties of Nuclear Matter and Phase Transition in Nuclei"** is the outcome of genuine research work carried out by me under the guidance and supervision of **Dr. T. R. Routray**, Prof., Dept. of Physics, Sambalpur University and **Dr. B. Behera**, Retd. Prof., Dept. of Physics, Sambalpur University. I also declare that the same has not been submitted by me to any other institution for any other degree.

Aliva Pradhan

(Aliva Pradhan)

Dr. T. R. Routray, Ph.D.
Prof. in Physics
P.G. Department of Physics,
Sambalpur University,
Jyoti Vihar, Burla.

Dr. B. Behera, Ph.D.
Retd. Prof. in Physics
P.G. Department of Physics,
Sambalpur University,
Jyoti Vihar, Burla.

CERTIFICATE

This is to certify that the thesis entitled **"Studies on Nuclear Equation of State, Properties of Nuclear Matter and Phase Transition in Nuclei"** submitted by **Aliva Pradhan** for the award of degree of **Doctor of Philosophy (Science)** to **Sambalpur University** is a record of bonafide research work carried out by her under our joint supervision and guidance. This work is original and to the best of our knowledge has not been submitted elsewhere for award of any degree or diploma in any other university or institution. In our opinion the thesis has fulfilled the requirements according to the regulations and has reached the standard necessary for submission. We further certify that to the best of our knowledge Aliva Pradhan bears a good moral character.

B. Behera

(Dr. B. Behera)

Date: 9-9-2010.

T R Routray 9.9.10

(Dr. T. R. Routray)

Date: 9-9-2010.

ACKNOWLEDGEMENT

I express my deep sense of gratitude to my esteemed supervisors Prof. Basudeb Behera, Retd. Prof., Dept. of Physics, Sambalpur University and Dr. Tushar Ranjan Routray, Prof., Dept. of Physics, Sambalpur University for their untiring guidance, supervision, moral support and constant encouragement during the entire course of the present work.

I express my thanks to the H.O.D., Dept. of Physics, Sambalpur University for allowing me to carry out the work in the department and providing me all the facilities available in the department. I am indebted to all the staff members of the Department of Physics for their immense help throughout the research period.

I am also very much thankful to Dr. S. K. Patra and Dr. P.K. Sahu, Institute of Physics, Bhubaneswar for their valuable suggestions and help in partial completion of the present work. I acknowledge with thanks, The Director, Institute of Physics, Bhubaneswar for the generous help in allowing me to make full use of the technical and academic facilities of their esteemed institute.

I take this opportunity to express my gratitude to all my friends and family members who encouraged, helped and co-operated me during this work. I owe my earnest gratefulness to my husband Dr. Prahallad Padhan and daughter Adyasha for their patience and support during my work. Words can not describe my indebtedness to my parents whose love and encouragement inspired me to carry out the research work.

Finally, I express my sincere thanks to the University Grants Commission, India for partial financial support through Major Research Project.

Aliva Pradhan

Date: 9.9.2010

Aliva Pradhan

LIST OF PUBLICATIONS

- T. R. Routray, B. Sahoo, A. Pradhan and B. Behera, *Liquid-gas phase transition in asymmetric nuclear matter*, DAE-BRNS Symposium on Nuclear Physics Vol. 44B, (2001) 356.

- B. Behera, T. R. Routray, A. Pradhan and B. Sahoo, *Thermal evolution of nuclear matter properties*, DAE-BRNS Symposium on Nuclear Physics Vol. 46B, (2003) 416.

- T. R. Routray, A. Pradhan, B. Sahoo and B. Behera, *Effective mass in asymmetric nuclear matter*, DAE-BRNS Symposium on Nuclear Physics Vol. 46B, (2003) 418.

- B. Behera, T. R. Routray and A. Pradhan, *Momentum and density dependence of isovector part of nuclear mean field*, Modern physics letters A 20, (2005) 2639.

- B. Behera, T. R. Routray, A. Pradhan, S. K. Patra and P. K. Sahu, *Momentum and density dependence of the isospin part of nuclear mean field and equation of state of asymmetric nuclear matter*, Nucl. Phys. A 753, (2005) 367.

- B. Behera , T.R. Routray, A. Pradhan, S.K. Patra, and P.K. Sahu, *Nuclear Mean Field and Equation of State of Asymmetric Nuclear Matter*, DAE-BRNS Symposium on Nuclear Physics Vol. 50, (2005) 52.

- B. Behera, T. R. Routray, A. Pradhan, S. K. Patra and P. K. Sahu, *Nuclear mean field and equation of state of asymmetric nuclear matter*, Nucl. Phys. A 794, (2007) 132.

CONTENTS

LIST OF FIGURES

LIST OF TABLES

CHAPTER 1

NUCLEON NUCLEON INTERACTION AND EQUATION OF STATE OF NUCLEAR MATTER

1.1. Introduction

The equation of state (EOS) of nuclear matter is under investigation for the past 70 years. Despite extensive research the EOS of nuclear matter still remains elusive. Nuclear EOS at extreme conditions has become a major area of research in nuclear physics in the past decade. Currently an increasing attention is being given to the study of EOS of highly isospin asymmetric dense nuclear matter because of its implications and connections beyond standard nuclear physics [1–22] such as astrophysical phenomena like supernova explosion and neutron star structure as well as for the new experimental possibilities offered by the Radioactive Ion Beam (RIB) facilities.

Nuclear matter is an idealized infinite system of nucleons where the difference between neutrons and protons is neglected and single particle effects are not considered. These conditions lead to constant density and the absence of Coulomb energy, pairing and surface effects. These features make it an attractive medium for testing and comparing bulk nuclear properties. Although nuclear matter is hypothetical some of its properties give an insight to bulk properties of nuclei. Considering nuclear matter as starting point to test properties of real finite nuclei makes the calculations easier to handle which otherwise involves complex many–body equations. There are two limiting states of infinite nuclear matter, the symmetric nuclear matter (SNM) containing equal number of neutrons and protons and the pure neutron matter (PNM) with only neutrons present. These two states have fundamentally different properties. The SNM is bound (ground state) while the PNM does not exist in a bound state and represents the highest excited state of nuclear matter. In between the two extreme cases of SNM and PNM lies the asymmetric nuclear matter (ANM) characterized by an asymmetry parameter σ, with

$$\sigma = \frac{\rho_n - \rho_p}{\rho} \qquad \text{...(1.1)}$$

where ρ_n and ρ_p are the neutron and proton densities and $\rho = \rho_n + \rho_p$ is the total density of nuclear matter. As can be seen from Eq. (1.1) the value of the asymmetry parameter σ always lies between 0 (SNM) and 1 (PNM). Since nucleon–nucleon (NN) interaction is generally attractive upto a separation distance of 1 to 2 *fm* but becomes repulsive at small distances (< 0.5 *fm*), nuclear matter is difficult to compress. As a result most stable nuclei are at approximately the same density called the saturation density ρ_0 ($\approx 0.16\, fm^{-3}$) and higher densities do not occur naturally on earth. However, heavy–ion (HI) collision reactions may produce matter of density in the range (2–3)ρ_0 in terrestrial laboratories, in the interiors of neutron stars the density of matter may reach about (8–10)ρ_0 [9] and matter at densities about 4ρ_0 may be present in the core collapse of type II supernovae [23].

Intermediate energy heavy–ion collision experiments provide a unique opportunity to obtain a piece of dense nuclear matter in the laboratory. Besides the many radioactive beam facilities that already exists a number of new next generation RIB facilities are being constructed or planned all over the world [1]. These facilities provide the opportunity to study the properties of dense isospin asymmetric nuclear matter that has a large neutron proton ratio.

Matter found in neutron star is an ideal example of highly asymmetric dense nuclear matter. In fact it is one of the densest forms of matter known in the observable universe. In the interior of neutron stars density of matter can be as high as 8–10 times normal nuclear matter density ρ_0 [9]. Thus neutron star can serve as a laboratory to study dense isospin asymmetric nuclear matter. New advance telescopes and observatories are enabling astrophysicists to discover a large number of neutron stars in the form of radio pulsars, X–ray binaries, etc. and measure more accurate data from them. These data can be very helpful in the study of EOS of highly dense asymmetric nuclear matter.

On one hand, large number of experimental data coming from the HI collision experiments as well as observational data from neutron stars propose to constrain the high density behaviour of nuclear EOS. On the other hand, for analysis of these HI reactions and study of properties of neutron star knowledge of nuclear EOS is required.

The EOS of nuclear matter, described as the relationship between energy density or pressure (as function of density and temperature), density and temperature is determined from the underlying NN interaction and summarizes the properties of nuclear matter. Despite intensive studies the nuclear EOS, especially the EOS of ANM, still remains elusive. Although the properties of nuclear matter at saturation density are now known to a good precision, it appears a challenge to the possibility of predicting the nuclear EOS on the basis of NN interaction in the density range upto a few times the saturation density. The growing experimental facilities for the study of nuclear reactions induced by high energy intense RIB and their analysis in terms of transport model calculations have provided an opportunity for the first time to explore the EOS of highly asymmetric dense nuclear matter experimentally [1–3, 24–33].

After exhaustive research the EOS of symmetric nuclear matter (SNM) at normal nuclear matter density ρ_0 is now known to a good precision. Recent measurements from collective flow [3] and sub–threshold kaon production in relativistic nucleon–nucleon collision [24] have been able to constrain the EOS of SNM in the density range $2\rho_0 - 5\rho_0$. However, the isospin dependent part of nuclear EOS, especially the density dependence of nuclear symmetry energy and momentum and density dependence of nuclear symmetry potential, particularly at high density and high momentum, is still largely unknown [28, 29, 31–33]. In the last decade the density dependence of nuclear symmetry energy has received much attention in nuclear physics research. Knowledge of nuclear symmetry energy plays a major role in understanding the dynamics of heavy–ion collision, the structure of exotic nuclei far from beta stability line and the cooling mechanism of protoneutron stars [8, 9]. Although the value of nuclear symmetry energy at normal nuclear matter density ρ_0 is now known to a good approximation from empirical liquid drop mass formula [34, 35] its high density behaviour is still under intense investigation.

Theoretically the EOS of nuclear matter has been under investigation for the past several decades using a large number of different NN interactions. Since the NN interactions are not well known and because of the complexities of nuclear many body theories, various approaches using a number of techniques are employed to analyse the EOS of nuclear matter. Different approaches which are used to study the nuclear EOS can be roughly divided into two groups: phenomenological and microscopic approaches. The behaviour of EOS of SNM as predicted by these different approaches are comparable at sub–normal to normal nuclear matter densities; however, they differ widely in prediction of EOS of SNM at supra–normal densities. On the other hand, the behaviour of asymmetric nuclear matter (ANM) as predicted by different theoretical calculations is widely different at both low and high densities [36, 37]. Especially, the high density behaviour of nuclear symmetry energy predicted by these different approaches are very different from each other and can be classified into two groups. One group predicts a monotonically increasing behaviour of nuclear symmetry energy and the other group predicts that symmetry energy decreases after attaining a maximum value and ultimately becomes negative with increase in density. The nuclear symmetry energy is directly related to the proton fraction of beta–stable nuclear matter found in the interior of neutron stars. The two different types of behaviour of symmetry energy will affect the cooling mechanism of neutron stars [9, 38].

Another most important quantity in calculation of nuclear EOS is the single particle potential or the nuclear mean field. The study of momentum and density dependence of nuclear symmetry potential or the isovector part of nuclear mean field is very important since it can not only provide information on the isospin dependence of the inmedium NN interaction but also help in understanding structure and reactions of radioactive nuclei. All theoretical prediction on momentum dependence of isovector part of nuclear mean field can be classified into two distinct groups depending on whether it decreases or increases with increase in momentum. Another important property directly linked to nucleon mean fields is the effective nucleon mass. Uncertainty in the momentum dependence of isovector part of nuclear mean field further leads to controversy in neutron–proton effective mass splitting in asymmetric nuclear matter.

In view of this in this chapter we have given an outline of different approaches used to study the nuclear EOS in section 1.1. A brief discussion on status of various nuclear matter properties as found from literatures is given in section 1.2. Finally in section 1.3 the motivation and plan of the present thesis work is outlined.

1.2. The nucleon–nucleon interaction

One of the most fundamental challenges in theoretical nuclear physics is to understand the underlying interactions between constituents of nuclei or the nucleon–nucleon (NN) interaction. A large number of different NN interactions using different lines and methods have been developed in the past several decades. The NN interaction is the basic ingredient in the calculation of nuclear EOS. Various approaches, involving different physical approximations and numerical techniques, used to construct the EOS of nuclear matter from these different NN interactions can be broadly classified into two groups; microscopic and phenomenological approach. Here we will discuss in brief some important methods used to construct NN interaction and calculate the nuclear EOS. We have also mentioned important literatures under these approaches analysing nuclear EOS and properties of nuclear matter especially dense asymmetric nuclear matter.

1.2.1. Microscopic approach

In the past few decades significant progress has been made in development of microscopic many body approach and its application in nuclear physics. In microscopic approach the input is a two body NN interaction described by "realistic" potentials. The theoretical basis to construct these realistic potentials is the meson–exchange theory of nuclear forces. In this scheme nucleons, nucleon resonances and mesons such as π, ρ and ω are incorporated in a potential representation. The various parameters in the potential are then adjusted to reproduce the experimental data for the two body problem (e.g. deuteron properties, NN phase shifts etc.). Then one has to solve the complicated many body problem to get the EOS. Various methods used to solve the manybody problem and to study nuclear EOS are the nonrelativistic (i) Variational calculation using different combination of two and three nucleon interactions [15, 16, 39–44], (ii) Brueckner–Hartree–Fock (BHF) to Brueckner–Bethe–Goldstone (BBG) calculation [45–56], and the relativistic (iii) Dirac–Brueckner–Hartree–Fock (DBHF) calculations using realistic NN interaction derived from relativistic meson field theory [57–73].

1.2.1.1. The variational method

The variational method is one of the popular non relativistic microscopic models to evaluate the ground state of many–body systems and it is extensively used to study the nuclear EOS. The variational method based on hypernetted chain summation techniques (VCS) [15] provides a means to study the ground state energy and wave function of nuclear matter from realistic models of nuclear forces. In this method a variational trial wave function Ψ_v is constructed and is used to evaluate the Rayleigh–Ritz upper bound to the ground state energy. The parameters in Ψ_v are determined by the variational principle, i.e., by imposing that the mean value of the Hamiltonian is minimum. The trial function Ψ_v is chosen in such a way that it gives a good representation of the full many–body wave function and the expectation value of the Hamiltonian is accurately evaluated. The variational trial wave function Ψ_v is expressed as the product of two–body correlation operators acting on an unperturbed ground–state:

$$\Psi_v = \prod_{i<j} F_{ij} \Phi , \qquad \ldots(1.2)$$

where Φ is the properly antisymmetrized Fermi–gas wave function and F_{ij} are two body correlation operators. The key quantity in this method is the complex correlation operator F_{ij} which represents the correlations induced by the complicated NN potential. F_{ij} can be expanded in the same spin–isospin, spin–orbit and tensor operators appearing in the NN interaction. Expectation values of the full Hamiltonian are evaluated for the correlation operator trial function in a diagrammatic cluster expansion with the help of Fermi Hypernated Chain–Single Operator Chain (FHNC–SOC) integral equations.

In a variational frame work the nuclear EOS has been calculated by Friedman and Pandharipande [39] using Urbanna V_{14} plus three nucleon interaction (TNI) model; Wiringa, Ficks and Fabrocini [15] using different combinations of two and three body interactions; and various other authors [41, 42]. Many excellent review papers on this method exist in literature, see, e.g. [43, 44].

1.2.1.2. BBG to BHF methods

The non–relativistic BHF approach can be interpreted as a mean field theory in the lowest order non–relativistic BBG theory. The BBG method is a general many body method particularly suited for nuclear systems. For the past few decades this method has been used extensively to study the EOS of nuclear matter. For excellent review articles see ref. [55, 56].

The BBG theory is based on the linked cluster expansion of the ground state energy. The perturbation expansion of the energy per particle in this approach can be ordered according to the number of hole lines in the corresponding diagrams, and it shows a rapid convergence at low densities. The diagram with given number n of hole lines describe the n–particle correlations in the system. The BHF approximation is obtained by truncating the expansion at the two hole–line level. At the two hole line approximation the corresponding summation of diagrams lead to the BHF approximation that incorporates in an exact way the two–particle correlations. The inmedium effective NN interaction is replaced by the G–matrix, which can be considered the generalization of scattering T–matrix to the case of two particles in a medium. The G–matrix satisfies the Bethe–Goldstone equation. An auxiliary single particle potential U is introduced to minimize the effect of correlations and speed up the rate of convergence of the expansion. In other words, the choice of U is such that the contribution from higher order correlations, i.e., contributions from three or more hole lines is minimum. Since the auxiliary potential U appears in the definition of the single particle energies, the G–matrix depends on the choice of the auxiliary potential U. This implies a self–consistent determination of the auxiliary potential U. In the original Brueckner theory the auxiliary potential U was assumed to be zero above the Fermi momentum. This is called the 'standard choice' or 'gap choice' of the auxiliary potential. Beside the gap choice of the auxiliary potential another choice can be the so called 'continuous choice' [74]. In this case the definition of the potential is extended to momenta larger than the Fermi momentum, thus making the potential a continuous function through the Fermi surface. In principle the final result of the BBG calculation should be independent of the choice of the auxiliary single–particle potential. However, the convergence rate of the expansion can depend on the particular choice of U adopted in the calculations. Day and Wiringa [75] within the frame work of BBG theory with the 'standard choice' or 'gap choice' for the single particle auxiliary potential has proved the convergence of the hole–line expansion. During the last decade, important progress in BBG theory has been made by calculating the three–hole line contributions which require solving the Faddeev equation for the inmedium three body problem, i.e. the Bethe–Faddeev equation [76]. The resulting EOS of nuclear matter is found to a high degree of accuracy to be independent of the choice of auxiliary potential. Furthermore, it has been shown that the continuous choice BHF calculations give result much closer to those from BBG cal with three hole–line contributions than the gap choice calculation [77], indicating that continuous choice is more optimal than the gap choice in BHF calculations. Now a days the continuous choice is usually used [78].

1.2.1.3. Dirac–Brueckner–Hartree–Fock method

The failure of nonrelativistic two body interactions in producing the correct saturation properties of nuclear matter, discussed in detail later in this chapter, led to improvisations like introduction of meson and isobar degrees of freedom [79] in addition to nuclear degrees of freedom. One of the most important developments was the replacement of nonrelativistic Schrodinger equation with relativistic Dirac equation to describe the single particle motion in nuclear matter [58, 59]. This approach is called the Dirac–Brueckner (DB) approach. In most DB calculations a one–boson–exchange (OBE) potential is used to describe the bare NN interaction. The OBE potential is defined as a sum of one–particle–exchange amplitudes of certain bosons with given mass and coupling. Usually six nonstrange bosons with mass below 1 GeV are used. So

$$V_{OBEP} = \sum_{\alpha=\pi,\eta,\rho,\omega,\delta,\sigma} V_{\alpha}^{OBE} \qquad \ldots(1.3)$$

with π and η pseudoscalar, σ and δ scalar and ρ and ω vector particles. The two nucleon scattering is described covariently by relativistic Bethe–Salpeter equation [80]. The BS equation, the relativistic counterpart of the non relativistic Bethe–Goldstone equation, is very difficult to solve, and it is customary to reduce the four–dimensional integral equation to a three–dimensional covariant quasipotential equation. The reduction of the four–dimensional integral depends on the method adopted and is not unique [81]. The Thomson reduction method and Blankenbecler–Sugar methods are examples of the different methods used to reduce the four dimensional integral equation to a three dimensional one [81]. In solving the Bethe–Salpeter equation the Pauli principle is respected and the intermediate scattering states are projected out of the Fermi sea. The inmedium T–matrix which is obtained from the BS equation plays the role of an effective two–body interaction which contains all short–range and many–body correlation in the ladder approximation. The summation of *T*–matrix interactions with occupied states inside the Fermi sphere finally gives the self–energy Σ in the DBHF approximation. This constitutes a self–consistency problem and the self–energy Σ and *T*–matrix are calculated by method of iteration. The DB approach which is a relativistic extension of Brueckner theory was first proposed by the Brooklyn group [82]. They have used first order perturbation theory in calculating the relativistic effect. Brockmann and Machleidt [59, 60] and ter Haar and Malfliet [58] have performed a full self consistency calculation in the determination of the relativistic single particle energies and wave functions. The DBHF method can be developed in another way by introducing the inmedium relativistic *G*–matrix to describe the two–body correlations. Harowitz and Serot [83] have discussed in detail the derivation of the relaticvistic *G*–matrix.

1.2.2. The phenomenological approach

Although quite less fundamental than the microscopic approach phenomenological approach is extensively used to study nuclear EOS. Here the input is a density dependent effective NN interaction. In this approach the parameters appearing in the phenomenological interaction are adjusted to fit the properties of many finite nuclei (e.g. binding energies, radii) and the empirical saturation properties of nuclear matter. Both relativistic and non–relativistic approaches are used. The relativistic ones use relativistic mean field (RMF) theory, with effective interaction being represented by a Lagrangian dependent on a number of coupling constants, which is fitted to saturation properties of nuclear matter and observables of the ground states of finite nuclei [84]. The equations of motion for baryons and mesons are solved self–consistently using Hartree technique. In non–relativistic approach Hartree–Fock or extended Thomas–Fermi–Strutinsky–Integral [85] techniques are used to solve for the nucleonic equations of motion based on a Hamiltonian utilizing an effective NN interaction of the Skyrme [86, 17], Gogny [87–90] or separable monopole (SMO) [91, 92] types. These models can be surprisingly successful for describing dense matter upto (2–3)ρ_0 depending on the choice of the effective interaction. EOS constructed under these restrictions work very well even when extrapolated to higher densities.

1.2.2.1. Relativistic Mean Field approach

The relativistic mean field (RMF) theory in the frame work of quantum hadrodynamics (QHD) is a very popular approximation to calculate nuclear EOS since Walecka first gave it in 1974 [93]. In this approach the effective interaction is represented by a Lagrangian having nucleons and mesons as the degrees of freedom. The various mesons considered are: a scalar meson σ and a vector meson ω treated as classical fields generating scalar and vector interactions and a vector meson ρ giving the isovector contribution. The interaction Lagrangian contains a number of coupling constants which are fitted from saturation properties of nuclear matter and observables of ground state of finite nuclei. Although the earlier RMF models, having only linear coupling terms, were successful in producing qualitative properties of nuclei they predicted too high compressibility and failed to produce surface properties. In order to overcome this deficiency Boguta and Bodmer [94] introduced a nonlinear (NL) density dependent term in the σ field, a concept which is used by most of the recent works. The additional density dependent term helped in reducing nuclear matter incompressibility to reasonable limits. Later Sugahara and Toki [95, 96] extended the self coupling to other meson fields. A scalar isovector δ meson is also added [97, 98] to the interaction Lagrangian to describe the isovector contributions.

Recently another method the density dependent (DD) nucleon–meson coupling was developed by various authors [99–104] to predict correct experimental results. In this model the coupling constants are calculated from scattering results. Both NL self–coupling of meson field and DD nucleon–meson coupling have been successfully used to study the EOS of nuclear matter. Recently L.W. Chen *et al.* [105] have studied 23 different parameter sets used in RMF approach to study the isospin dependent bulk and single particle properties of ANM.

1.2.2.2. Non relativistic effective interaction method

In non relativistic phenomenological models the most popular effective NN interaction is the Skyrme type effective interaction whose analytic form leads to considerable simplification of nuclear calculations. The standard form of the Skyrme effective interaction is

$$V(\vec{r}_1,\vec{r}_2)=t_0(1+x_0P_\sigma)\delta(\vec{r})+\frac{1}{2}t_1(1+x_1P_\sigma)\left[\vec{P}'^2\delta(\vec{r})+\delta(\vec{r})\vec{P}^2\right]+t_2(1+x_2P_\sigma)\vec{P}'\cdot\delta(\vec{r})\vec{P}$$
$$+\frac{1}{6}t_3(1+x_3P_\sigma)\left[\rho(\vec{R})\right]^\sigma\delta(\vec{r})+iW_0(\vec{\sigma}_1+\vec{\sigma}_2)\cdot\left[\vec{P}'\times\delta(\vec{r})\vec{P}\right], \quad ...(1.4)$$

where $\vec{r}=\vec{r}_1-\vec{r}_2$ is the relative coordinates of the two particles, $\vec{R}=(\vec{r}_1+\vec{r}_2)/2$ is the center of mass coordinate $P_\sigma=(1+\vec{\sigma}_1\cdot\vec{\sigma}_2)/2$ is the spin operator. The parameters t_i, x_i, σ and W_0 are adjusted from basic physical properties such as saturation of infinite nuclear matter, binding energies of some doubly magic nuclei and other simple nuclear experimental observables.

The Skyrme interaction has been widely used in mean field models since the last several decades and there are several known parametrisations of it which reproduce experimental data for the ground states of finite nuclei and for observables of finite nuclear matter at the saturation density, giving more or less comparable agreement with experimental or expected empirical data. In its most sophisticated versions, the Skyrme type interaction can predict binding energies of nuclei with an overall error of less than 0.7 *MeV* [106]. However, at higher densities than saturation density, these parametrisations predict widely varying behaviour for observables of nuclear matter.

Behera *et al.* [107, 108] have used a Skyrme type NN interaction to successfully study the EOS of symmetric nuclear matter. In order to improve the description of nuclear system with large neutron excess Chabanat *et al.* [17, 18] have parametrized the Skyrme interaction using constraints from variational calculations [15] to study the EOS of neutron rich and pure neutron matter. Rikovska Stone *et al.* [19] have investigated about 90 different Skyrme parametrisations to examine how successful they are in predicting the expected properties of infinite nuclear matter and generating plausible neutron star models. Some notable examples of literature found on study of nuclear EOS using Skyrme interactions are as follow: Lattimer, *et al.* [109] have used a modified Skyrme interaction to model thermodynamical properties of hot, dense nuclear matter; Onsi *et al.* [85] have used several Skyrme interactions in their investigation of the EOS of homogeneous nuclear matter under conditions appropriate for a collapsing star, employing the ETFSI approximation; Pethick [110] have used a modified SIII interaction to study neutron star crust in beta equilibrium.

Cao, Lombardo *et al.* [111] have tried to derive a Skyrme type parametrisation of an effective interaction suitable for Hartree–Fock calculations of finite as well as infinite system.

The Gogny model is also a very powerful option to study the EOS of nuclear matter. This interaction was first postulated by Decharge and Gogny [87]. The Gogny interaction is given as

$$V(\vec{r}) = \sum_{i=1,2} (W_i + B_i P_\sigma - H_i P_\tau - M_i P_\sigma P_\tau) e^{-r^2/\mu_i^2} + t_0(1 + x_0 P_\sigma)\rho^\sigma(\vec{R})\delta(\vec{r}) \\ + iW_0(\vec{\sigma}_1 + \vec{\sigma}_2)\cdot\left[\vec{P}' \times \delta(\vec{r})\vec{P}\right] \quad \text{...(1.5)}$$

Recently Das *et al.* [30] used the Gogny interaction to derive an effective momentum and isospin dependent potential that can be used in transport model calculations for HI collision reactions.

1.3. Transport models

Apart from these theoretical models, heavy ion collision experiments are also used to study the nuclear EOS. Intermediate energy heavy–ion collision experiments provide a unique opportunity to obtain a piece of dense nuclear matter in the laboratory. However, for analysis of these reactions the properties of nuclear matter at high density is required which can only be obtained from theoretical investigations [112, 113]. To interpret data from these collisions and to extract accurately properties of nuclear matter, advanced transport model calculations are employed. Mainly two types of semiclassical transport models are used: the Boltzmann–Uehling–Ulenbeck (BUU) [112] and the Quantum Molecular Dynamical (QMD) model [113]. In these transport model calculations usually very simple parametrisation of mean fields and energy density are used. In earlier transport model calculations momentum independent mean fields were used. Later the momentum dependence of mean field was found to play very crucial role in these calculations [112–114]. For many years now momentum dependent mean fields are used in simulation of heavy–ion collision experiments to study properties of nuclear matter. Several isospin dependent semiclassical transport models have been developed in the past few years to analyse nuclear reactions from intermediate energy to high energy HI collision experiments [115–122].

1.4. Properties of nuclear matter

Although nuclear matter itself is hypothetical, properties of SNM and some properties of ANM at equilibrium provide a physical insight to the bulk properties of nuclear matter. Here we have defined some of the properties of nuclear matter required to understand the nuclear EOS and a concise study on these properties as reported in literatures has been done.

1.4.1. Saturation properties of nuclear matter

The most important property of nuclear matter which defines the nuclear EOS is the pressure of nuclear matter. In SNM the pressure P(ρ) can be expressed as [123]

$$P(\rho) = \rho^2\{de(\rho)/d\rho\} \qquad ..(1.6)$$

where $e(\rho)$ is the energy per particle in SNM.

The above equation is sometimes called the nuclear EOS which gives the relation between pressure and energy density in nuclear matter. From the above equation it is evident that the behaviour of $P(\rho)$ with density ρ depends entirely upon the density dependence of energy per particle $e(\rho)$.

All theoretical models on nuclear EOS predict that SNM is bound i.e. the energy per particle in SNM decreases with density up to a particular density and then increases giving a saturation point at a particular density called saturation density ρ_0. For any model of nuclear EOS to be successful the first requirement is to reproduce the correct saturation properties of nuclear matter and properties of finite nuclei from experimental data. The value of energy per particle $e(\rho_0)$ at the saturation density ρ_0 is usually determined via the liquid drop model. The value of $e(\rho_0)$ is taken to be the value of the volume coefficient a_v in liquid drop model determined by fitting with the binding energies of a large number of nuclei. This procedure gives $e(\rho_0) = -(16.0 \pm 0.2)$ MeV [17]. Heiselberg and Hjorth–Jensen [123] has reported a lower value of $e(\rho_0) = -(15.6 \pm 0.2)$ MeV. The value of ρ_0 is expected to be $\rho_0 = 0.16 \pm 0.005\ fm^{-3}$ based on calculating the charge distribution in heavy nuclei [17]. A more conservative value of $\rho_0 = 0.17 \pm 0.02\ fm^{-3}$ is given in ref. [124] where the error bar includes uncertainties in the neutron density distribution and a correction for possible density inhomoginity in nuclear interior.

The early nonrelativistic microscopic approaches like BBG and variational approaches based on purely two–body NN interactions failed to reproduce the correct saturation properties. Usually called the Coester band phenomena [125], the energy per particle at saturation and/or the saturation density calculated by these models were either very low or high and lied in a band in the binding energy versus density plot that did not meet the empirical saturation region. Further, saturation results obtained from BHF calculations differed from those of variational calculation using the same NN potential. Inclusion of contributions from three–hole line contributions in the BHF calculations [76] gave saturation results that agreed reasonably well with those from advanced variational calculations [16]. The saturation point was also shifted off the Coester band. However, the improvement is not sufficient enough and accurate saturation point is still not producible by nonrelativistic microscopic models. In ref. [56] it has been pointed out that these discrepancies from non relativistic many body models are due to the adopted Hamiltonian and not due to many body treatment. This deficiency in the nonrelativistic microscopic approaches can be remedied by including many body forces, especially three body forces and relativistic effects. In fact most recent Brueckner calculation [54] including a three body force in the interaction estimates the value of $\rho_0 \approx 0.18\ fm^{-3}$ and $e(\rho_0) \approx -14.8\ MeV$. The relativistic DBHF models, on the other hand, reproduce correct saturation properties of symmetric nuclear matter. All phenomenological models predict correct saturation points.

Another property of interest in the study of EOS of nuclear matter is the incompressibility modulus $K(\rho)$. For SNM the incompressibility $K(\rho)$ is given as

$$K(\rho) = 9\frac{dP(\rho)}{d\rho} \qquad \text{...(1.7)}$$

The value of incompressibility $K(\rho_0)$ at saturation density ρ_0 provides an important constrain on nuclear EOS. The larger the value of $K(\rho_0)$, the more steeply the EOS will increase with density. This is generally referred to as the "stiffness" or "softness" of the EOS. The value of $K(\rho_0)$ is model dependent and is still not known precisely. Experimentally the value of $K(\rho_0)$ can be calculated from measurement of centroid energy of isoscalar giant monopole resonance (ISGMR) and isoscalar giant dipole resonance (ISGDR) based on a microscopic random phase approximation (RPA) using a given effective interaction [21, 22, 126, 127]. Nonrelativistic Hartree–Fock based RPA calculation of ISGMR with the use of zero range Skyrme and finite range

Gogny interactions predict the value of $K(\rho_0)$ = 210–220 *MeV* [127]. Recent RMF based RPA [128] calculation for ISGMR report the value of $K(\rho_0)$ = 250–270 *MeV*. Nonrelativistic HF+RPA calculation for ISGDR data [129] however predicts a lower value of 160–180 *MeV* for $K(\rho_0)$. In a recent paper Shlomo *et al.* [127] have shown that the difference between non–relativistic and relativistic results from ISGMR data is due to the difference in the value of nuclear symmetry energy $J_\tau(\rho_0)$ and its slope as predicted by these models.

1.4.2. Symmetry energy, proton fraction and neutron star properties

One of the most important property of ANM is the nuclear symmetry energy $J_\tau(\rho)$ which plays a crucial role in the evaluation of EOS of ANM is defined as

$$J_\tau(\rho) = \frac{1}{2\rho}\left[\frac{\partial^2 H(\rho_n, \rho_p)}{\partial \sigma^2}\right]_{\sigma = 0} \quad \ldots(1.8)$$

where σ is the asymmetry parameter related to neutron and proton density by the relation $\sigma = (\rho_n - \rho_p)/\rho$.

The nuclear symmetry energy, particularly its high density behaviour, is in center of attention of nuclear physicists because of its direct impact on observables from heavy–ion collision induced by radioactive beams and of its connection to astrophysical phenomena like chemical composition and related mechanisms in the process of formation of neutron stars. The nuclear symmetry energy is directly related to the value of proton fraction of beta stable matter found in the interior of neutron stars. Despite intensive research the behaviour of nuclear symmetry energy at high density still eludes nuclear physicists.

The behaviour of nuclear symmetry energy $J_\tau(\rho)$ about supranormal and normal nuclear matter density is somewhat similar as calculated by different theoretical models. The value of $J_\tau(\rho_0)$ at normal nuclear matter density ρ_0 is directly related to the asymmetry coefficient in Bethe–Weizsäcker semiempirical mass formula [130] and experimentally the value of $J_\tau(\rho_0)$ can be extracted from a systematic study of masses of atomic nuclei based on, e.g., liquid droplet model or the macroscopic–microscopic model. In ref. [131] the value of $J_\tau(\rho_0)$ has been reported to be 32.5 ± 0.5 *MeV* as calculated from a large set of experimental data in the finite range droplet model. Tondeur *et al.* [132] have reported a lower value of 28 *MeV* from a fit of nuclear ground state binding energies in a mean field model with a Skyrme interaction. Non–relativistic Hartree–Fock theories [14] predict the value of $J_\tau(\rho_0)$ in the range about 26–35 *MeV* depending on the nuclear interaction used in the calculation. The RMF models [105] however, usually predict a somewhat higher value of $J_\tau(\rho_0)$ at about 35 – 44 *MeV*. Recent calculations from continuous choice BHF approach using different NN potentials give the value of $J_\tau(\rho_0)$ in the range 28.5 – 32.6 *MeV* [78].

However, the behaviour of nuclear symmetry energy at high density, which is important for understanding properties of neutron star, as predicted by different theoretical calculations differs significantly from each other. Based on the behaviour of nuclear symmetry energy at high density all theoretical calculations can be divided into two groups, one where $J_\tau(\rho)$ increases monotonically and the other where it decreases after reaching a maximum value and then ultimately becomes negative with increasing density. It should be mentioned here that an increasing $J_\tau(\rho)$ makes a neutron star neutron rich while a decreasing behaviour of $J_\tau(\rho)$ makes the neutron star ultimately pure neutron matter.

Recently Stone *et. al.* [19] have examined 87 different Skyrme interactions on the basis of their predictions on equilibrium proton fraction and EOS of beta–stable matter as well as neutron star properties. It is found that only 27 of the interactions pass the test which have a monotonically increasing behaviour of $J_\tau(\rho)$ over a wide range of density. For the other interactions considered in ref. [19] with increase in density $J_\tau(\rho)$ reaches a maximum value and then decreases until it becomes negative. Microscopic calculations based on realistic nucleon–nucleon interactions as well as RMF calculations also predict a monotonically increasing behaviour of $J_\tau(\rho)$.

Experimental studies of isospin–sensitive observables in intermediate energy reactions involving radioactive beams have been quite useful in providing some constraints on the density dependence of nuclear symmetry energy at subsaturation densities [1]. Further experiments from future radioactive beam facilities are expected to provide constraints on the high density behaviour of nuclear symmetry energy $J_\tau(\rho)$. In ref. [31] it has been reported that to extract the high density behaviour of nuclear symmetry energy, the momentum and density dependence of the isovector part of nuclear mean field have to be determined simultaneously from an analysis of the experimental observables sensitive to the differences between neutron and proton flow data in highly asymmetric dense nuclear matter in terms of isospin dependent transport model calculations.

1.4.3. Nuclear mean field and nucleon effective mass

The nuclear mean field is a key ingredient in the study of properties of both finite and infinite nuclear systems, particularly in calculations of nuclear equation of state (EOS) and simulation of dynamical evolution of heavy–ion (HI) collisions at intermediate and high energies.

In earlier studies on HI collision dynamics using transport models like Boltzmann–Uehling–Uhlenbeck(BUU) [112] usually a simple density dependent but momentum independent form of the mean field was used, such as the Skyrme parametrisation

$$U(\rho) = A(\rho/\rho_0) + B(\rho/\rho_0)^{\gamma} \qquad ...(1.9)$$

where, the parameter A is attractive, B is repulsive and $\gamma > 1$. Analysis of heavy–ion collision data at intermediate energies, using such momentum independent mean field, demanded a stiff EOS with incompressibility of $\approx 380\ MeV$ [112]. Later in ref. [112] using GBD parametrisation it was shown that if a reasonable momentum dependence is introduced in the nuclear mean field, a rather soft EOS with a incompressibility $\approx$ 200 MeV is consistent in the interpretation of experimental data. Aichelin *et al.* [133] have also showed that introduction of momentum dependence mean field strongly augmented transverse momenta. Subsequently there were many important investigations [114, 134–137] which strongly suggest that momentum dependence of the nuclear mean field is an unavoidable feature for a fundamental understanding of nuclear matter properties and for the successful interpretation of heavy–ion collision dynamics at intermediate and high energies.

The momentum and density dependence of nuclear mean field in SNM has been extensively studied over the past couple of decades using various microscopic as well as phenomenological approaches. Phenomenological effective interactions have been widely used to study the isoscalar part of nuclear mean field at both zero temperature and at finite temperature. In the Skyrme interaction and the Seylor–Blanchard type effective interactions the momentum dependent part of mean field in

SNM is repulsive and has a quadratic dependence of momentum. On the other hand, the momentum dependent part of mean field in SNM derived from a general finite range effective interaction is attractive and is strong at very low momenta. With increase in momentum this part of mean field weakens and vanishes asymptotically at very large momenta. This behaviour of the mean field is an essential feature for a successful interpretation of nucleon–nucleus scattering data at intermediate energies [114, 134–137,]. The microscopic DBHF calculations also exhibit this type of momentum dependence of nuclear mean field in SNM [61, 62].

The nuclear mean field in SNM using a short range momentum dependent effective interaction of conventional forms, such as Yukawa, Gaussian or exponential, has been analysed by Behera *et al.* [107, 108]. They report the momentum dependent part of nuclear mean field is strongly attractive at lower momenta and with increase in momentum it vanishes and then becomes repulsive at high momenta for all the three forms considered. The momentum dependent part of the mean field calculated over a wide range of density and momentum has been compared to that from microscopic calculation by Wiringa [40] using realistic Hamiltonians containing two–body and three–body interactions which fit nucleon–nucleus scattering data, nuclear binding energies of few body system and saturation property of nuclear matter. The momentum dependence of nuclear mean field over a wide range of momentum and density calculated in [108] agrees quite well with that obtained by Wiringa [40] for all the three realistic interactions UV14+UVII, UV14+TNI and AV14+UVII considered. The results are however shown to be in better agreement with those of UV14+UVII and UV14+TNI.

Li and Machleidt [61, 62] have calculated the nuclear mean field in SNM in the DBHF approach using Bonn meson–exchange model for the NN interaction with the approximation that the scalar and vector mean fields are momentum independent although the nuclear mean field is momentum dependent. The nuclear mean field obtained from the DBHF parameterization shows an increasing behaviour with momentum. Comparing the result with phenomenological parameterizations of momentum dependent mean field used in transport models they report a similar bahaviour with variation in momentum. Although, at low momentum the microscopic mean field considered shows stronger momentum dependence than the phenomenological models, at high momenta the momentum dependence in microscopic mean field disappears while it becomes stronger for phenomenological mean fields considered.

Experimental observables from HI collision provide significant constraints on the momentum dependence of mean fields up to a density about $2.3\rho_0$ [3]. Analysis of elliptic flow data in HI collision by Danielewicz [114] show that the momentum and density dependence of nuclear mean field in SNM calculated from microscopic DBHF calculation and the variational interactions UV14+TNI and UV14+UVII agree quite well with that obtained from the parametrisation giving an acceptable description of the flow data. However, the potentials obtained from the nonrelativistic BBG approach with Paris interaction and the variational AV14+UVII interaction were found to be unacceptably weak to produce the correct experimental data at supranormal densities.

So far we were discussing on momentum and density dependence of mean field of SNM where the neutron and proton mean fields are not distinguished from each other. From the discussion till now we see that exhaustive theoretical and experimental studies show the nuclear mean field in SNM to be momentum as well as density dependent and the momentum dependence of mean field can be constrained from experimental observables up to a few times normal nuclear matter density. We will now concentrate on nuclear mean field in isospin asymmetric nuclear matter (ANM).

The momentum and density dependence of mean field in ANM is poorly known [1, 28, 29, 31–33]. Unlike SNM where the single particle potential felt by a neutron and a proton is same in ANM the single particle potential felt by a neutron is different than that from a proton. The knowledge of momentum and density dependence of isovector part of nuclear mean field or the symmetry potential is very important for understanding structure and reactions of radioactive nuclei. Simultaneous study of both momentum and density dependence of symmetry potential is essential for determination of density dependence of nuclear symmetry energy [31]. Therefore momentum dependence of symmetry potential is crucial for constraining the high density behaviour of symmetry energy. In the earlier dynamical simulation of HI collisions the momentum dependence of symmetry potential was seldom taken into account. Recently Li *et al.* [13, 31] showed that experimental observables such as neutron–proton differential flow, π^-/π^+ ratio etc. are quite sensitive to momentum dependence of symmetry potential.

The isovector part of nuclear mean field is defined as the difference between the neutron and proton mean fields normalized to asymmetry. The momentum and density dependence of isovector part of mean field as predicted by different theoretical model calculations discussed in section 1.2 are rather extremely divergent and even contradicting. All theoretical predictions on the momentum dependence of isovector part of nuclear mean field can be classified into two distinct and opposite groups depending on whether it decreases or increases with momentum.

The effective nucleon mass is a very important property of nuclear matter which is directly related to the nuclear mean field. It characterizes the propagation of a nucleon in the nuclear medium. Knowledge about nucleon effective mass in neutron rich matter is important for understanding the reaction dynamics of nuclear collisions induced by radioactive beams, such as the degree and rate of isospin diffusion and neutron–proton differential collective flow [31–33]. Unfortunately, until now there is no definite answer to the question of whether neutron effective mass is greater or proton effective mass is greater in asymmetric nuclear matter.

In connection with the splitting of neutron and proton effective masses in asymmetric nuclear matter it should be mentioned here that the results obtained from different theoretical calculations can be roughly classified in to two groups; one in which the neutron effective mass goes above the proton one and the other showing a splitting in the opposite direction .

1.5. Plan of the thesis

The aim of this present thesis is to analyse the EOS of nuclear matter, starting from symmetric nuclear matter (SNM) to the extreme case of asymmetry, pure neutron matter (PNM), at a large range of density, momentum and temperature using a simple effective interaction. Emphasis will be given to the EOS of ANM and analysis of the puzzling behaviour of nucleon mean fields and symmetry energy as reported from various theoretical and experimental calculations.

In chapter 1 a short introduction emphasizing the importance of determining the EOS of dense ANM is given. Different theoretical approaches used to describe the EOS of nuclear matter on the basis of the underlying nucleon–nucleon interaction has been reviewed briefly in this chapter. The behaviour of nuclear EOS and some of the reported properties of nuclear matter at saturation conditions has been discussed. The contradicting behaviour of nuclear symmetry energy as shown by different theoretical calculations has been discussed in brief. It has been discussed that momentum dependence of nuclear mean field, which is a key ingredient in the study of nuclear EOS, is an unavoidable feature for the fundamental understanding of nuclear matter properties and for successful interpretation of HI collision dynamics. The momentum and density dependence of nuclear mean field as reported by various theoretical approaches has been discussed. The two types of behaviour of the isovector part of nuclear mean field with variation in momentum and the effective nucleon mass splitting has been discussed.

In chapter 2 the momentum and density dependence aspects of nuclear matter is analysed using a general finite range effective interaction. It is shown that the more fundamental quantity for the study of nuclear EOS is the nuclear mean field. The study of nuclear mean field at Fermi momentum accounts for the density dependent aspect of nuclear EOS, while, the momentum dependence aspect of nuclear EOS can be sealed from the momentum dependence of the effective mass. For example, in ANM, the isovector part of mean field around Fermi momentum gives the density dependence of nuclear symmetry energy. On the other hand, momentum dependence of isovector part of nuclear mean field at a given density accounts for the nucleon effective mass splitting in ANM. It is explicitly shown that the puzzle regarding the EOS of ANM can be solved by solving the density and momentum dependence of nuclear mean field and density dependence of nuclear symmetry energy. In this chapter it is shown that to study the momentum dependence of nuclear mean field we need only the exchange part of the effective interaction, where as to study the density dependence of nuclear mean field at densities other than normal nuclear matter density knowledge of both direct and exchange part of the effective interaction is necessary. From this chapter it emerges that a simple density dependent finite range effective interaction of conventional form can be used to analyse the EOS of ANM.

In chapter 3 a simple density dependent finite range effective interaction having Yukawa form for the short range interaction part is considered to analyse the nuclear EOS. The EOS of ANM and properties of nuclear matter at zero temperature are defined for this simple density dependent finite range effective interaction. Since

SNM and PNM form the two boundaries of the EOS of ANM and a complete description of EOS of ANM is equivalent to separate description of EOS of SNM and PNM, the parameters involved in the description of EOS of SNM and PNM are determined. To determine the parameters of the interaction we have used existing empirical/experimental data and simple physical considerations. A number of parameter sets were obtained. Some parameters of the interaction are kept open to analyse their effect on the EOS of ANM. The EOS and properties of nuclear matter such as nuclear mean field, effective nucleon masses, nuclear symmetry energy, energy per particle, pressure, chemical potentials, nuclear incompressibility and speed of sound has been calculated at a large range of density, momentum and asymmetry for the different parameter sets. Two different trends for the effective nucleon mass splitting are shown in this chapter for two different parameter sets. The contradicting behaviour of isovector part of nuclear mean field is examined in detail in this chapter. Also the extremely divergent and contradicting behaviour of nuclear symmetry energy is shown in this chapter for different parameter sets.

Chapter 4 concerns the thermal evolution and liquid–gas phase transition in ANM. The EOS of ANM at finite temperature ($T\neq0$) is constructed for the simple density dependent finite range effective interaction and thermal evolution of ANM at a wide range of density, temperature and asymmetry is shown. The liquid–gas phase transition in ANM is also discussed in brief.

In chapter 5 it is shown that to understand the evolution and structure of neutron stars it is important to understand the EOS of ANM. On the other hand, observables from neutron star properties can put important constrain on the EOS of ANM. In this chapter the EOS of beta–stable matter found in the interiors of neutron star is constructed. We have put further constrain on the high density behaviour of nuclear symmetry energy by adjusting the interaction parameters on the basis of an approximate universal high density behaviour of asymmetric contribution to the nucleonic part of energy density of neutron star matter. The properties of neutron star are calculated for the simple finite range effective interaction.

Finally a brief summary and future scope of the present work is given in chapter 6.

CHAPTER 2

MOMENTUM AND DENSITY DEPENDENCE OF NUCLEAR MEAN FIELD FOR A GENERAL FINITE RANGE EFFECTIVE INTERACTION

2.1. Introduction

The study of momentum and density dependence of the nuclear mean fields in isospin asymmetric nuclear matter is very important topic for fundamental reasons: it will provide better understanding of the isoscalar and isovector parts of the inmedium interactions as well as for the new experimental possibilities offered by RIB facilities.

The two most important quantities in the study of neutron and proton mean field properties and EOS of ANM are the isoscalar and isovector parts of the nuclear mean field, $u(k, \rho)$ and $u_\tau(k, \rho)$, respectively. The isoscalar part $u(k, \rho)$ can be defined as

$$u(k,\rho) = \lim_{Y_p \to 1/2} \frac{u^n(k,\rho,Y_p) + u^p(k,\rho,Y_p)}{2} \qquad \text{...(2.1)}$$

and the isovector part $u_\tau(k, \rho)$ is defined as the difference between neutron and proton mean fields normalized to the asymmetry (1-2Y_p), given as

$$u_\tau(k,\rho) = \lim_{Y_p \to 1/2} \frac{u^n(k,\rho,Y_p) - u^p(k,\rho,Y_p)}{2(1-2Y_p)} \qquad \text{....(2.2).}$$

In the above equations $u^n(k, \rho, Y_p)$ and $u^p(k, \rho, Y_p)$ are the zero-temperature neutron and proton mean fields expressed as functions of momentum k, total nucleon density $\rho = \rho_n + \rho_p$ and proton fraction $Y_p = \rho_p/\rho$.

As seen from Chapter 1 the momentum and density dependence of nuclear mean fields in both SNM and ANM has been studied extensively using various theoretical approaches. Many theoretical models predict a rather similar behaviour of momentum and density dependence of isoscalar and isovector parts of nuclear mean field around Fermi momentum $k = k_f$ at saturation and sub-saturation densities but differ considerably from each other when extrapolated to high momenta and high densities.

Since non-relativistic finite range effective interactions provide the simplest possible way to study the EOS of nuclear matter, in this chapter we have used a general finite range effective interaction to construct the nuclear matter EOS and use it to study the momentum and density dependence of isoscalar and isovector parts of nuclear mean field. The expressions for EOS of nuclear matter at zero temperature ($T = 0$) and at finite temperature ($T \neq 0$) has been given for a general effective interaction in sections 2.2 and 2.3 respectively. To study the momentum dependence of neutron and proton mean fields the difference between these two quantities has been studied in section 2.4. In that section it has been shown that the difference between neutron and proton mean fields is directly connected to the sign of the difference between neutron and proton effective masses and hence can lead to the neutron and proton effective mass splitting study. In section 2.5 the isoscalar and isovector parts of nuclear mean field are given for the general effective interaction. In section 2.6 a brief discussion has been given on how the knowledge of certain nuclear matter properties, although our present knowledge on these properties is very low, can lead to the solution of the whole problem. Finally in section 2.7 a brief summary has been given.

2.2. EOS of ANM for general effective interaction at finite temperature

To derive the equation of state (EOS) of asymmetric nuclear matter (ANM) from a general nucleon-nucleon effective interaction we consider four different effective interactions, namely, the direct and the exchange effective interactions between like (l) and unlike (ul) nucleons: $v_d^{l}(r)$, $v_d^{ul}(r)$, $v_{ex}^{l}(r)$ and $v_{ex}^{ul}(r)$, assuming charge symmetry (i.e. $v^{nn}(r) = v^{pp}(r)$). These four different interactions are given as

$$v_d^{\,l}(r) = \frac{1}{4}v^{se}(r) + \frac{3}{4}v^{to}(r) \qquad \text{...(2.3)}$$

$$v_d^{ul}(r) = \frac{1}{8}v^{se}(r) + \frac{3}{8}v^{te}(r) + \frac{1}{8}v^{so}(r) + \frac{3}{8}v^{to}(r). \qquad \text{...(2.4)}$$

$$v_{ex}^{l}(r) = \frac{1}{4}v^{se}(r) - \frac{3}{4}v^{to}(r) \qquad \text{...(2.5)}$$

and

$$v_{ex}^{ul}(r) = \frac{1}{8}v^{se}(r) + \frac{3}{8}v^{te}(r) - \frac{1}{8}v^{so}(r) - \frac{3}{8}v^{to}(r). \qquad \text{...(2.6)}$$

The quantities $v^{se}(r)$, $v^{te}(r)$, $v^{so}(r)$ and $v^{to}(r)$ represent effective interactions in the specified states averaged over angles, spins, and isopsins of the two interacting nucleons. The symbols *e/o* and *t/s* represent respectively the parity (even/odd) and the spin (triplet/singlet) of the two nucleon states. These effective interactions depend on the relative separation distance r between the two nucleons as well as on the total nucleon density $\rho = \rho_n + \rho_p$ of ANM. The neutron and proton densities ρ_n and ρ_p are generated by their respective single particle Fermi-Dirac momentum distribution functions $f_T^n(\vec{k})$ and $f_T^p(\vec{k})$ subject to the normalization

$$\rho_{n,\,p} = \int f_T^{n,p}(\vec{k})\ d^3k. \qquad \text{...(2.7)}$$

The energy density functional in asymmetric nuclear matter $H_T(\rho_n, \rho_p)$ at temperature T obtained from these effective interactions is given as,

$$\begin{aligned}H_T(\rho_n,\rho_p) &= \int [f_T^n(\vec{k}) + f_T^p(\vec{k})](c^2\hbar^2k^2 + M^2c^4)^{1/2}d^3k + \frac{1}{2}(\rho_n^2+\rho_p^2)\int v_d^l(r)d^3r \\ &+ \rho_n\rho_p\int v_d^{ul}(r)d^3r + \frac{1}{2}\iint [f_T^n(\vec{k})f_T^n(\vec{k}') + f_T^p(\vec{k})f_T^p(\vec{k}')]g_{ex}^l(|\vec{k}-\vec{k}'|)d^3k d^3k' \\ &+ \frac{1}{2}\iint [f_T^n(\vec{k})f_T^p(\vec{k}') + f_T^p(\vec{k})f_T^n(\vec{k}')]g_{ex}^{ul}(|\vec{k}-\vec{k}'|)d^3k d^3k'.\end{aligned} \qquad \text{...(2.8)}$$

The momentum dependent interactions $g_{ex}^{l,ul}(|\vec{k}-\vec{k}'|)$ are Fourier transforms of the respective exchange interactions $v_{ex}^{l,ul}(r)$,

$$g_{ex}^{l,ul}(|\vec{k}-\vec{k}'|) = \int e^{i(\vec{k}-\vec{k}')\cdot\vec{r}}v_{ex}^{l,ul}(r)d^3r. \qquad \text{...(2.9)}$$

The energy density functional $H_T(\rho_n,\rho_p)$ has separate contributions to the kinetic energy density from neutrons as well as protons. In Eq. (2.8) relativistic relation between kinetic energy and momentum has been used to take account of possible relativistic effects that may arise at high density and/or temperature. Similarly the potential energy density has separate contributions from interactions between like and unlike nucleons.

In asymmetric nuclear matter the single particle energy felt by a neutron is different than that by a proton. The neutron and proton single particle energies $\epsilon_T^{n,p}(k,\rho_n,\rho_p)$ can be obtained as the respective functional derivatives of the energy density $H_T(\rho_n,\rho_p)$ given in Eq. (2.8) and are expressed as

$$\epsilon_T^{n,p}(k,\rho_n,\rho_p) = (c^2\hbar^2k^2 + M^2c^4)^{1/2} + u_T^{n,p}(k,\rho_n,\rho_p). \qquad \ldots(2.10)$$

In the above equation the first term is the kinetic energy of neutron and proton under consideration and $u_T^{n,p}(k,\rho_n,\rho_p)$ are the neutron and proton single particle potentials or mean fields respectively. The neutron mean field $u_T^{n,p}(k,\rho_n,\rho_p)$ at temperature T is given as

$$\begin{aligned}
u_T^n(k,\rho_n,\rho_p) &= \left[\rho_n \int v_d^l(r)d^3r + \rho_p \int v_d^{ul}(r)d^3r\right] \\
&+ \left[\int f_T^n(\vec{k}')g_{ex}^l(|\vec{k}-\vec{k}'|)d^3k' + f_T^p(\vec{k}')g_{ex}^{ul}(|\vec{k}-\vec{k}'|)d^3k'\right] \\
&+ \left[\frac{(\rho_n^2+\rho_p^2)}{2}\int\frac{\partial v_d^l(r)}{\partial\rho_n}d^3r + \rho_n\rho_p\int\frac{\partial v_d^{ul}(r)}{\partial\rho_n}d^3r\right. \\
&+ \frac{1}{2}\iint\left[f_T^n(\vec{k})f_T^n(\vec{k}') + f_T^p(\vec{k})f_T^p(\vec{k}')\right]\frac{\partial g_{ex}^l(|\vec{k}-\vec{k}'|)}{\partial\rho_n}d^3k\,d^3k' \\
&\left.+ \frac{1}{2}\iint\left[f_T^n(\vec{k})f_T^p(\vec{k}') + f_T^p(\vec{k})f_T^n(\vec{k}')\right]\frac{\partial g_{ex}^{ul}(|\vec{k}-\vec{k}'|)}{\partial\rho_n}d^3k\,d^3k'\right]
\end{aligned} \qquad \ldots(2.11)$$

Similarly the proton mean field $u_T^p(k,\rho_n,\rho_p)$ at temperature T is given as

$$\begin{aligned}u_T^{p}(k,\rho_n,\rho_p) = &\left[\rho_p \int v_d^{l}(r)d^3r + \rho_n \int v_d^{ul}(r)d^3r\right] \\ &+\left[\int f_T^p(\vec{k}')g_{ex}^{l}(|\vec{k}-\vec{k}'|)d^3k' + f_T^n(\vec{k}')g_{ex}^{ul}(|\vec{k}-\vec{k}'|)d^3k'\right] \\ &+\left[\frac{(\rho_n^2+\rho_p^2)}{2}\int \frac{\partial v_d^{l}(r)}{\partial \rho_p}d^3r + \rho_n\rho_p \int \frac{\partial v_d^{ul}(r)}{\partial \rho_p}d^3r\right. \\ &+\frac{1}{2}\iint\left[f_T^p(\vec{k})f_T^p(\vec{k}') + f_T^n(\vec{k})f_T^n(\vec{k}')\right]\frac{\partial g_{ex}^{l}(|\vec{k}-\vec{k}'|)}{\partial \rho_p}d^3k d^3k' \\ &\left.+\frac{1}{2}\iint\left[f_T^p(\vec{k})f_T^n(\vec{k}') + f_T^n(\vec{k})f_T^p(\vec{k}')\right]\frac{\partial g_{ex}^{ul}(|\vec{k}-\vec{k}'|)}{\partial \rho_p}d^3k d^3k'\right]\end{aligned} \qquad \ldots(2.12)$$

From Eqs. (2.11) and (2.12) it is observed that the nucleon mean fields or single particle potentials $u_T^{n,p}(k,\rho_n,\rho_p)$ have three distinct parts; a direct part, an exchange part which is momentum dependent and a rearrangement part arising out of any explicit dependence of the four different effective interactions on total nucleon density ρ.

In the calculation of EOS of ANM the most important entities are the neutron and proton single particle momentum distribution functions $f_T^n(\vec{k})$ and $f_T^p(\vec{k})$. In terms of Fermi-Dirac distribution functions the single particle momentum distribution functions are expressed as

$$f_T^{n,p}(\vec{k}) = \frac{g}{(2\pi)^3} n_T^{n,p}(\vec{k}), \qquad \ldots(2.13)$$

where $n_T^{n,p}(\vec{k})$ are the neutron and proton occupation probability given by

$$n_T^{n,p}(\vec{k}) = \left\{\exp\left[\left(\epsilon_T^{n,p}(k,\rho_n,\rho_p) - \mu_T^{n,p}\right)/T\right]+1\right\}^{-1}, \qquad (2.14)$$

g is the spin-isospin degeneracy factor and $\mu_T^{n,p}$ are the chemical potentials for neutrons and protons respectively.

From Eqs. (2.10)-(2.14) it is evident that a self-consistent calculation is required to evaluate the single particle momentum distribution functions $f_T^n(\vec{k})$ and $f_T^p(\vec{k})$. A method of successive iteration, starting from the single particle energies at zero temperature $\epsilon^{n,p}(k,\rho_n,\rho_p)$ can be implemented to evaluate the single particle momentum distribution functions $f_T^n(\vec{k})$ and $f_T^p(\vec{k})$ self-consistently [140] at a given total nucleon density ρ and temperature T. This procedure gives simultaneously the neutron and proton Fermi-Dirac distribution functions $f_T^{n,p}(\vec{k})$, the single particle energies $\in_T^{n,p}(k,\rho_n,\rho_p)$ and the chemical potentials $\mu_T^{n,p}$, using which the energy density $H_T(\rho_n,\rho_p)$ as well as the complete EOS of ANM can be calculated at temperature T and total nucleon density ρ.

An important property of asymmetric nuclear matter related directly to the nucleon mean fields is the effective nucleon mass. The nucleon effective masses usually arise from the momentum dependence of the mean fields $u_T^{n,p}(k,\rho_n,\rho_p)$ and are defined through the relation

$$\left\{\frac{1}{k}\frac{d}{dk}(c^2\hbar^2k^2+M^2c^4)^{1/2}\right\}_{M=M^*}=\frac{1}{k}\frac{\partial\in_T(k,\rho_n,\rho_p)}{\partial k}. \qquad \ldots(2.15)$$

Using the relation for $\in_T^{n,p}(k,\rho_n,\rho_p)$ the ratio of effective nucleon masses to the actual mass can be written as

$$\left[\frac{M^*(k,\rho_n,\rho_p)}{M}\right]_T^{n,p}=\left\{\left[\left(1+\frac{\hbar^2k^2}{M^2c^2}\right)^{-1/2}+\frac{M}{\hbar^2k}\frac{\partial u_T{}^{n,p}(k,\rho_n,\rho_p)}{\partial k}\right]^{-2}-\frac{\hbar^2k^2}{M^2c^2}\right\}^{1/2} \qquad \ldots(2.16)$$

The momentum and density dependence of the neutron and proton single particle energies $\in^{n,p}(k,\rho_n,\rho_p)$ at zero temperature play an important role in the thermal evolution of EOS of ANM. As discussed earlier in this section, the nucleon mean fields $\in^{n,p}(k,\rho_n,\rho_p)$ are the basic input in the self-consistent evaluation of the single particle momentum distribution functions at $T \neq 0$. In view of this, we have derived the nucleon mean fields and EOS of ANM at zero temperature ($T=0$) in the next section.

2.3. EOS of ANM for general effective interaction at zero temperature

To evaluate the EOS of ANM at zero temperature ($T=0$) no more self-consistent calculation is required, which was necessary for the case of $T \neq 0$. As the single particle momentum distribution functions at zero temperature take the form of step functions the EOS of ANM can be calculated analytically.

The single particle momentum distribution functions at zero temperature are given as step functions,

$$f^{n,p}(k)=\frac{g}{(2\pi)^3}\theta(k_{n,p}-k), \qquad \ldots(2.17)$$

where k_n, and k_p are the neutron and proton momentum at Fermi surface and using Eq. (2.9) are related to neutron and proton densities ρ_n and ρ_p by the relation

$$\rho_{n,p}=\frac{k_{n,p}^3}{3\pi^2}. \qquad \ldots(2.18)$$

Using the zero-temperature momentum distribution functions the energy density functional $H(\rho_n, \rho_p)$ in ANM at zero temperature can be expressed in the form

$$H(\rho_n,\rho_p)=\frac{3Mc^2}{8}\sum_{i=n,p}\frac{\rho_i}{x_i^3}\left[2x_iu_i^3-x_iu_i-\ln(x_i+u_i)\right]+\frac{1}{2}(\rho_n^2+\rho_p^2)\int v_d^l(r)d^3r$$
$$+\rho_n\rho_p\int v_d^{ul}(r)d^3r+\frac{9}{2}\int\left[\rho_n^2\frac{j_1^2(k_nr)}{(k_nr)^2}+\rho_p^2\frac{j_1^2(k_pr)}{(k_pr)^2}\right]v_{ex}^l(r)d^3r$$
$$+9\rho_n\rho_p\int\frac{j_1(k_nr)}{(k_nr)}\frac{j_1(k_pr)}{(k_pr)}v_{ex}^{ul}(r)d^3r \qquad \ldots(2.19)$$

where $\quad x_i=\dfrac{\hbar k_i}{Mc}$ and $u_i=(1+x_i^2)^{1/2}$, $i=n,p$ $\qquad \ldots(2.20)$

and $\quad j_1$ is spherical Bessel functions of order 1.

Similarly the neutron and proton single particle energies $\epsilon^{n,p}(k,\rho_n,\rho_p)$ at zero temperature are given as

$$\epsilon^{n,p}(k,\rho_n,\rho_p)=(c^2\hbar^2k^2+M^2c^4)^{1/2}+u^{n,p}(k,\rho_n,\rho_p), \qquad \ldots(2.21)$$

where $u^{n,p}(k,\rho_n,\rho_p)$ are the neutron and proton mean fields at zero temperature in ANM, given as

$$u^n(k,\rho_n,\rho_p)=\left[\rho_n\int v_d^l(r)d^3r+\rho_p\int v_d^{ul}(r)d^3r\right]$$
$$+\left[3\rho_n\int j_0(kr)\frac{j_1(k_nr)}{k_nr}v_{ex}^l(r)d^3r+3\rho_p\int j_0(kr)\frac{j_1(k_pr)}{k_pr}v_{ex}^{ul}(r)d^3r\right]$$
$$+\left[\frac{(\rho_n^2+\rho_p^2)}{2}\int\frac{\partial v_d^l(r)}{\partial\rho_n}d^3r+\rho_n\rho_p\int\frac{\partial v_d^{ul}(r)}{\partial\rho_n}d^3r\right.$$
$$\left.+\frac{9}{2}\int\left\{\rho_n^2\frac{j_1^2(k_nr)}{(k_nr)^2}+\rho_p^2\frac{j_1^2(k_pr)}{(k_pr)^2}\right\}\frac{\partial v_d^l(r)}{\partial\rho_n}d^3r+9\rho_n\rho_p\int\frac{j_1(k_nr)}{(k_nr)}\frac{j_1(k_pr)}{(k_pr)}\frac{\partial v_{ex}^{ul}(r)}{\partial\rho_n}d^3r\right]$$

$\ldots(2.22)$,

$$u^p(k,\rho_n,\rho_p)=\left[\rho_p\int v_d^l(r)d^3r+\rho_n\int v_d^{ul}(r)d^3r\right]$$
$$+\left[3\rho_p\int j_0(kr)\frac{j_1(k_pr)}{k_pr}v_{ex}^l(r)d^3r+3\rho_n\int j_0(kr)\frac{j_1(k_nr)}{k_nr}v_{ex}^{ul}(r)d^3r\right]$$
$$+\left[\frac{(\rho_n{}^2+\rho_p^2)}{2}\int\frac{\partial v_d^l(r)}{\partial\rho_p}d^3r+\rho_n\rho_p\int\frac{\partial v_d^{ul}(r)}{\partial\rho_p}d^3r\right.$$
$$\left.+\frac{9}{2}\int\left\{\rho_p{}^2\frac{j_1^2(k_pr)}{(k_pr)^2}+\rho_n{}^2\frac{j_1^2(k_nr)}{(k_nr)^2}\right\}\frac{\partial v_{ex}^l(r)}{\partial\rho_p}d^3r+9\rho_n\rho_p\int\frac{j_1(k_pr)}{(k_pr)}\frac{j_1(k_nr)}{(k_nr)}\frac{\partial v_{ex}^{ul}(r)}{\partial\rho_p}d^3r\right]$$

...(2.23)

In the above equations j_0 is the spherical Bessel function of order 0.

The nuclear symmetry energy $J_\tau(\rho)$ which plays a crucial role in the evaluation of EOS of ANM was defined in chapter 1 as

$$J_\tau(\rho)=\frac{1}{2\rho}\left[\frac{\partial^2 H(\rho_n,\rho_p)}{\partial\sigma^2}\right]_{\sigma=0} \qquad ...(2.24)$$

where σ is the asymmetry parameter related to neutron and proton density by the relation $\sigma=(\rho_n-\rho_p)/\rho$. For a general effective interaction $J_\tau(\rho)$ can be derived from Eqs. (2.19) and (2.24) as

$$J_\tau(\rho)=\frac{Mc^2}{6}\frac{x_f^2}{u_f}+\frac{\rho}{4}\int\left[v_d^l(r)-v_d^{ul}(r)\right]d^3r$$
$$+\frac{\rho}{4}\int j_0^2(k_fr)\left[v_{ex}^l(r)-v_{ex}^{ul}(r)\right]d^3r-\frac{\rho}{4}\int j_1^2(k_fr)\left[v_{ex}^l(r)+v_{ex}^{ul}(r)\right]d^3r$$

...(2.25)

where $x_f=\dfrac{\hbar k_f}{Mc}$, $\quad u_f=(1+x_f^2)^{1/2}$, ...(2.26)

and k_f is the Fermi momentum in symmetric nuclear matter (SNM) connected to the total nucleon density ρ by the relation

$$\rho=\frac{2k_f^3}{3\pi^2} \qquad ...(2.27)$$

The effective nucleon masses at zero temperature in ANM can be expressed as

$$\left[\frac{M^*(k,\rho_n,\rho_p)}{M}\right]^{n,p}=\left\{\left[\left(1+\frac{\hbar^2k^2}{M^2c^2}\right)^{-1/2}+\frac{M}{\hbar^2k}\frac{\partial u^{n,p}(k,\rho_n,\rho_p)}{\partial k}\right]^{-2}-\frac{\hbar^2k^2}{M^2c^2}\right\}^{1/2} \qquad (2.28)$$

From the above equation it is evident that momentum dependence of the nucleon effective masses depend on the behaviour of nucleon mean fields with momentum.

2.4. Momentum dependence of nucleon mean fields for general effective interaction

The momentum and density dependence of neutron and proton mean fields are very crucial in understanding a number of phenomena involving inmedium interactions. The importance of the study has increased manifold with the growing experimental facilities available for study of HI collision using Radioactive Ion Beams [1]. In this section, the momentum dependence of neutron and proton mean fields has been studied for a general effective interaction.

In the study of EOS of asymmetric nuclear matter (ANM), the most important quantity is the difference between neutron and proton mean fields,

$$u_T^{n-p}(k,\rho_n,\rho_p)=u_T^n(k,\rho_n,\rho_p)-u_T^p(k,\rho_n,\rho_p), \tag{2.29}$$

From Eqs. (2.11) and (2.12) it is evident that the rearrangement parts in neutron and proton nuclear mean fields will cancel out and the functional $u_T^{n-p}(k,\rho_n,\rho_p)$ at a given temperature T in terms of total nucleon density ρ and proton fraction $Y_p=\rho_p/\rho$ can be expressed as

$$\begin{aligned} u_T^{n-p}(k,\rho,Y_p)&=(1-2Y_p)\rho\int[v_d^l(r)-v_d^{ul}(r)]d^3r \\ &+\int[f_T^n(\vec{k}')-f_T^p(\vec{k}')][g_{ex}^l(|\vec{k}-\vec{k}'|)-g_{ex}^{ul}(|\vec{k}-\vec{k}'|)]d^3k'. \end{aligned} \tag{2.30}$$

This result shows that the first term of $u_T^{n-p}(k,\rho_n,\rho_p)$ is independent of temperature and momentum and is directly proportional to $(1\text{-}2Y_p)$, the proportionality factor depending only on the total nucleon density ρ. On the other hand, the second term has a very complicated dependence on temperature T, momentum k, total nucleon density ρ and proton fraction Y_p. However, in the limit of very large k, the functionals $g_{ex}^{l,ul}(|\vec{k}-\vec{k}'|)$ appearing inside the integral in eqn. (2.30) can be approximated for a finite range exchange interaction by $g_{ex}^{l,ul}(k)$ and hence the functional $u_T^{n-p}(k,\rho,Y_p)$ can be expressed as

$$u_T^{n-p}(k,\rho,Y_p)\xrightarrow[k\to\infty]{}(1-2Y_p)\rho\left[\int\left[v_d^l(r)-v_d^{ul}(r)\right]d^3r+\left[g_{ex}^l(k)-g_{ex}^{ul}(k)\right]\right] \tag{2.31}$$

This result is very important in the sense that at large k the functional $u_T^{n-p}(k,\rho,Y_p)$ is independent of temperature and is directly proportional to neutron proton asymmetry (1-2Y_p).

To examine the momentum dependence of $u_T^{n-p}(k,\rho,Y_p)$ we introduce a dimensionless quantity,

$$\frac{M}{\hbar^2 k}\frac{\partial u_T^{n-p}(k,\rho,Y_p)}{\partial k}=\frac{M}{\hbar^2 k}\frac{\partial}{\partial k}\left[\int [f_T^n(\vec{k}')-f_T^p(\vec{k}')][g_{ex}^l(|\vec{k}-\vec{k}'|)-g_{ex}^{ul}(|\vec{k}-\vec{k}'|)]d^3k'\right] \quad ...(2.32)$$

It is important to note that the functionals $\frac{M}{\hbar^2 k}\frac{\partial u_T^{n,p}(k,\rho,Y_p)}{\partial k}$ are directly connected to neutron and proton effective masses $\left[\frac{M^*(k,\rho_n,\rho_p)}{M}\right]_T^{n,p}$ as evident from Eq. (2.16).

It should be mentioned here that knowledge about neutron and proton effective masses in highly asymmetric matter is important for understanding isospin diffusion, neutron-proton differential flow in HI reaction dynamics. However, the question of whether neutron effective mass is larger than proton effective mass in ANM is still open. Different theoretical calculations predict contradicting result and almost nothing is known experimentally about the neutron-proton effective mass splitting.

In case of Skyrme parametrization of the EOS of ANM the functional $\frac{M}{\hbar^2 k}\frac{\partial u_T^{n-p}(k,\rho,Y_p)}{\partial k}$ has a very simple structure,

$$\frac{M}{\hbar^2 k}\frac{\partial u_T^{n-p}(k,\rho,Y_p)}{\partial k}=(1-2Y_p)\frac{M}{4\hbar^2}\left[t_2(2x_2+1)-t_1(2x_1+1)\right]\rho, \quad ...(2.33)$$

which is not only proportional to neutron-proton asymmetry parameter (1-2Y_p) but also independent of temperature T and momentum k. The sign of the parameter B = [t_2 (2x_2 + 1) – t_1 (2x_1 + 1)] will determine whether the proton effective mass is above the neutron one or the other way around. For all Skyrme parametrizations [19, references therein] with x_1 = x_2 = 0 the value of B is negative. Other Skyrme parametrizations such as SGII, RATP, SKP, SKX, SKXm and SkSC have also negative values of the parameter B. In all these cases the neutron effective mass is above the proton effective mass irrespective of temperature, momentum and density.

above the proton effective mass irrespective of temperature, momentum and density. On the other hand, the Skyrme-Lyon parametrisations Sly-a and Sly-b and SkI1-SkI6 give positive values of the parameter B and in these cases the proton effective mass is above the neutron one. For Skyrme parametrizations such as SkSC4 and T6 for which $x_1 = x_2 = -0.5$ the parameter B vanishes and the neutron and proton effective masses are identical.

From Eq. (2.32) it can be observed that for finite range effective interactions the dimensionless quantity $\frac{M}{\hbar^2 k}\frac{\partial u_T^{n-p}(k,\rho,Y_p)}{\partial k}$ has a very complicated dependence on temperature T, momentum k, total density ρ and proton fraction Y_p. Only in the limit of large k the functional $\frac{M}{\hbar^2 k}\frac{\partial u_T^{n-p}(k,\rho,Y_p)}{\partial k}$ will simplify and can be given as

$$\frac{M}{\hbar^2 k}\frac{\partial u_T^{n-p}(k,\rho,Y_p)}{\partial k} \underset{large\ k}{\sim} (1-2Y_p)\rho\frac{M}{\hbar^2 k}\left[\frac{dg_{ex}^{l}(k)}{dk}-\frac{dg_{ex}^{ul}(k)}{dk}\right] \qquad \ldots(2.34)$$

From the above equation it is evident that if the asymptotic behaviour of $\frac{M}{\hbar^2 k}\frac{\partial u_T^{n-p}(k,\rho,Y_p)}{\partial k}$ is positive then neutron effective mass is less than the proton effective mass for given values of k, ρ and Y_p and the other way around for negative values of $\frac{M}{\hbar^2 k}\frac{\partial u_T^{n-p}(k,\rho,Y_p)}{\partial k}$ for large k.

For Gogny effective interactions the behaviour of $\frac{M}{\hbar^2 k}\frac{\partial u_T^{n-p}(k,\rho,Y_p)}{\partial k}$ at large k can be calculated analytically and the result can be written as,

$$\frac{M}{\hbar^2 k}\frac{\partial u_T^{n-p}(k,\rho,Y_p)}{\partial k} \underset{k\to\infty}{\sim} (1-2Y_p)\rho\frac{M}{2\hbar^2}\sum_{i=1,2}\alpha_i^5\left(\frac{W_i}{2}+B_i\right)\exp\left(-\alpha_i^2 k^2/4\right). \qquad \ldots(2.35)$$

For large values of k the contribution coming from the long range part of Gogny effective interactions (α_2 = 1.2 *fm*) can be safely ignored compared to the contributions from the short range part ($\alpha_1 = 0.7$ *fm*). Thus the sign of ($W_1/2 + B_1$) for the short range part of Gogny effective interactions will determine whether asymptotically for large k the neutron effective mass is above the proton effective mass or the other way around. Among the different sets of Gogny effective interactions used by Blaizot *et al.* [141] this parameter is positive for D1S and D250 and therefore asymptotically for large k the proton effective mass goes above the neutron effective mass. On the other hand, ($W_1/2 + B_1$) is negative for D1, D260, D280 and D300 and as a result the neutron effective mass goes above the proton effective mass asymptotically for large k.

Since the asymptotic behaviour of $\frac{M}{\hbar^2 k}\frac{\partial u_T^{n-p}(k,\rho,Y_p)}{\partial k}$ is proportional to the total nucleon density ρ and the neutron-proton asymmetry parameter ($1-2Y_p$), the splitting of neutron and proton effective masses mentioned above may be small around normal nuclear matter density ρ_0 and therefore can be neglected in finite nuclei where both ρ and ($1-2Y_p$) are rather small [142]. However, this difference in neutron and proton effective masses may be quite relevant for transport properties of energetic nucleons in highly asymmetric dense nuclear matter that can be formed in high energy heavy-ion collisions with radioactive ion beams.

2.5. Isoscalar and isovector parts of nuclear mean field for general effective interaction

At zero temperature the difference between neutron and proton mean fields can be calculated from eqns. (2.22) and (2.23) as

$$u^{n-p}(k,\rho,Y_p)=(1-2Y_p)\rho\int[v_d^l(r)-v_d^{ul}(r)]d^3r$$
$$+\int\left[\rho_n\frac{3j_1(k_n r)}{k_n r}-\rho_p\frac{3j_1(k_p r)}{k_p r}\right][v_{ex}^l(r)-v_{ex}^{ul}(r)]j_0(kr)d^3r, \qquad \ldots(2.36)$$

The direct part of $u^{n-p}(k,\rho,Y_p)$ is same as that of $u_T^{n-p}(k,\rho,Y_p)$ and similarly, the exchange part has a complicated dependence on momentum k, total nucleon density ρ and proton fraction Y_p. However, in case of zero temperature $u^{n-p}(k,\rho,Y_p)$ can be simplified in two cases. In the limit of large k, it will take the same form as at finite temperature given in Eq. (2.31). The second simplification arises from the fact that the exchange term in $u^{n-p}(k,\rho,Y_p)$ is approximately proportional to ($1-2Y_p$). The proportionality factor of exchange part can be approximated in terms of a Taylor expansion of the functional $\left[\rho_n\frac{3j_1(k_n r)}{k_n r}-\rho_p\frac{3j_1(k_p r)}{k_p r}\right]$ about Y_p =1/2 as,

$\left[\rho_n \frac{3j_1(k_n r)}{k_n r} - \rho_p \frac{3j_1(k_p r)}{k_p r}\right]$ = (1-2 Y_p) ρ $j_0(k_f r)$+ terms with higher odd integral powers of (1-2 Y_p). ...(2.37)

Using Eqs. (2.2) and (2.37) and neglecting higher order powers of (1-2Y_p) the isovector part of nuclear mean field $u_\tau(k, \rho)$ can now be approximated as

$$u_\tau(k,\rho) = \frac{\rho}{2}\left[\int [v_d^l(r) - v_d^{ul}(r)]d^3r + \int j_0(kr) j_0(k_f r)[v_{ex}^l(r) - v_{ex}^{ul}(r)]d^3r\right] \quad ...(2.38)$$

A common problem which frequently arises in comparing the momentum dependence of the isovector part of nuclear mean field $u_\tau(k, \rho)$ derived from different effective interactions is the difference in the density dependence of the nuclear symmetry energy $J_\tau(\rho)$ for these interactions. In view of this it is desirable to separate out the density dependence of $J_\tau(\rho)$ from the isovector part of nuclear mean field $u_\tau(k, \rho)$.

The nuclear symmetry energy $J_\tau(\rho)$ given in Eq. (2.25) can be put in the form,

$$J_\tau(\rho) = \frac{\hbar^2 k_f^2}{6M}\left[\left\{\frac{M^*(k,\rho)}{M}\right\}^2 + \frac{\hbar^2 k^2}{M^2c^2}\right]^{-1/2}_{k=k_f} + \frac{\rho}{4}\int [v_d^l(r) - v_d^{ul}(r)]d^3r$$
$$+\frac{\rho}{4}\int [v_{ex}^l(r) - v_{ex}^{ul}(r)] j_0^2(k_f r) d^3r \quad ...(2.39)$$

where, $M^*(k, \rho)/M$ is the zero-temperature nuclear effective mass in SNM defined as

$$\frac{M^*(k,\rho)}{M} = \left[\left\{\left(1+\frac{\hbar^2k^2}{M^2c^2}\right)^{-1/2} + \frac{M}{\hbar^2 k}\frac{\partial u(k,\rho)}{\partial k}\right\}^{-2} - \frac{\hbar^2k^2}{M^2c^2}\right]^{1/2} \quad ...(2.40)$$

In the above equation $u(k, \rho)$ is the zero-temperature mean field in SNM, conventionally called the isoscalar part of nuclear mean field, which can be obtained from Eqs. (2.22) and (2.23) as

$$u(k,\rho) = \rho\int v_d(r)d^3r + \rho\int j_0(kr)\frac{3j_1(k_f r)}{(k_f r)} v_{ex}(r)d^3r$$
$$+\frac{\rho^2}{2}\int \frac{\partial v_d(r)}{\partial \rho}d^3r + 9\frac{\rho^2}{2}\int \frac{j_1^2(k_f r)}{(k_f r)^2}\frac{\partial v_{ex}(r)}{\partial \rho}d^3r \quad ...(2.41)$$

Here $v_d(r)$ and $v_{ex}(r)$ are the direct and exchange parts of the effective interaction, respectively and satisfy the relation

$$v_d(r) = \frac{v_d^l(r) + v_d^{ul}(r)}{2} \text{ and } v_{ex}(r) = \frac{v_{ex}^l(r) + v_{ex}^{ul}(r)}{2} \qquad \text{...(2.42)}$$

It should be mentioned here that the single particle energy in SNM $\in(k,\rho)$ defined as

$$\in(k,\rho) = (c^2\hbar^2k^2 + M^2c^4)^{1/2} + u(k,\rho) \qquad \text{...(2.43)}$$

satisfies the Hugenholtz-Van Hove (HV) theorem at Fermi surface, i.e.,

$$\in(k=k_f,\rho) = e(\rho) + \rho\frac{de(\rho)}{d\rho}. \qquad \text{...(2.44)}$$

In the above equation $e(\rho)$ is the energy per nucleon in SNM given as

$$e(\rho) = \frac{3Mc^2}{8x_f^3}\left[2x_f u_f^3 - x_f u_f - \ln(x_f + u_f)\right] + \frac{\rho}{2}\int v_d(r)d^3r + \frac{9\rho}{2}\int\frac{j_1^2(k_f r)}{(k_f r)^2}v_{ex}(r)d^3r$$

...(2.45)

Now the isovector part of the nuclear mean field $u_\tau(k, \rho)$ defined in eqn. (2.38) is connected to the nuclear symmetry energy $J_\tau(\rho)$ given in eqn. (2.39) through the relation,

$$u_\tau(k,\rho) = 2J_\tau(\rho) - \frac{\hbar^2k_f^2}{3M}\left[\left(\frac{M^*(k,\rho)}{M}\right)^2 + \frac{\hbar^2k^2}{M^2c^2}\right]_{k=k_f}^{-1/2} + u_\tau^{ex}(k,\rho) \qquad \text{...(2.46)}$$

where, $u_\tau^{ex}(k,\rho) = \frac{\rho}{2}\int[j_0(kr) - j_0(k_f r)][v_{ex}^l(r) - v_{ex}^{ul}(r)]j_0(k_f r)d^3r.$ ...(2.47)

Analogous to Eqs. (2.36) and (2.47) the zero-temperature mean field in SNM or the isoscalar part of mean field $u(k, \rho)$ can also be expressed with the help of HV theorem given in Eq. (2.44) as

$$u(k,\rho) = e(\rho) + \rho\frac{de(\rho)}{d\rho} - \left(c^2\hbar^2k_f^2 + M^2c^4\right)^{1/2} + u^{ex}(k,\rho), \qquad \text{...(2.48)}$$

where, $u^{ex}(k,\rho) = \frac{3\rho}{2}\int[j_0(kr) - j_0(k_f r)]\frac{j_1(k_f r)}{(k_f r)}[v_{ex}^l(r) + v_{ex}^{ul}(r)]d^3r$ ...(2.49)

It should be mentioned here that in eqns. (2.46)-(2.47) there is a connection to very old open problems; the momentum and density dependence of the Lane potentials [143] $v_l = 4\, u_\tau(k, \rho)$, which is now seen in a much more general framework.

It is important to note that only finite range parts of the exchange interactions between like and unlike nucleons can contribute to $u_\tau(k, \rho)$ and $u_\tau^{ex}(k, \rho)$. Moreover, these two functionals vanish at the Fermi momentum $k = k_f$ and the isoscalar and isovector part of nuclear mean field at Fermi momentum is given as

$$u_\tau(k=k_f,\rho)=2J_\tau(\rho)-\frac{\hbar^2 k_f^{\,2}}{3M}\left[\left(\frac{M^*(k,\rho)}{M}\right)^2+\frac{\hbar^2k^2}{M^2c^2}\right]_{k=k_f}^{-1/2} \qquad \ldots(2.50)$$

and $$u(k=k_f,\rho)=e(\rho)+\rho\frac{de(\rho)}{d\rho}-\left(c^2\hbar^2k_f^2+M^2c^4\right)^{1/2} \qquad \ldots(2.51)$$

From Eqs. (2.50) and (2.51) it is clearly evident that nuclear matter properties like energy per particle, chemical potentials, pressure, incompressibility and speed of sound in both SNM and ANM are determined by the behaviour of isoscalar and isovector parts of nuclear mean field at the Fermi momentum $k = k_f$ and follow in a trivial way once the density dependence of nuclear symmetry energy $J_\tau(\rho)$ and energy per particle $e(\rho)$ in SNM are fixed. In view of this, different EOS of ANM sharing the same density dependence of $e(\rho)$ and $J_\tau(\rho)$ but having quite different momentum dependence of the functionals $u_\tau(k, \rho)$ and $u_\tau^{ex}(k, \rho)$ will lead to almost the same results for properties like energy per particle, chemical potentials, pressure and incompressibility in both SNM and ANM. However, these different EOS can give rise to significantly different predictions on experimental observables sensitive to the differences between neutron and proton flow data in highly asymmetric dense nuclear matter. The whole problem now divides naturally into two parts:

1. momentum and density dependence of the functionals $u_\tau(k, \rho)$ and $u_\tau^{ex}(k, \rho)$
2. density dependence of $e(\rho)$ and $J_\tau(\rho)$.

Since in chapter 1 we have already discussed some properties of these functionals in detail we give an outline of our present knowledge of these functionals which determine the EOS of nuclear matter in the next section.

2.6. Discussion

As discussed in chapter 1 in the past couple of decades intensive theoretical and experimental study has been done on the momentum and density dependence of isoscalar part of nuclear mean field. Now the momentum dependence of isoscalar part of nuclear mean field $u(k, \rho)$ is well established and experimental observables provide significant constraints on the momentum and density dependence of $u(k, \rho)$ [3,114].

On the other hand, the momentum and density dependence of isovector part of nuclear mean field is poorly known. Different theoretical calculations predict quite different and even contradicting results. The extremely divergent and even contradicting behaviour of isovector part of nuclear mean field $u_\tau(k, \rho)$ with momentum as predicted by different theoretical calculations is exhibited for Skyrme and Gogny effective interactions.

The functional $u_\tau^{ex}(k, \rho)$ which determines the momentum dependence of isovector part of nuclear mean field can be calculated analytically for Gogny effective interactions and the result is given by

$$u_\tau^{ex}(k,\rho) = -\frac{1}{3\pi^{1/2}} \sum_{i=1,2} \left(\frac{W_i}{2} + B_i\right) \left[\frac{x_i^2}{z_i} \left\{ \exp[-(z_i - x_i)^2/4] - \exp[-(z_i + x_i)^2/4] \right\} - x_i(1 - e^{-x_i^2}) \right] \quad \ldots(2.52)$$

where $z_i = \alpha_i k_i$, $x_i = \alpha_i k_f$ and α_i, W_i, B_i are the parameters of the Gogny interaction.

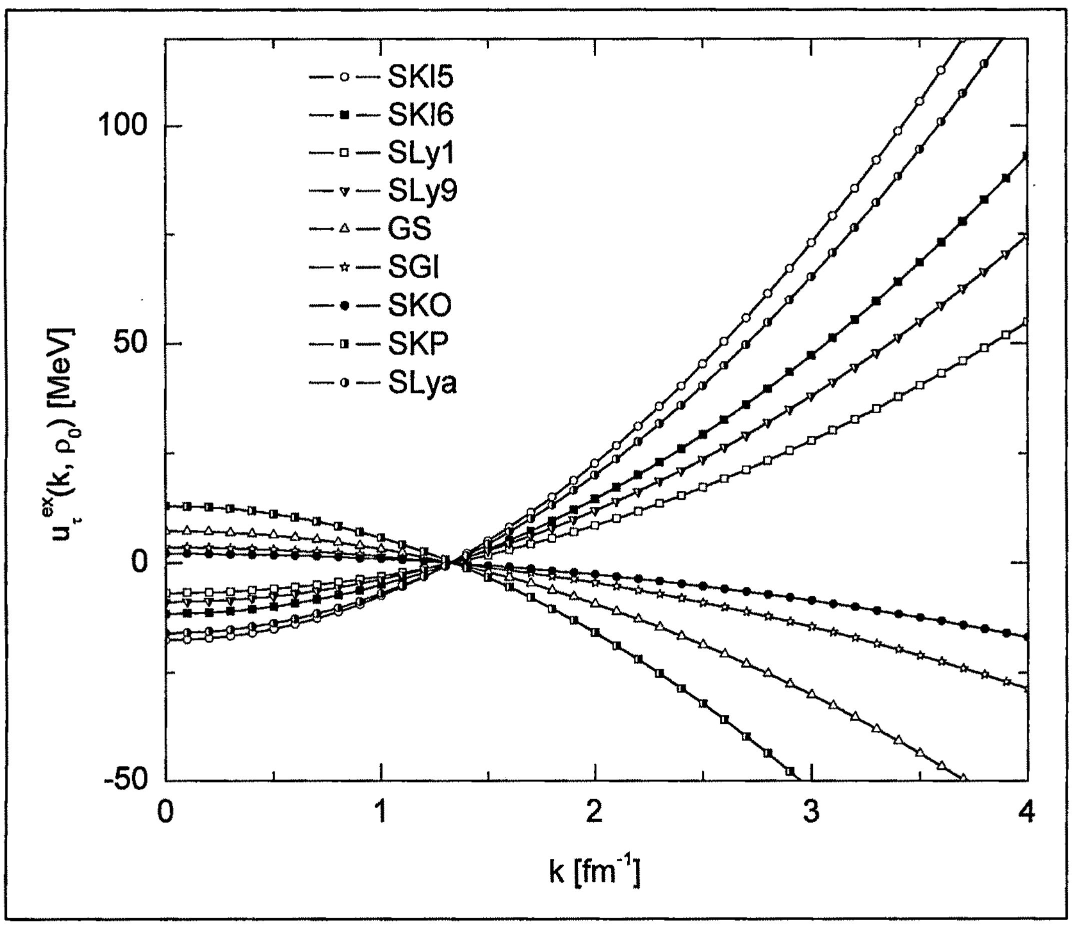

Figure 2.1: Momentum dependence of the functional $u_\tau^{ex}(k, \rho_0)$ for Skyrme parametrisations.

For the Skyrme parametrization $u_\tau^{ex}(k, \rho)$ has a very simple form,

$$u_\tau^{ex}(k,\rho)=\frac{1}{16}\left[t_2(2x_2+1)-t_1(2x_1+1)\right](k^2-k_f^2)\rho \qquad \text{...(2.53)}$$

Eqns. (2.52) and (2.53) clearly exhibit the difference in the high momentum behaviour of $u_\tau^{ex}(k, \rho)$ for Skyrme and Gogny type effective interactions. While for Skyrme parametrization $u_\tau^{ex}(k, \rho)$ either increases or decreases monotonically with increase in k, it approaches a definite value

$$u_\tau^{ex}(k\to\infty,\rho)=\frac{1}{3\pi^{1/2}}\sum_{i=1,2}\left(\frac{W_i}{2}+B_i\right)x_i\left(1-e^{-x_i^2}\right) \qquad \text{...(2.54)}$$

in the limit of $k\to\infty$ for Gogny parametrizations.

In Fig. 2.1 the extremely divergent and even contradicting behaviour of $u_\tau^{ex}(k, \rho_0)$ with momentum is shown as a function of momentum k at normal density ρ_0 for nine different Skyrme parametrizations [19, references therein] SKI5, SKI6, SLy1, SLy9, SLy-a, GS, SGI, SKO and SKP. While $u_\tau^{ex}(k, \rho_0)$ increases monotonically for the Skyrme interactions SKI5, SKI6, SLy1, SLy9 and SLy-a it decreases monotonically for GS, SGI, SKO and SKP with increase in momentum.

In Fig. 2.2 the momentum dependence of $u_\tau^{ex}(k, \rho_0)$ is shown for six different Gogny interactions [141] DIS, D260, D250, D280, D300 and D1. The Gogny interactions D260, D280, D300 and D1 exhibit a decreasing trend with increase in momentum and for large k approach a definite negative value depending on the interaction considered. The variation of $u_\tau^{ex}(k, \rho_0)$ with momentum for the Gogny interaction DIS and D250 is rather different from the other interactions shown in Fig. 2.2. In these cases $u_\tau^{ex}(k, \rho_0)$ gradually decreases with increase in k, becomes negative and attains a minimum value and then gradually increases with further increase in k and approaches a value, depending on the interaction considered, in the limit of $k\to\infty$.

It is important to note that a decreasing trend of momentum dependence of the isovector part of nuclear mean field corresponds to neutron effective mass being greater than proton effective mass whereas an increasing trend corresponds to the other way around.

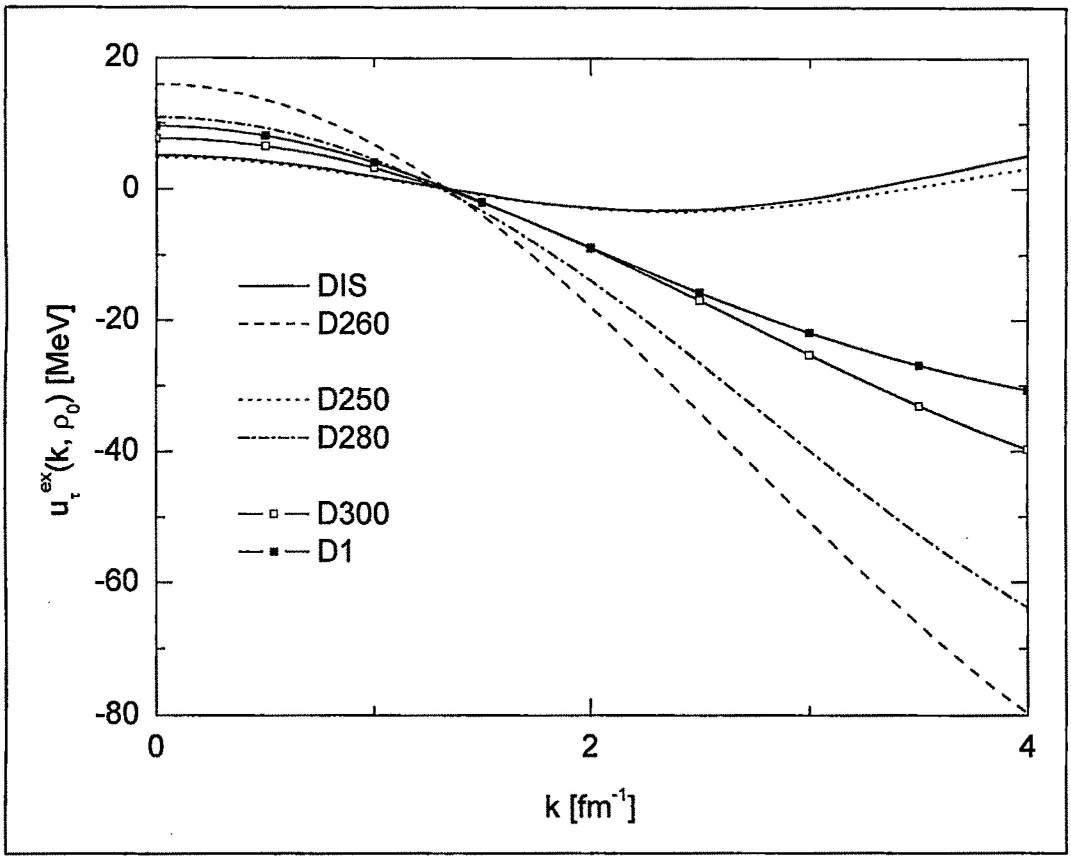

Figure 2.2: Momentum dependence of the functional $u_\tau^{ex}(k, \rho_0)$ for Gogny interactions.

The density dependence of energy per particle $e(\rho)$ in SNM is usually described in terms of the equilibrium density ρ_0, energy per particle $e(\rho_0)$ at this density and the stiffness parameter $\rho de(\rho)/d\rho$ related to pressure in SNM. The values of equilibrium density or saturation density ρ_0 and energy per particle $e(\rho_0)$ at this density are known within a good precision from experimental/empirical data. The value of $e(\rho_0)$, determined from liquid drop model fits on the binding energies of a large number of nuclei is $e(\rho_0) = -(16 \pm 0.2)\ MeV$ (excluding rest mass energy) [17]. The saturation density or the normal nuclear matter density ρ_0 is expected to be $\rho_0 = 0.16 \pm 0.005\ fm^{-3}$ based on calculating the charge distribution in heavy nuclei. However, the value of the stiffness parameter is not known precisely. Recent analysis of nucleon flow data in high energy heavy-ion collisions performed at National Superconducting Cyclotron Laboratory (NSCL) have been able to constrain the stiffness parameter upto some extent [3]. The value of nuclear incompressibility $K(\rho_0)$ in SNM at normal nuclear matter density ρ_0, which is related to the stiffness parameter, is also not known precisely. The value of $K(\rho_0)$ is model dependent and different theoretical calculations give the value of $K(\rho_0)$ in the range 200 – 240 MeV [21,22].

On the other hand, there are no experimental/empirical constraints on the high density behaviour of nuclear symmetry energy $J_\tau(\rho)$ [3]. The high density behaviour of $J_\tau(\rho)$ predicted by different theoretical calculations is rather extremely divergent and even contradicting [27-28]. In fact, even the sign of the symmetry energy above a density $3\rho_0$ is still very uncertain [31]. Analysis of the differences between neutron and proton flow data in high energy heavy-ion collisions have yet to pin down the high density behaviour of $J_\tau(\rho)$ [27-33]. The only constraint available is the value of nuclear symmetry energy $J_\tau(\rho_0)$ at normal nuclear matter density ρ_0. The value of $J_\tau(\rho_0)$ calculated from liquid drop mass formula is ≈ 30 MeV [131]. However, different theoretical calculations which give a good account of EOS of SNM predict the value of $J_\tau(\rho_0)$ in the range 24 to 40 MeV.

2.7. Summary

In this chapter we constructed the EOS of asymmetric nuclear matter at temperature T ($T \neq 0$) and at zero temperature ($T = 0$) for a general effective interaction. It was shown that in the study of EOS of nuclear matter the more important quantity is the difference between neutron and proton mean fields $u_T^{n-p}(k,\rho,Y_p)$. To study the momentum dependence of $u_T^{n-p}(k,\rho,Y_p)$, the functional $\frac{M}{\hbar^2 k}\frac{\partial u_T^{n-p}(k,\rho,Y_p)}{\partial k}$ was introduced which is directly connected to neutron and proton effective mass splitting. In fact the sign of the functional $\frac{M}{\hbar^2 k}\frac{\partial u_T^{n-p}(k,\rho,Y_p)}{\partial k}$ determines whether neutron effective mass is greater than proton effective mass or the vice versa. It was shown that the sign of the functional $\frac{M}{\hbar^2 k}\frac{\partial u_T^{n-p}(k,\rho,Y_p)}{\partial k}$ and as a result the sign of the splitting of neutron and proton effective masses depends on the parameters of the interaction. This was shown for popular parametrisations of Skyrme and Gogny interactions.

To study the momentum and density dependence of nuclear mean field the isoscalar and isovector parts of nuclear mean field $u(k, \rho)$ and $u_\tau(k, \rho)$, respectively, were defined for a general phenomenological effective interaction. The behaviour of $u_\tau(k, \rho)$ and $u(k, \rho)$ around Fermi momentum $k = k_f$ were found to be connected to the density dependence of nuclear symmetry energy $J_\tau(\rho)$ and energy per particle $e(\rho)$ in SNM respectively. The momentum dependence of $u_\tau(k, \rho)$ and $u(k, \rho)$ were separated out in terms of simple functionals $u_\tau^{ex}(k, \rho)$ and $u^{ex}(k, \rho)$ which vanish at the Fermi momentum $k = k_f$ and involves only the finite range parts of the exchange interactions between like and unlike nucleons. The existing uncertainty in the value of nuclear symmetry energy $J_\tau(\rho)$ even at normal nuclear matter density was discussed. The conflicting behaviour of the functional $u_\tau^{ex}(k, \rho)$ predicted by different theoretical models was shown for the Skyrme and Gogny effective interactions with several parameter sets.

In this chapter it was seen that to study the momentum dependence of isoscalar and isovector part of nuclear mean field we need the knowledge of only the exchange part of the effective interaction. However, to study the density dependence of the isovector and isoscalar part of nuclear mean field at densities other than the normal nuclear matter density ρ_0 we require the knowledge of not only the exchange part of the interaction but also the direct part of the interaction. Further, to study the momentum and density dependence of neutron and proton mean fields, density dependence of nuclear symmetry energy and properties of nuclear matter also we need the full form of the interaction.

In view of this in the next chapter we have built a simple density dependent short range effective interaction of conventional form to study the density and momentum dependence of nuclear mean field, the density dependence of nuclear symmetry energy and properties of nuclear matter.

CHAPTER 3

NUCLEAR EQUATION OF STATE AND THE PROPERTIES OF NUCLEAR MATTER FOR A SIMPLE SHORT RANGE EFFECTIVE INTERACTION

3.1. Introduction

In chapter 2 we observed that a general finite range interaction can simulate the momentum and density dependence of nuclear mean fields and analyse the nuclear equation of state (EOS). In view of this we have chosen a simple density dependent finite range effective interaction of conventional form, such as Yukawa, Gaussian or exponential, which was successfully used by Behera, *et al.* [108] to simulate the momentum dependence of mean field in symmetric nuclear matter (SNM) and study EOS of SNM. We will use this interaction to analyze the EOS of nuclear matter, especially the EOS of ANM and neutron star matter.

The simple density dependent finite range effective interaction is given as

$$v_{eff}(r) = t_0(1+x_0P_\sigma)\delta(r) + \frac{t_3}{6}(1+x_3P_\sigma)\left[\frac{\rho(R)}{1+b\rho(R)}\right]^\gamma \delta(r) + (W + BP_\sigma - HP_\tau - MP_\sigma P_\tau)f(r) \quad \ldots(3.1)$$

In the above equation t_0, t_3, x_0, x_3, b, γ, W, B, H and M are the parameters of the interaction. P_σ and P_τ are the Pauli spin and isospin operators, respectively and $\delta(r)$ is the Dirac delta function. In Eq. (3.1) the first term is independent of density while the second term takes the density dependence aspect of the interaction into account. The third term contains the short range interaction $f(r)$ of conventional forms, such as Yukawa, Gaussian or exponential specified by a single parameter α, the range of the interaction. In this thesis work we have used only the Yukawa form for the short range interaction $f(r)$. For Yukawa form $f(r)$ is given as

$$f(r) = \frac{e^{-r/\alpha}}{r/\alpha}. \qquad \ldots(3.2)$$

where α is the range of the interaction.

This interaction is very similar to Skyrme–type interactions except for two differences. The first one is the short–range interaction $(W + BP_\sigma - HP_\tau - MP_\sigma P_\tau) f(r)$ in place of the t_1 and t_2 terms in Skyrme–type interactions. This replacement is necessary to provide a description leading to vanishing attractive interaction between nucleons of very large relative momenta, an important feature for the successful interpretation of heavy–ion collision data at intermediate and high energies. The second modification is the denominator in the density dependent term of the effective interaction which is necessary to prevent the supraluminous behaviour of nuclear matter at very high density [144].

A major advantage of using this simple finite range effective interaction is that it leads to analytical calculations of all zero–temperature nuclear matter properties with a minimum number of adjustable parameters, as we will see in the subsequent sections, although the results are not simple. Behera *et al.* [108] have used this interaction to study the properties of SNM at wide range of densities and temperature. It was shown that the SNM properties such as energy density, pressure, chemical potential and incompressibility calculated with different functional forms of the effective interaction are almost same over a wide range of density and temperature. However, the functional form of the finite range part of the interaction was shown to be important in determining the high momentum behaviour of the nuclear mean field in SNM. At higher momenta the exchange part of mean field in SNM was found to be more repulsive for Yukawa form of short range interaction than the Gaussian one. On comparing the results of exchange part of nuclear mean field in SNM using Yukawa form of short range part with those obtained by Wiringa [40] it was found that both the results are quite similar over a wide range of momenta and densities for the realistic Hamiltonians considered in ref. [40], in particular with the Hamiltonian UV14+UVII. It should be mentioned here that the momentum and density dependence of single particle potential for the interaction UV14+UVII agree well with those extracted from analysis of elliptic flow data in HI collisions [114].

In this chapter we have considered a simple density dependent effective interaction given in Eq. (3.1) with short range part having Yukawa form. The nucleon mean fields and the EOS of asymmetric nuclear matter at zero temperature (T = 0) has been constructed using this interaction in section 3.2. Since SNM and PNM constitute the two boundaries of ANM in section 3.3 we have constructed the EOS of SNM and PNM. In section 3.4 we have determined the interaction parameters involved in the EOS of SNM and PNM. The variation of pressure with density in SNM and PNM has been discussed in the same section. In section 3.5 we have calculated the effective nucleon mass and the isovector part of nuclear mean fields. The two types of behaviour of isovector part of nuclear mean fields and effective nucleon masses, as discussed in chapter 2, has been analysed over a wide range of momentum and density for different parameter sets. In section 3.6 we have analysed the high density behaviour of nuclear symmetry energy using the parameters obtained in section 3.4. The slope and curvature parameters of nuclear symmetry energy around normal nuclear matter density have also been calculated in this section. Properties of nuclear matter such as energy per particle, pressure, chemical potential, incompressibility and velocity of sound in nuclear medium has been calculated in section 3.7. In section 3.8 we have given a brief summary of this chapter.

3.2. EOS of ANM at zero temperature for the simple short range interaction

In chapter 2 the EOS of ANM for a general effective interaction was constructed using four different effective interactions, $v_d^l(r)$, $v_d^{ul}(r)$, $v_{ex}^l(r)$ and $v_{ex}^{ul}(r)$. For the simple effective interaction used here, these four different interactions can be expressed as

$$v_d^l(r) = \frac{t_0}{4}(1-x_0)\delta(r) + \frac{t_3}{24}(1-x_3)\rho^\gamma\delta(r) + \left(W + \frac{B}{2} - H - \frac{M}{2}\right)f(r) \quad \ldots(3.3)$$

$$v_d^{ul}(r) = \frac{t_0}{4}(2+x_0)\delta(r) + \frac{t_3}{24}(2+x_3)\rho^\gamma\delta(r) + \left(W + \frac{B}{2}\right)f(r) \quad \ldots(3.4)$$

$$v_{ex}^l(r) = \frac{t_0}{4}(1-x_0)\delta(r) + \frac{t_3}{24}(1-x_3)\rho^\gamma\delta(r) + \left(M + \frac{H}{2} - B - \frac{W}{2}\right)f(r) \quad \ldots(3.5)$$

$$v_{ex}^{ul}(r)=\frac{t_0}{4}(2+x_0)\delta(r)+\frac{t_3}{24}(2+x_3)\rho^{\gamma}\delta(r)+\left(M+\frac{H}{2}\right)f(r). \qquad ...(3.6)$$

Using these four equations and the EOS of ANM at zero temperature as given in chapter 2 for a general finite range effective interaction we have constructed the EOS of ANM at zero temperature for the simple density dependent short range interaction given in Eq. (3.1).

The energy density $H(\rho_n, \rho_p)$ in ANM at zero temperature which was given in Eq. (2.19) for a general effective interaction can now be derived for the simple short range effective interaction given in Eq. (3.1) and is expressed as

$$H(\rho_n,\rho_p)=\frac{3Mc^2}{8}\sum_{i=n,p}\frac{\rho_i}{x_i^3}\left[2x_iu_i^3-x_iu_i-\ln(x_i+u_i)\right]$$
$$+\frac{1}{2}\left[\frac{\varepsilon_0^l}{\rho_0}+\frac{\varepsilon_\gamma^l}{\rho_0^{\gamma+1}}\left(\frac{\rho}{1+b\rho}\right)^{\gamma}\right](\rho_n^2+\rho_p^2)+\left[\frac{\varepsilon_0^{ul}}{\rho_0}+\frac{\varepsilon_\gamma^{ul}}{\rho_0^{\gamma+1}}\left(\frac{\rho}{1+b\rho}\right)^{\gamma}\right]\rho_n\rho_p$$
$$+\frac{\varepsilon_{ex}^l\rho_n^2}{2\rho_0}J_\alpha(\rho_n)+\frac{\varepsilon_{ex}^{ul}\rho_p^2}{2\rho_0}J_\alpha(\rho_p)+\frac{9\varepsilon_{ex}^{ul}\rho_n\rho_p}{\rho_0\int f(r)d^3r}\int\frac{j_1(k_nr)}{k_nr}\frac{j_1(k_pr)}{k_pr}f(r)d^3r$$

$$...(3.7)$$

where $$J_\alpha(\rho_i)=\frac{9}{\int f(r)d^3r}\int\frac{j_1^{\,2}(k_ir)}{(k_ir)^2}f(r)d^3r,\; i=n,\ p \qquad ...(3.8)$$

In Eq. (3.7) $\varepsilon_0^{\,l}$, $\varepsilon_0^{\,ul}$, $\varepsilon_\gamma^{\,l}$, $\varepsilon_\gamma^{\,ul}$, $\varepsilon_{ex}^{\,l}$ and $\varepsilon_{ex}^{\,ul}$ are the strength parameters for interactions between like (*l*) and unlike (*ul*) nucleons related to the interaction parameters through the relations given below,

$$\varepsilon_0^l=\rho_0\left[\frac{t_0}{2}(1-x_0)+\left(W+\frac{B}{2}-H-\frac{M}{2}\right)\int f(r)d^3r\right] \qquad ...(3.9)$$

$$\varepsilon_\gamma^l=\frac{t_3}{12}(1-x_3)\rho_0^{\gamma+1} \qquad ...(3.10)$$

$$\varepsilon_{ex}^l=\rho_0\left[\left(M+\frac{H}{2}-B-\frac{W}{2}\right)\int f(r)d^3r\right] \qquad ...(3.11)$$

$$\varepsilon_0^{ul}=\rho_0\left[\frac{t_0}{2}(2+x_0)+\left(W+\frac{B}{2}\right)\int f(r)d^3r\right] \qquad ...(3.12)$$

$$\varepsilon_\gamma^{ul}=\frac{t_3}{12}(2+x_3)\rho_0^{\gamma+1} \qquad ...(3.13)$$

and $$\varepsilon_{ex}^{ul} = \rho_0\left[\left(M+\frac{H}{2}\right)\int f(r)d^3r\right]. \qquad ...(3.14)$$

The neutron and proton mean fields $u^n(k, \rho_n, \rho_p)$ and $u^p(k, \rho_n, \rho_p)$ at zero temperature can be given as

$$u^n(k,\rho_n,\rho_p) = \varepsilon_0^l\frac{\rho_n}{\rho_0}+\varepsilon_0^{ul}\frac{\rho_p}{\rho_0}+\frac{\varepsilon_\gamma^l}{\rho_0^{\gamma+1}}\left(\frac{\rho}{1+b\rho}\right)^\gamma\rho_n+\frac{\varepsilon_\gamma^{ul}}{\rho_0^{\gamma+1}}\left(\frac{\rho}{1+b\rho}\right)^\gamma\rho_p$$
$$+\frac{1}{2}\frac{\varepsilon_\gamma^l}{\rho_0^{\gamma+1}}\frac{\gamma\rho^{\gamma-1}}{(1+b\rho)^{\gamma+1}}(\rho_n^2+\rho_p^2)+\frac{\varepsilon_\gamma^{ul}}{\rho_0^{\gamma+1}}\frac{\gamma\rho^{\gamma-1}}{(1+b\rho)^{\gamma+1}}\rho_n\rho_p \qquad ...(3.15)$$
$$+\frac{\varepsilon_{ex}^l}{\rho_0}\rho_n I_\alpha(k,\rho_n)+\frac{\varepsilon_{ex}^{ul}}{\rho_0}\rho_p I_\alpha(k,\rho_p)$$

$$u^p(k,\rho_n,\rho_p) = \varepsilon_0^l\frac{\rho_p}{\rho_0}+\varepsilon_0^{ul}\frac{\rho_n}{\rho_0}+\frac{\varepsilon_\gamma^l}{\rho_0^{\gamma+1}}\left(\frac{\rho}{1+b\rho}\right)^\gamma\rho_p+\frac{\varepsilon_\gamma^{ul}}{\rho_0^{\gamma+1}}\left(\frac{\rho}{1+b\rho}\right)^\gamma\rho_n$$
$$+\frac{1}{2}\frac{\varepsilon_\gamma^l}{\rho_0^{\gamma+1}}\frac{\gamma\rho^{\gamma-1}}{(1+b\rho)^{\gamma+1}}(\rho_n^2+\rho_p^2)+\frac{\varepsilon_\gamma^{ul}}{\rho_0^{\gamma+1}}\frac{\gamma\rho^{\gamma-1}}{(1+b\rho)^{\gamma+1}}\rho_n\rho_p \qquad ...(3.16)$$
$$+\frac{\varepsilon_{ex}^l}{\rho_0}\rho_p I_\alpha(k,\rho_p)+\frac{\varepsilon_{ex}^{ul}}{\rho_0}\rho_n I_\alpha(k,\rho_n)$$

where $$I_\alpha(k,\rho_i) = \frac{3}{\int f(r)d^3r}\int j_0(kr)\frac{j_1(k_i r)}{k_i r}f(r)d^3r\ ,\ i=n,p \qquad ...(3.17)$$

It should be mentioned here that the functional $J_\alpha(k, \rho_i)$ and $I_\alpha(k, \rho_i)$ given in Eqs. (3.8) and (3.17) can be solved analytically for Yukawa form of $f(r)$ [107].

The pressure $P(\rho_n, \rho_p)$ in ANM at zero temperature is defined as

$$P(\rho_n,\rho_p) = \rho_n\mu^n+\rho_p\mu^p-H(\rho_n,\rho_p) \qquad ...(3.18)$$

where the neutron and proton chemical potentials $\mu^{n,p}(\rho_n, \rho_p)$ in ANM at zero temperature are defined as

$$\mu^{n,p}(\rho_n,\rho_p) = \frac{\partial H(\rho_n,\rho_p)}{\partial\rho_{n,p}} \qquad ...(3.19)$$

The nuclear symmetry energy $J_\tau(\rho)$ can be derived from the expression of energy density functional $H(\rho_n, \rho_p)$ given in Eq. (3.7) and is given as

$$J_\tau(\rho) = \frac{Mc^2}{6}\frac{x_f^2}{u_f} + \frac{\rho(\varepsilon_0^l - \varepsilon_0^{ul})}{4\rho_0} + \frac{\rho^{\gamma+1}(\varepsilon_\gamma^l - \varepsilon_\gamma^{ul})}{4\rho_0^{\gamma+1}}$$
$$+ \frac{\rho(\varepsilon_{ex}^l - \varepsilon_{ex}^{ul})}{4\rho_0 \int f(r)d^3r}\int j_0^2(k_f r) f(r) d^3r - \frac{\rho(\varepsilon_{ex}^l + \varepsilon_{ex}^{ul})}{4\rho_0 \int f(r)d^3r}\int j_1^2(k_f r) f(r) d^3r$$

...(3.20)

The incompressibility $K(\rho_n, \rho_p)$ at zero temperature is expressed as

$$K(\rho_n,\rho_p) = \frac{9}{\rho}\left(\rho_n\frac{\partial P(\rho_n,\rho_p)}{\partial\rho_n} + \rho_p\frac{\partial P(\rho_n,\rho_p)}{\partial\rho_p}\right) = 9\frac{\partial P(\rho_n,\rho_p)}{\partial\rho}. \quad ...(3.21)$$

The speed of sound in nuclear medium is defined as

$$\frac{v^2}{c^2} = \frac{\partial P(\rho)}{\partial H(\rho)} \quad ...(3.22)$$

It should be mentioned here that speed of sound in nuclear matter should never be greater than velocity of light. However, some models predict speed of sound to be greater than that of light at very high density. This phenomenon called the supraluminosity should always be prevented.

3.2.1. Empirical parabolic law for EOS of ANM

Assuming charge symmetry in nuclear interactions ($v^{nn} = v^{pp}$) the energy density $H(\rho_n, \rho_p)$ of ANM can be expanded into a Taylor series about $\sigma = 0$ ($Y_p=1/2$) and is given as

$$H(\rho_n,\rho_p) = H(\rho) + \frac{\sigma^2}{2!4}\left[\frac{\partial^2 H(\rho_n,\rho_p)}{\partial\sigma^2}\right]_{\sigma=0} + \frac{\sigma^4}{4!16}\left[\frac{\partial^4 H(\rho_n,\rho_p)}{\partial\sigma^4}\right]_{\sigma=0} + \ldots..$$

...(3.23)

Neglecting terms with higer order powers of σ than the second order power the energy density $H(\rho_n, \rho_p)$ is very often written as

$$H(\rho_n,\rho_p) = H(\rho) + \sigma^2\rho J_\tau(\rho) \quad ...(3.24)$$

where $H(\rho)$ is the energy density in SNM and $J_\tau(\rho)$ is the nuclear symmetry energy. The above equation is called empirical parabolic law for EOS of ANM and this quadratic form of EOS is frequently used in many nuclear calculations.

The difference in neutron and proton chemical potentials $[\mu^n(\rho_n, \rho_p)-\mu^p(\rho_n, \rho_p)]$ which is a crucial input in the calculation of proton fraction in beta–stable matter can be approximated using this quadratic form of energy density as

$$\left[\mu^n(\rho_n,\rho_p)-\mu^p(\rho_n,\rho_p)\right]=4\sigma J_\tau(\rho) \qquad \text{...(3.25)}$$

The pressure $P(\rho_n, \rho_p)$ and the nuclear matter incompressibility $K(\rho_n, \rho_p)$ in ANM can also be approximated as

$$P(\rho_n,\rho_p)=\rho\frac{dH(\rho)}{d\rho}+\sigma^2\rho^2\frac{dJ_\tau(\rho)}{d\rho}-H(\rho) \qquad \text{...(3.26)}$$

$$K(\rho_n,\rho_p)=9\rho\left[\frac{d^2H(\rho)}{d\rho^2}+2\sigma^2\frac{dJ_\tau(\rho)}{d\rho}+\sigma^2\rho\frac{d^2J_\tau(\rho)}{d\rho^2}\right] \qquad \text{...(3.27)}$$

3.3 EOS of SNM and PNM

3.3.1. EOS of SNM

In symmetric nuclear matter (SNM) the energy per particle $e(\rho)$ and the mean field $u(k, \rho)$ can be derived from Eqs. (2.45) and (2.41) for the simple effective interaction given in Eq. (3.1) as

$$e(\rho)=\frac{3mc^2}{8x_f^3}[2x_f u_f^3-x_f u_f-\ln(x_f+u_f)]+\frac{\varepsilon_0}{2}\frac{\rho}{\rho_0}+\frac{\varepsilon_\gamma}{2\rho_0^{\gamma+1}}\left(\frac{\rho}{1+b\rho}\right)^\gamma\rho+\frac{\varepsilon_{ex}\rho}{2\rho_0}J_\alpha(\rho) \qquad \text{...(3.28)}$$

and $$u(k,\rho)=\varepsilon_0\frac{\rho}{\rho_0}+\frac{\varepsilon_\gamma}{\rho_0^{\gamma+1}}\left(\frac{\rho}{1+b\rho}\right)^{\gamma+1}(1+b\rho+\frac{\gamma}{2})+\frac{\varepsilon_{ex}\rho}{\rho_0}I_\alpha(k,\rho) \qquad \text{...(3.29)}$$

where $x_f=\frac{\hbar k_f}{Mc}$, $u_f=(1+x_f^2)^{1/2}$, $k_f=(3\pi^2\rho/2)^{1/3}$; $J_\alpha(\rho)$ and $I_\alpha(k, \rho)$ can be obtained from Eqs. (3.8) and (3.17) respectively.

The strength parameters ε_0, ε_γ and ε_{ex} required to describe the EOS of SNM satisfy the conditions

$$\varepsilon_0^l+\varepsilon_0^{ul}=2\varepsilon_0 \;;\quad \varepsilon_\gamma^l+\varepsilon_\gamma^{ul}=2\varepsilon_\gamma \quad \text{and} \quad \varepsilon_{ex}^l+\varepsilon_{ex}^{ul}=2\varepsilon_{ex}. \qquad \text{...(3.30)}$$

The pressure $P(\rho)$ in SNM can be calculated from the following relations.

$$P(\rho)=\rho^2\frac{de(\rho)}{d\rho}=\rho\,\mu(\rho)-H(\rho) \qquad \text{...(3.31)}$$

where $H(\rho)$ is the energy density and $\mu(\rho)$ is the chemical potential of SNM given as

$$H(\rho) = \rho\, e(\rho) \quad \text{and} \quad \mu(\rho) = dH(\rho)/d\rho. \qquad \ldots(3.32)$$

The nuclear incompressibility $K(\rho)$ in SNM and the speed of sound in nuclear medium is defined as

$$K(\rho) = 9\frac{dP(\rho)}{d\rho} = 18\rho\frac{de(\rho)}{d\rho} + 9\rho^2\frac{d^2e(\rho)}{d\rho^2} \qquad \ldots(3.33)$$

and $$\frac{v^2}{c^2} = \frac{dP(\rho)}{dH(\rho)} \qquad \ldots(3.34)$$

3.3.2. EOS of PNM

The energy per particle $e^n(\rho)$ and mean field $u^n(k, \rho)$ in zero–temperature PNM can be written as

$$e^n(\rho) = \frac{3Mc^2}{8x_n^3}[2x_n u_n^3 - x_n u_n - \ln(x_n + u_n)] + \frac{\varepsilon_0^l}{2}\frac{\rho}{\rho_0} + \frac{\varepsilon_\gamma^l}{2\rho_0^{\gamma+1}}\left(\frac{\rho}{1+b\rho}\right)^\gamma \rho + \frac{\varepsilon_{ex}^l \rho}{2\rho_0} J_\alpha(\rho) \qquad \ldots(3.35)$$

and $$u^n(k,\rho) = \varepsilon_0^l\frac{\rho}{\rho_0} + \frac{\varepsilon_\gamma^l}{\rho_0^{\gamma+1}}\left(\frac{\rho}{1+b\rho}\right)^{\gamma+1}(1 + b\rho + \frac{\gamma}{2}) + \frac{\varepsilon_{ex}^l \rho}{\rho_0} I_\alpha(k,\rho) \qquad \ldots(3.36)$$

where $x_n = \frac{\hbar k_n}{Mc}$, $u_n = (1 + x_n^2)^{1/2}$ and $k_n = (3\pi^2\rho)^{1/3}$.

The pressure in zero temperature PNM is given by the relation

$$P^n(\rho) = \rho^2\frac{de^n(\rho)}{d\rho} \qquad \ldots(3.37)$$

3.4. Determination of interaction parameters

From Eq. (3.7) it can be observed that to describe the EOS of ANM for a simple density dependent finite range effective interaction given in Eq. (3.1) we need to determine nine adjustable interaction parameters, namely, γ, b, α, ε_0^l, ε_γ^l, ε_{ex}^l, ε_0^{ul}, ε_γ^{ul} and ε_{ex}^{ul}. From the definition of energy density in ANM given in Eq. (3.7) and from the relation between exchange strength parameters given in Eq. (3.30) it is quite evident that a complete description of EOS of ANM is equivalent to separate description of EOS of SNM and PNM. Hence to determine these nine interaction parameters required to describe the EOS of ANM we will determine the parameters involved in the EOS of SNM and PNM from simple physical conditions and available empirical/experimental data.

3.4.1. Adjustment of parameters involved in EOS of SNM

As seen from section 3.3.1 we require altogether six adjustable parameters namely ε_0, ε_γ, γ, b, ε_{ex} and α to describe the EOS of SNM completely. To start with we have used the values of exchange strength parameters ε_{ex} and the range parameter α as given in ref. [108] for Yukawa form of the interaction. In ref. [108] the parameters α and ε_{ex} have been determined by an optimization procedure requiring to give a reasonable account of momentum dependence of the zero–temperature mean field in SNM at normal density ρ_0 over a wide range of momentum as demanded by optical model fits to nucleon–nucleus scattering data [138, 139] at intermediate energies. The values of the two parameters ε_{ex} and α for the Yukawa form of the exchange interaction are $\varepsilon_{ex} = -121.8\ MeV$ and $\alpha = 0.4044\ fm$ which gives an effective nucleon mass $M^*(k = k_{f0}, \rho_0)/M = 0.67$ at the Fermi surface corresponding to normal nuclear matter density ρ_0. It should be mentioned here that we have used standard values of $Mc^2 = 939\ MeV$, $e(\rho_0) = 923\ MeV$ and $(c^2\hbar^2 k_{f_0}^2 + M^2c^4)^{1/2} = 976\ MeV$ (corresponding to $\rho_0 = 0.1658\ fm^{-3}$) in this thesis work.

In this work we have kept the value of the parameter γ open. For a particular value of γ we have calculated the remaining three parameters b, ε_0 and ε_γ. The parameter b appearing in the density dependent part of the interaction is constrained by requiring to prevent the supraluminous behaviour of zero temperature SNM at high densities. An approximate result [144] can be obtained in the form

$$b\rho_0 \geq \left\{ \left[\frac{Mc^2}{S_{f_0} - e(\rho_0)} \right]^{\frac{1}{\gamma+1}} - 1 \right\}^{-1}, \qquad \ldots(3.38)$$

where
$$S_{f_0} = \left\{ \frac{Mc^2}{4x_f^3} [3x_f u_f + 2x_f^3 u_f - 3\ln(x_f + u_f)] \right\}_{\rho=\rho_0}. \qquad \ldots(3.39)$$

Since density dependence of the form ρ^γ have been very successful in predicting binding energies and radii of many nuclei, we take the lower limit of $b\rho_0$ in the above inequality.

To determine the remaining two parameters, we express the parameters ε_0 and ε_γ in terms of $e(\rho_0)$ and $\rho de(\rho)/d\rho|_{\rho=\rho 0}$ using Eqs. (3.28) and (3.31). Then we use the saturation conditions of symmetric nuclear matter

$$e(\rho_0) = 923\ MeV \qquad \text{and} \qquad \rho de(\rho)/d\rho|_{\rho=\rho 0} = 0$$

to solve the two equations and get the parameters ε_0 and ε_γ.

Following the above procedure we have calculated values for b, ε_0 and ε_γ for different values of γ. The parameter γ which determines the stiffness of the EOS of SNM at high densities can be constrained by using the pressure–density relationship extracted from analysis of flow data in high energy HI collisions [3].

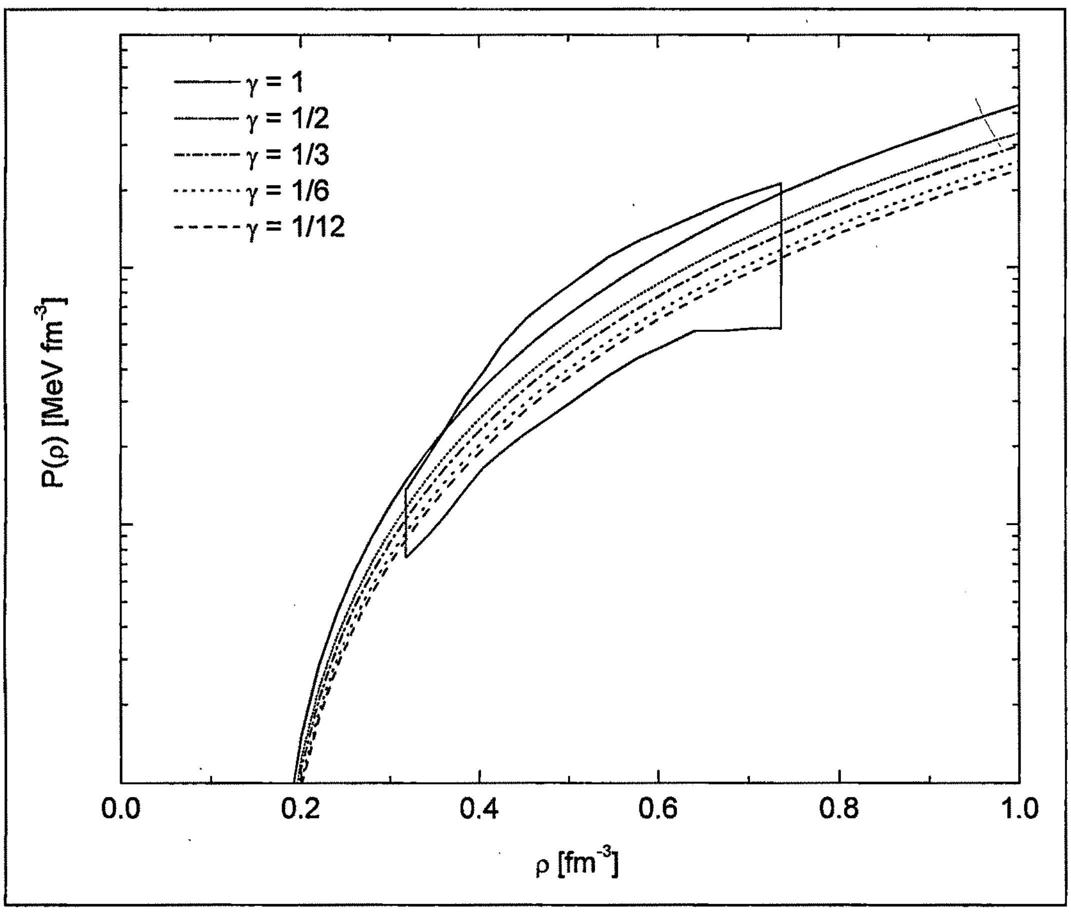

Figure 3.1: Pressure–density relationship for five different EOS of SNM with γ = 1/12, 1/6, 1/3, 1/2 and 1 compared with EOS of Danielewicz *et al.* [3] extracted from flow data in HI collisions and depicted by the bounded region.

Recently Danielewicz *et al.* [3] have assessed the pressure–density relationship in zero–temperature SNM in the density range $2 \leq \rho/\rho_0 \leq 4.6$ from an analysis of experimental data on flow of matter in high energy heavy–ion collisions. This experimental determination of nuclear EOS has provided for the first time an important test for all theoretical models that extrapolate the EOS from the properties of finite nuclei near normal density and from nucleon–nucleon scattering, in terms of laboratory measurements of high density matter. The pressure–density relationship in zero–temperature SNM assessed from analysis of flow of matter in high energy heavy–ion collisions is depicted in Fig. 3.1 by the bounded region in the density range $0.32\ fm^{-3} \leq \rho \leq 0.736\ fm^{-3}$ (i.e., $2.0 \leq \rho/\rho_0 \leq 4.6$, with $\rho_0 = 0.16\ fm^{-3}$). In the same figure, the pressure–density curves calculated for different values of the parameter γ are also shown for comparison. It can be seen from the figure that experimentally allowed region approximately constrains the value of γ in the range $1/12 \leq \gamma \leq 1$. While all EOSs of SNM in this range of γ give similar results at saturation and sub–saturation densities they differ considerably from each other when extrapolated to high densities.

Transport model calculations have also demonstrated that sub–threshold K^+ production in high energy HI collisions can provide a suitable tool to constrain the EOS of SNM at densities $\rho \leq 3\rho_0$ [24]. Theoretical analysis of the data implies a behaviour of the EOS in the considered density range consistent with the flow data constraint shown in Fig. 3.1.

In Fig. 3.2 we have shown the energy per particle in SNM $e(\rho)$ about normal nuclear matter density ρ_0 for γ = 1/12, 1/6, 1/3, 1/2 and 1. The saturation point is depicted by the Coester rectangle [125] for comparison. The saturation curves for all γ values mentioned above are quite the same inside the depicted rectangle and pass through the middle of the allowed empirical region. From this figure it can be seen that at higher densities the curves differ very much from each other.

The behaviour of EOSs of SNM around normal nuclear matter density ρ_0 is determined by energy per particle $e(\rho_0)$ and incompressibility $K(\rho_0)$. While different theoretical models predict similar values for $e(\rho_0)$, they differ widely in the values of $K(\rho_0)$. The value of $K(\rho_0)$ for the allowed range of γ in Fig. 3.1 varies from 190 MeV to 287 MeV. It should be noted here that the centroid energies for giant monopole resonances in finite nuclei depend mainly on the value of $K(\rho_0)$ [126, 141]. Studies on monopole vibrations in finite nuclei using Gogny type effective interactions [126] as well as Skyrme–type interactions [21, 22] have approximately constrained the value of nuclear matter incompressibility $K(\rho_0)$ in the range 200–240 MeV. This range of $K(\rho_0)$ constrains the value of γ in the range 1/6 to 1/2 for the simple interaction considered here.

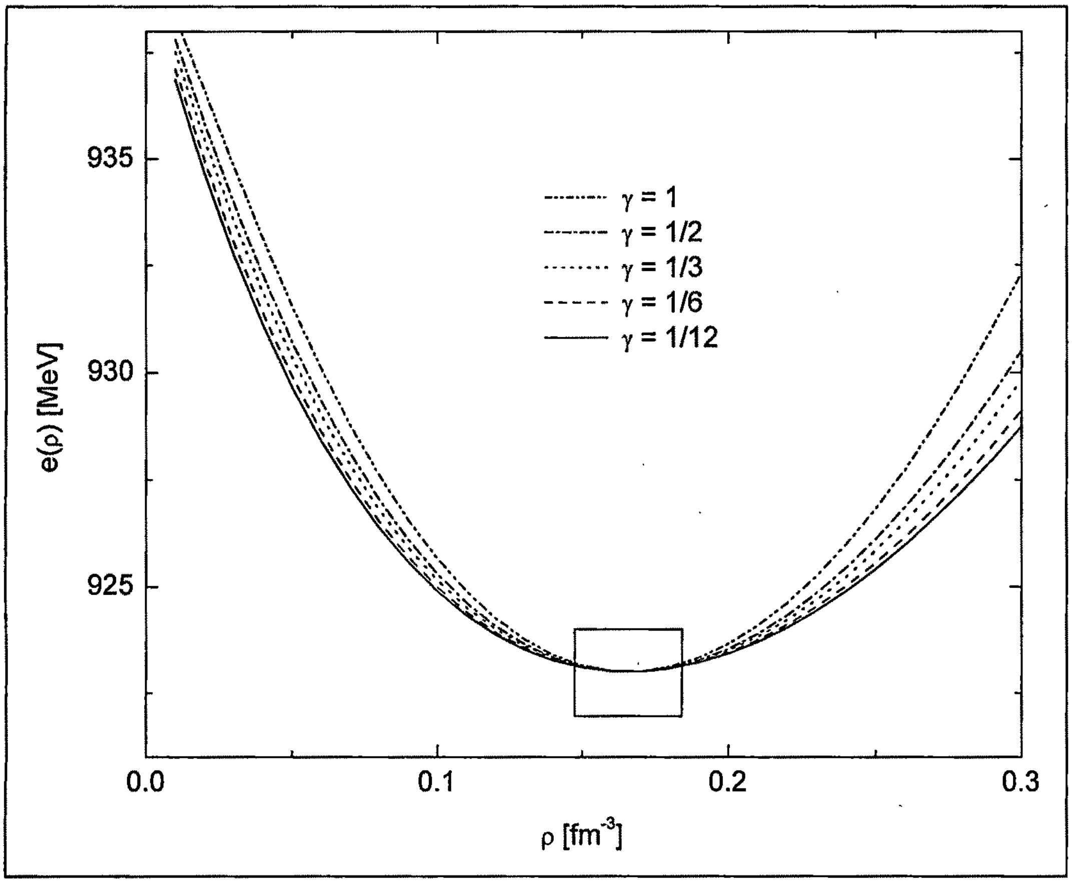

Figure 3.2: Energy per particle $e(\rho)$ in SNM as function of density ρ for γ = 1/12, 1/6, 1/3, 1/2 and 1. The empirical region of saturation is depicted by the Coester rectangle.

In this section we saw how the parameters α, γ, b, ε_0, ε_γ and ε_{ex} can be adjusted the properties and EOS of SNM. In Table 3.1 we have listed the values of the parameters required to describe the EOS of SNM. In the same table we have also given the value of $K(\rho_0)$ for the representative values of γ.

Table 3.1: The values of interaction parameters for SNM b, ε_0 and ε_γ for different values of the exponent γ along with the values of nuclear incompressibility $K(\rho_0)$ at normal density $\rho_0 = 0.1658\ fm^{-3}$. The values of exchange strength parameter and range parameter taken from ref. [108] are $\varepsilon_{ex} = -121.8\ MeV$ and $\alpha = 0.4044\ fm$ which give $M^*(k = k_{f0}, \rho_0)/M = 0.67$.

γ	ε_0 [MeV]	ε_γ [MeV]	b [fm^3]	$K(\rho_0)$ [MeV]
1/12	-401.5819	418.4447	0.2086	190.92
1/6	-194.9526	212.1658	0.2684	201.48
1/3	-91.9532	110.0007	0.407	221.46
1/2	-57.8575	76.9146	0.5668	239.92
1	-24.2697	47.4836	1.1375	287.03

Since, $\varepsilon_0 = (\varepsilon_0^{\,l} + \varepsilon_0^{\,ul})/2$, $\varepsilon_\gamma = (\varepsilon_\gamma^{\,l} + \varepsilon_\gamma^{\,ul})/2$ and $\varepsilon_{ex} = (\varepsilon_{ex}^{\,l} + \varepsilon_{ex}^{\,ul})/2$, a complete description of neutron and proton mean field properties and EOS of ANM would require the correct splittings of the three parameters ε_0, ε_γ and ε_{ex} into two specific channels $\varepsilon_0^{\,l}(\varepsilon_0^{\,ul})$, $\varepsilon_\gamma^{\,l}(\varepsilon_\gamma^{\,ul})$ and $\varepsilon_{ex}^{\,l}(\varepsilon_{ex}^{\,ul})$ for interactions between like (l) and unlike (ul) nucleons. However, there are no experimental/empirical constraint on the splittings of these three parameters except for the value of nuclear matter symmetry energy $J_\tau(\rho_0)$ at normal density. Different choices of these splittings can therefore lead to different results for nuclear matter properties. We now consider the EOS of PNM and try to adjust the parameters $\varepsilon_0^{\,l}$, $\varepsilon_\gamma^{\,l}$ and $\varepsilon_{ex}^{\,l}$ using simple physical conditions and the value of nuclear symmetry energy $J_\tau(\rho_0)$ at normal density. Once the values of $\varepsilon_0^{\,l}$, $\varepsilon_\gamma^{\,l}$ and $\varepsilon_{ex}^{\,l}$ are fixed we can have the values of $\varepsilon_0^{\,ul}$, $\varepsilon_\gamma^{\,ul}$ and $\varepsilon_{ex}^{\,ul}$.

3.4.2. Adjustment of parameters involved in EOS of PNM

As seen from EOS of PNM given in the section 3.3.2 we require six parameters α, γ, b, $\varepsilon_0^{\,l}$, $\varepsilon_\gamma^{\,l}$ and $\varepsilon_{ex}^{\,l}$ to describe PNM. Since the parameters α, γ and b are fixed from the EOS of SNM in the previous section; a complete description of EOS of PNM requires the knowledge of three additional parameters, namely, ε_0^l, ε_γ^l and ε_{ex}^l. Unlike the case of zero–temperature SNM there are no experimental/empirical constraints on the behaviour of EOS of PNM [3]. The only constrain available is the value of the nuclear symmetry energy $J_\tau(\rho_0)$ at normal nuclear matter density ρ_0. As discussed in chapter 1 and chapter 2 the value of $J_\tau(\rho_0)$ as predicted by different theoretical calculations is in the range 28 to 34 MeV. Calculations from liquid drop mass formula give the value of $J_\tau(\rho_0) \approx 30$ MeV. Moreover, the high density behaviour of $J_\tau(\rho_0)$ is extremely divergent as predicted by different model calculations [27, 28]. Our knowledge on momentum dependence of the mean field in PNM is still worse and different calculations have predicted quite different and contradicting results. In the absence of any experimental/empirical constrains our objective is to analyse the EOS of PNM on the basis of simple physical considerations.

All reasonable nuclear interactions predict that the equilibrium density $\rho_0(\sigma)$ at which the energy per particle of ANM is minimum, decreases with increase in the asymmetry σ from zero onwards. As a result the binding energy per particle and the incompressibility in ANM at this equilibrium density also decrease with increase in σ. With further increase in asymmetry σ the minimum energy per particle disappears completely around a value $\sigma > 0.8$ which is in accordance with the well known fact that PNM is not bound by nuclear forces. In view of this PNM should not be predicted to be bound by any reasonable nuclear interaction and we impose the conditions,

$$P^n(\rho) > 0 \text{ and } \qquad dP^n(\rho)/d\rho > 0\,. \qquad \ldots(3.40)$$

While the first condition rules out the existence of any equilibrium density where the energy per particle $e^n(\rho)$ in PNM can have a minimum both the conditions are necessary to avoid any non physical behaviour leading to a collapse of PNM at any density. It can be remarked here that many existing parametrisation of effective interactions which are very successful in many nuclear calculations violate these two conditions [19]. We will now vary the three parameters ε_0^l, ε_γ^l and ε_{ex}^l and examine the EOS of PNM subject to this constrain.

It should be mentioned here that the neutron–proton effective mass splitting is solely determined from the splitting of the exchange strength parameter ε_{ex} into like and unlike channels ε_{ex}^l and ε_{ex}^{ul}. This will be shown clearly in section 3.5.1. However, the neutron–proton effective mass splitting is still an open problem in nuclear physics. Many attempts have been made to constrain these parameters from analysis of nucleon–nucleus scattering data at intermediate energies as well as experimental observables sensitive to the differences between neutron and proton flow data in high energy HI collisions. As we saw before in the previous section considerable progress have been made in constraining the strength parameter combination ($\varepsilon_{ex}^{l} + \varepsilon_{ex}^{ul}$) (i.e. the strength parameter ε_{ex} associated with SNM) [108]. On the other hand, the relative strength of the combination ($\varepsilon_{ex}^{l} - \varepsilon_{ex}^{ul}$) which determines the splitting of neutron–proton effective mass splitting is still largely unknown [30–33]. In view of this we have taken representative values of ε_{ex}^{l} in the range $0 \geq \varepsilon_{ex}^{l} \geq 2\varepsilon_{ex}$ (both ε_{ex} and ε_{ex}^{l} are negative) and then proceed to calculate the values of ε_0^{l} and ε_γ^{l}. To find the values of ε_0^{l} and ε_γ^{l} we express them in terms of $e^{n}(\rho_0)$ and $e^{n'}(\rho_0)$.

If we put $\sigma = 1$ in the quadratic expression for energy density in ANM given in Eq. (3.24) we get the definition of symmetry energy $J_\tau(\rho)$ as the difference between energy per particle in PNM and SNM, which can be expressed as

$$J_\tau(\rho) = e^{n}(\rho) - e(\rho) \qquad \ldots(3.41)$$

From the above Eq. we see that $e^{n}(\rho_0)$ and $e^{n'}(\rho_0)$ can be written as

$$e^{n}(\rho_0) = J_\tau(\rho_0) + e(\rho_0) \qquad \text{and} \qquad e^{n'}(\rho_0) = J_\tau'(\rho_0)$$

where $e^{n'}(\rho_0) = \rho(de^{n}/d\rho)|_{\rho=\rho 0}$ and $J_\tau'(\rho_0) = \rho(dJ_\tau(\rho)/d\rho)|_{\rho=\rho 0}$.

Solving the above equations we can get the values of ε_0^{l} and ε_γ^{l} subject to the condition that we know the values of $J_\tau(\rho_0)$, $e(\rho_0)$ and $J_\tau'(\rho_0)$. Since we do not have any knowledge of $J_\tau'(\rho_0)$ we vary its value. It was observed that if we vary the value of $J_\tau'(\rho_0)$, for a representative value of ε_{ex}^{l} in the range $0 \geq \varepsilon_{ex}^{l} \geq 2\varepsilon_{ex}$, given value of γ and a standard value of $J_\tau(\rho_0)$ at normal nuclear matter density, there is a critical value of $J_\tau'(\rho_0)$ above which the stability condition in PNM given in Eq. (3.40) is violated. Using that critical value of $J_\tau'(\rho_0)$ we find the value of ε_0^{l} and ε_γ^{l}. Using this critical value of $J_\tau'(\rho_0)$ we can obtain the stiffest EOS of PNM for a given value of ε_{ex}^{l}, γ and $J_\tau(\rho_0)$ that does not violate the constrain given in Eq. (3.40). This procedure is repeated for different values of γ, ε_{ex}^{l} and $J_\tau(\rho_0)$ over their admissible range and a number of parameter sets are calculated. It should be mentioned here that all the EOS of ANM corresponding to values of $J_\tau'(\rho_0)$ at and below the critical value of $J_\tau'(\rho_0)$ are allowed so far as the stability conditions in PNM are concerned. Thus we can have an infinite number of allowed EOS which satisfy the stability condition for PNM. In this chapter we will take this critical value of $J_\tau'(\rho_0)$, which gives the stiffest EOS of ANM, to analyse the density dependence of nuclear symmetry energy. In chapter 5 we have used EOS of beta–stable matter, found in the interior of neutron stars, to further constrain the value of $J_\tau'(\rho_0)$.

In table 3.2 we have listed the critical values of $J_\tau'(\rho_0)$, for which the stiffest EOS of PNM which did not violate the constraint discussed in Eq. (3.40), for different values of γ, ε_{ex}^l and $J_\tau(\rho_0)$. It should be mentioned here that $J_\tau'(\rho_0)$ is directly related to the slope of the symmetry energy at normal density ρ_0. While different theoretical models predict quite similar values of $J_\tau(\rho_0)$ they widely differ in the values of $J_\tau'(\rho_0)$. It can be seen from table 3.2(i)–(iii) that for a given value of $J_\tau(\rho_0)$ and γ, the critical values of $J_\tau'(\rho_0)$ do not vary much with variation in the value of exchange strength parameter ε_{ex}^l. However, for a given value of ε_{ex}^l and $J_\tau(\rho_0)$, the critical values of $J_\tau'(\rho_0)$ are very much sensitive to variation in the value of the parameter γ.

Table 3.2.i: Critical value of $J_\tau'(\rho_0)$ (in *MeV*), for which the stiffest EOS of PNM satisfies the stability condition given in Eq. (3.40), for different values of γ, ε_{ex}^l and $J_\tau(\rho_0) = 28\ MeV$.

ε_{ex}^l [*MeV*] / γ	*0*	$\varepsilon_{ex}/3$	$2\,\varepsilon_{ex}/3$	ε_{ex}	$4\varepsilon_{ex}/3$	$5\,\varepsilon_{ex}/3$	$2\,\varepsilon_{ex}$
1/12	***20.51***	***20.67***	***20.79***	***20.88***	***20.94***	***20.96***	***20.95***
1/6	***21.13***	***21.14***	***21.14***	***21.12***	***21.09***	***21.05***	***20.99***
1/3	***22.01***	***21.86***	***21.71***	***21.57***	***21.42***	***21.27***	***21.12***
1/2	***22.56***	***22.38***	***22.18***	***21.97***	***21.76***	***21.53***	***21.30***
1	***23.20***	***23.26***	***23.22***	***23.07***	***22.81***	***22.44***	***21.98***

Table 3.2.ii: Critical value of $J_\tau'(\rho_0)$ (in MeV), for which the stiffest EOS of PNM satisfies the stability condition given in Eq. (3.40), for different values of γ, ε_{ex}^l and $J_\tau(\rho_0) = 30\ MeV$.

ε_{ex}^l [MeV] / γ	0	$\varepsilon_{ex}/3$	$2\ \varepsilon_{ex}/3$	ε_{ex}	$4\varepsilon_{ex}/3$	$5\ \varepsilon_{ex}/3$	$2\ \varepsilon_{ex}$
1/12	23.75	23.98	24.17	24.31	24.44	24.53	24.59
1/6	24.57	24.64	24.67	24.71	24.72	24.72	24.71
1/3	25.84	25.70	25.56	25.41	25.27	25.13	24.98
1/2	26.77	26.54	26.31	26.07	25.82	25.57	25.31
1	28.34	28.25	28.06	27.79	27.41	26.95	26.40

Table 3.2.iii: Critical value of $J_\tau'(\rho_0)$ (in MeV), for which the stiffest EOS of PNM satisfies the stability condition given in Eq. (3.40), for different values of of γ, ε_{ex}^l and $J_\tau(\rho_0) = 32\ MeV$.

ε_{ex}^l [MeV] / γ	0	$\varepsilon_{ex}/3$	$2\ \varepsilon_{ex}/3$	ε_{ex}	$4\varepsilon_{ex}/3$	$5\ \varepsilon_{ex}/3$	$2\ \varepsilon_{ex}$
1/12	26.91	27.19	27.43	27.63	27.82	27.96	28.08
1/6	27.92	28.02	28.10	28.16	28.22	28.26	28.29
1/3	29.56	29.42	29.29	29.15	29.01	28.87	28.73
1/2	30.83	30.57	30.31	30.05	29.77	29.49	29.21
1	33.27	33.06	32.76	32.38	31.93	31.38	30.76

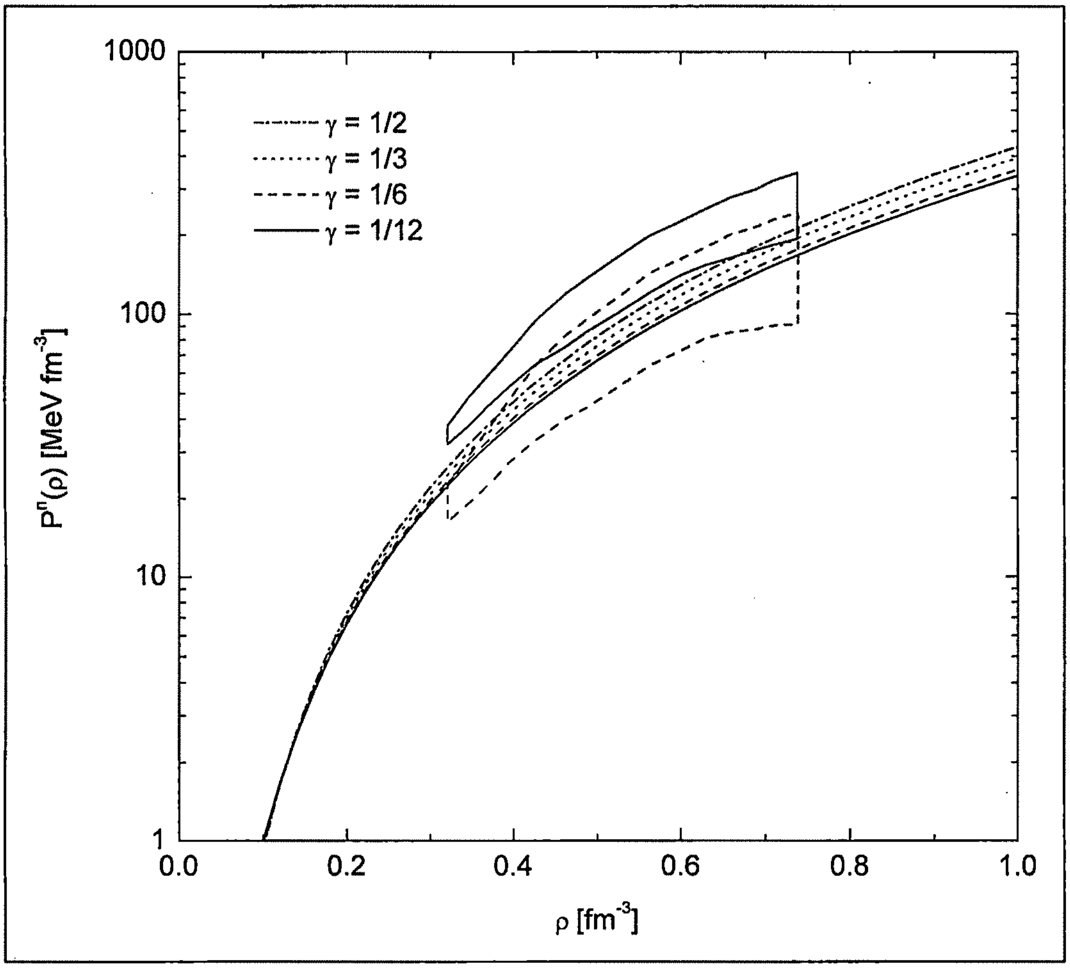

Figure 3.3: Pressure–density relationship for different EOS of PNM with $\varepsilon_{ex}^{l} = 4\varepsilon_{ex}/3$, $J_\tau(\rho_0) = 30$ *MeV* and $\gamma = 1/12$, 1/6, 1/3 and 1/2 compared with EOS of Danielewicz *et al.* [3] extracted from flow data in HI collisions and depicted by the bounded regions.

In Fig. 3.3 the pressure – density relationship in PNM assessed from flow of matter in high energy heavy–ion collision experiments in the density range $2 \leq \rho/\rho_0 \leq 4.6$ [3] depicted by the bounded regions have been shown. In the same figure the pressure density relation in PNM has been shown for the stiffest EOSs of the parameter sets $\varepsilon_{ex}^{l} = 4\varepsilon_{ex}/3$, $J_\tau(\rho_0) = 30$ *MeV* and $\gamma = 1/12$, 1/6, 1/3 and 1/2. It can be seen that all the curves considered here pass almost through the middle of the experimental region.

3.5. Nuclear mean fields and effective nucleon masses

In chapter 2 we analysed the momentum and density dependence of nuclear mean fields and effective nucleon masses for a general finite range effective interaction. It was seen that in the analysis of momentum dependence aspect of nuclear EOS the more important quantity is the difference in the neutron and proton mean fields $u^{n-p}(k,\rho,Y_p)$. For the simple finite range effective interaction considered in this chapter, $u^{n-p}(k,\rho,Y_p)$ can be obtained from Eqs. (3.15) and (3.16) and is given as

$$u^{n-p}(k,\rho,Y_p) = (1-2Y_p)\rho A(\rho) + G(k, \rho, Y_p), \qquad \ldots(3.42)$$

where $A(\rho) = \left[\frac{(\varepsilon_0^l - \varepsilon_0^{ul})}{\rho_0} + \frac{(\varepsilon_\gamma^l - \varepsilon_\gamma^{ul})}{\rho_0^{\gamma+1}}\left(\frac{\rho}{1+b\rho}\right)^\gamma\right]$, $\qquad \ldots(3.43)$

and $G(k,\rho,Y_p) = \frac{1}{\rho_0 \int f(r) d^3r} = \int \left[\rho_n \frac{3j_1(k_n r)}{k_n r} - \rho_p \frac{3j_1(k_p r)}{k_p r}\right] j_0(kr) f(r) d^3r. \quad \ldots(3.44)$

Again the functional $G(k, \rho, Y_p)$ has a complicated dependence on momentum k, total nucleon density ρ and the proton fraction Y_p and can be simplified for the two cases considered in chapter 2. In the limit of large k, $k >> k_n$, k_p the functional $G(k, \rho, Y_p)$ becomes very simple and for Yukawa form of finite range effective interaction it is given as,

$$G(k, \rho, Y_p) \underset{\text{large } k}{\sim} (1-2Y_p)\frac{\rho}{\rho_0}\frac{1}{1+k^2\alpha^2}. \qquad \ldots(3.45)$$

This result is very important in the sense that $G(k, \rho, Y_p)$ is directly proportional to the asymmetry parameter $(1-2Y_p)$, the proportionality factor being a very simple function of momentum k and total nucleon density ρ. However the actual values of k beyond which the asymptotic result in Eq. (3.45) will be valid depends on the total nucleon density ρ.

The second simplification arises by making a Taylor series expansion of the functional $\left[\rho_n \frac{3j_1(k_n r)}{k_n r} - \rho_p \frac{3j_1(k_p r)}{k_p r}\right]$ inside the integral in Eq. (3.44) about Y_p=1/2, and the functional $G(k, \rho, Y_p)$ is given by

$$G(k,\rho,Y_p) \approx \frac{(1-2Y_p)\rho}{\rho_0} L_\alpha(k,\rho). \qquad \ldots(3.46)$$

where, $$L_\alpha(k,\rho) = \frac{\int j_0(kr) j_0(k_f r) f(r) d^3r}{\int f(r) d^3r} \qquad \ldots(3.47)$$

For the present effective interaction having Yukawa form for finite range part the functional $L_\alpha(k, \rho)$ is given by the relation

$$L_\alpha(k,\rho) = \frac{1}{4xz} \ln\left\{\frac{1+(x+z)^2}{1+(x-z)^2}\right\}, \quad \text{where, } x = \alpha k \text{ and } z = \alpha k_f. \qquad \ldots(3.48)$$

The validity of Eqs. (3.45) and (3.46) are examined in Fig. 3.4. The dimensionless functional $G(k, \rho, Y_p)$ given in Eq. (3.44) is calculated analytically and is shown as a function of momentum k at three different densities, ρ_0, $3\rho_0$ and $5\rho_0$ for $Y_p = 0.1$ in Fig. 3.4. In the same figure the two approximate versions given in Eq. (3.45) and (3.46) are given for comparison. It is seen that the value of momentum k beyond which the asymptotic behaviour agrees with the exact one gradually increases with increase in density. The approximate version of $G(k, \rho, Y_p)$ in Eq. (3.45) although obtained from a Taylor expansion about $Y_p = 1/2$ compares quite well with the exact one even at $Y_p = 0.1$ over the entire range of momentum. However, at higher densities there is a small discrepancy between the two results at very low momenta which slowly increases as $Y_p \rightarrow 0$. This fact also justifies the linear isospin dependence of the famous Lane potential [143]. This discrepancy vanishes at higher momenta.

From Eq. (3.42) it can be seen that to study the momentum and density dependence of the functional $u^{n-p}(k,\rho,Y_p)$ we require the knowledge of the strength combinations $(\varepsilon_{ex}^{l} - \varepsilon_{ex}^{ul})$. It is important to mention here that the relative strength of the combination $(\varepsilon_{ex}^{l} - \varepsilon_{ex}^{ul})$ is still largely unknown [30–33]. In fact, even the sign of the combination $(\varepsilon_{ex}^{l} - \varepsilon_{ex}^{ul})$ is still uncertain [145]. However, considerable progress has been made in constraining the strength parameter combination $(\varepsilon_{ex}^{l} + \varepsilon_{ex}^{ul})$. In view of this we have chosen two different sets of exchange strength parameters set–A and set–B.

Set A: $\varepsilon_{ex}^{l} = \varepsilon_{ex}/3;\ \varepsilon_{ex}^{ul} = 5\varepsilon_{ex}/3$,

and Set B: $\varepsilon_{ex}^{l} = 5\varepsilon_{ex}/3;\ \varepsilon_{ex}^{ul} = \varepsilon_{ex}/3$

to study the momentum and density dependence of the neutron and proton mean fields and effective nucleon masses. It may be worth noticing here that the absolute value of $(\varepsilon_{ex}^{l} - \varepsilon_{ex}^{ul})$ does not change for the two different sets A and B.

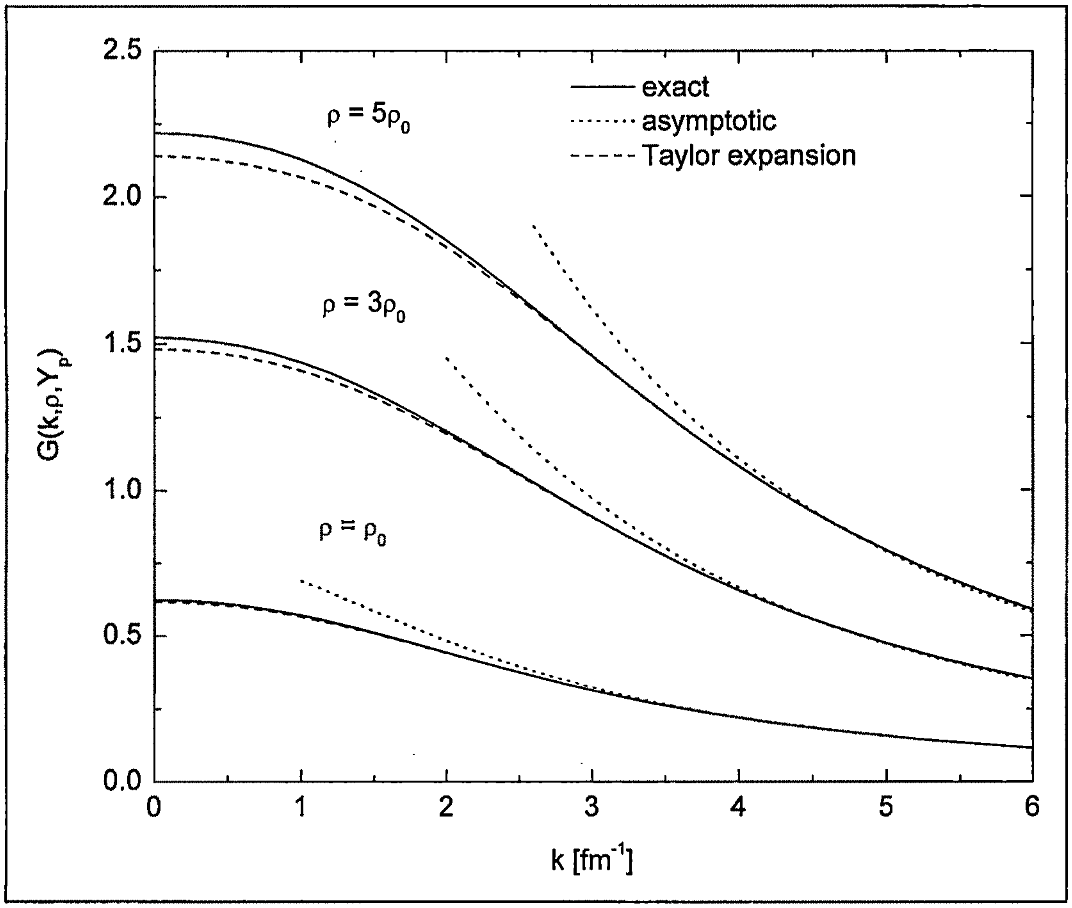

Figure 3.4: Momentum dependence of the functional $G(k, \rho, Y_p)$ given in Eq. (3.44) is shown at three different densities ($\rho = \rho_0$, $3\rho_0$ and $5\rho_0$) for $Y_p = 0.1$ and compared with its asymptotic and Taylor expansion versions in Eqs. (3.45), (3.46) and (3.47).

3.5.1. Momentum and density dependence of nucleon effective masses

The nucleonic effective mass is an important property that is related to the momentum dependence of the inmedium interaction of a nucleon. To study the momentum and density dependence of nucleon effective mass for the simple effective interaction considered in this chapter we analyse the dimensionless functional

$\frac{M}{\hbar^2 k}\frac{\partial u^{n-p}(k,\rho,Y_p)}{\partial k}$ introduced in chapter 2. It should be kept in mind that the dimensionless functional $\frac{M}{\hbar^2 k}\frac{\partial u^{n,p}(k,\rho,Y_p)}{\partial k}$ are directly connected to neutron and proton effective masses $\left[\frac{M^*(k,\rho_n,\rho_p)}{M}\right]^{n,p}$. The asymptotic behaviour of the dimensionless quantity $\frac{M}{\hbar^2 k}\frac{\partial u^{n-p}(k,\rho,Y_p)}{\partial k}$ calculated from Eqs. (3.42) and (3.45) for Yukawa form of exchange interaction is given by,

$$\frac{M}{\hbar^2 k}\frac{\partial u^{n-p}(k,\rho,Y_p)}{\partial k} \Rightarrow -2(1-2Y_p)\frac{M\rho}{\hbar^2}\frac{(\varepsilon_{ex}^{l}-\varepsilon_{ex}^{ul})\alpha^2}{\rho_0}\frac{1}{(1+\alpha^2 k^2)^2} \quad ..(3.49)$$

It should be noted here that the asymptotic behaviour of $\frac{M}{\hbar^2 k}\frac{\partial u^{n-p}(k,\rho,Y_p)}{\partial k}$ for large k given in Eq. (3.49) is positive for negative values of the exchange strength combination ($\varepsilon_{ex}^{l}-\varepsilon_{ex}^{ul}$). This means that $\frac{M}{\hbar^2 k}\frac{\partial u^{n}(k,\rho,Y_p)}{\partial k} > \frac{M}{\hbar^2 k}\frac{\partial u^{p}(k,\rho,Y_p)}{\partial k}$ and asymptotically the neutron effective mass $\left[\frac{M^*(k,\rho,Y_P)}{M}\right]_n$ is less than the proton effective mass $\left[\frac{M^*(k,\rho,Y_P)}{M}\right]_p$. On the other hand, the asymptotic behaviour of $\frac{M}{\hbar^2 k}\frac{\partial u^{n-p}(k,\rho,Y_p)}{\partial k}$ is negative for positive values of the exchange strength combination ($\varepsilon_{ex}^{l}-\varepsilon_{ex}^{ul}$) and asymptotically the proton effective mass will be less than the neutron effective mass. Since neither the value nor the sign of the exchange strength combination ($\varepsilon_{ex}^{l}-\varepsilon_{ex}^{ul}$) is known we show the splitting of nucleon effective masses for the two different parameter sets set–A and set–B mentioned earlier.

The two opposite types of behaviour of nucleon effective masses have been shown in Fig. 3.5, where the exact zero temperature neutron and proton effective masses, which can be calculated analytically using Eqs. (2.28), (3.15) and (3.16), and would involve only the exchange strength and range parameters, are plotted as functions of momentum k at $\rho = \rho_0$ and $Y_P = 0.1$ for two different sets of exchange strength parameters; Set A (Fig. 3.5(a)) and Set B (Fig. 3.5(b)). The asymptotic behaviour of neutron and proton effective masses are also shown in the same figures for comparison. The asymptotic results agree quite well with the exact results for $k \geq 3.5\, fm^{-1}$.

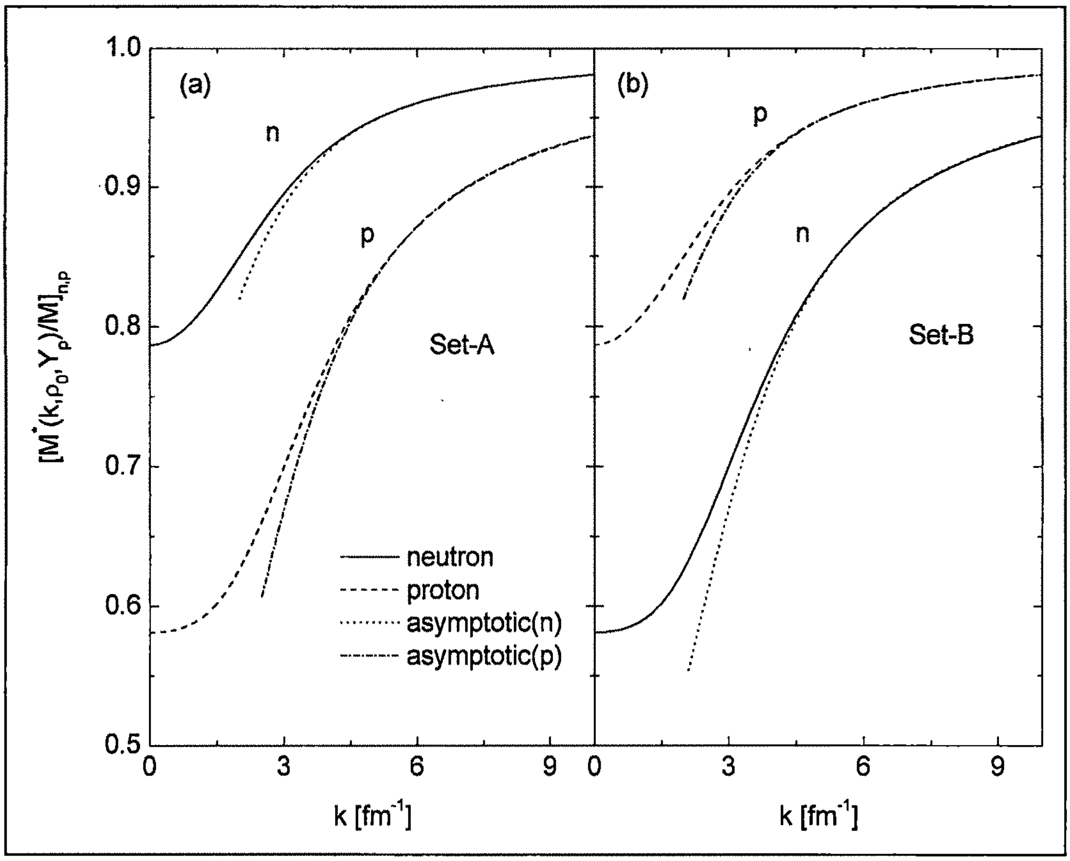

Figure 3.5: Neutron and proton effective masses shown as function of momentum k for $\rho = \rho_0$ and $Y_p = 0.1$ for the two different exchange parameter sets A and B (see text for details). The corresponding asymptotic behaviour is also shown for comparison.

The density dependence of these two opposite types of splitting of neutron and proton effective masses could also be quite important for the differences between neutron and proton transport properties in highly asymmetric dense nuclear matter. This has been shown for neutron and proton effective masses at $k = 0$ for the two sets of exchange strength parameters A and B in Figs. 3.6(a) and 3.6(b) respectively. The effective masses decrease with increase in density. However, the rate of decrease is considerably slowed down at higher densities.

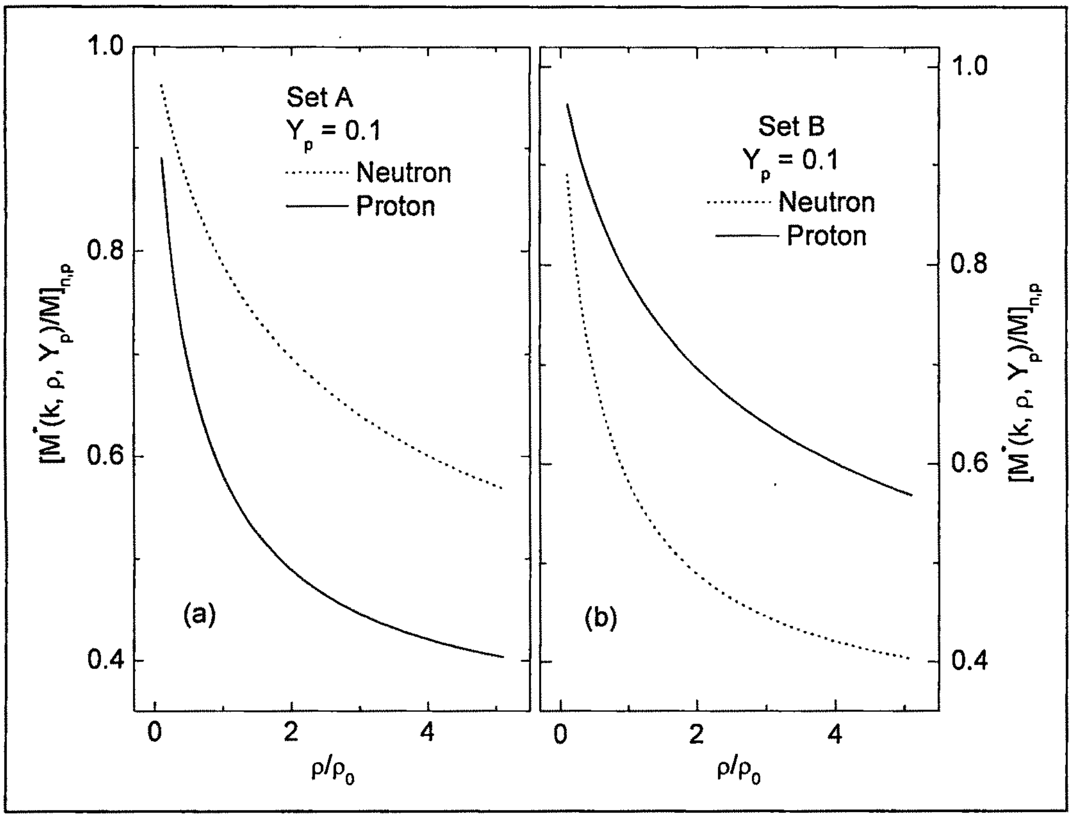

Figure 3.6: Density dependence of neutron and proton effective masses for k = 0 and Y_p = 0.1 for the two different exchange parameter sets A and B.

Since the absolute value of $(\varepsilon_{ex}^{l} - \varepsilon_{ex}^{ul})$ does not change for the two different sets A and B considered here, it should be noticed that the curves for the neutron effective mass in Figs. 3.5(a) and 3.6(a) are converted to the curves for the proton effective mass in Figs. 3.5(b) and 3.6(b) and conversely.

In connection with the splitting of neutron and proton effective masses in asymmetric nuclear matter it should be mentioned here that the results obtained from different theoretical calculations can be roughly classified in to two groups; one in which the neutron effective mass goes above the proton effective mass as in Figs. 3.5(a) and 3.6(a) and the other showing a splitting in the opposite direction similar to the trend shown in Figs. 3.5(b) and 3.6(b). The results obtained from Brueckner–Hartree–Fock (BHF) calculations using realistic nucleon–nucleon interactions [51, 52] like separable form of Paris potential, Argonne V_{14} potential and Argonne V_{14} plus a three body force exhibit a splitting where the neutron effective mass goes above the proton effective mass as in Figs. 3.5(a) and 3.6(a). Recently Li *et al.* [30–32] have studied effects of momentum dependent symmetry potentials on heavy–ion collisions induced by neutron rich nuclei in terms of simple parametrisations of neutron and proton single particle potentials guided by a Hartree–Fock calculation using Gogny effective interaction. This simple parametrisation of neutron and proton single particle potential also gives a splitting where neutron effective mass is above the proton one. On the other hand, the recent parametrisation, SLy–type [17, 19] of Skyrme forces give a splitting of neutron and proton effective masses in the opposite direction similar to the trend shown in Figs. 3.5(b) and 3.6(b). The results obtained in the microscopic relativistic Dirac–Brueckner calculations [71] as well as relativistic mean field (RMF) approximation using quantum hadrodynamics (QHD) [97, 142] also exhibit this type of splitting of neutron and proton effective masses.

In a recent work Rizzo *et al.* [33] have analysed the influence of the two opposite types of splitting of nucleon effective masses on flow data in HI collisions using two different simple GBD type parametrisations [140] of the energy density. It was shown that the two different types of results for effective mass splitting lead to rather different results for several observables in HI collisions. Following the same formalism as used by Rizzo *et al.*, Li [146] has analysed the effect of the two types of neutron and proton effective mass splitting on isovector part of nuclear mean field. Li has ruled out the possibility of neutron effective mass being smaller than proton effective mass on the basis that this type of neutron and proton effective mass splitting leads to wrong energy dependence of isovector part of nuclear mean field or the Lane potential.

3.5.2. Momentum and density dependence of isovector part of nuclear mean field

The isovector part of nuclear mean field $u_\tau(k, \rho)$ defined in chapter 2 in Eq. (2.38) for a general finite range effective interaction can now be given for the Yukawa form of short range interaction as,

$$u_\tau(k,\rho)=\frac{1}{2}\rho A(\rho)+\frac{(\varepsilon_{ex}^{l}-\varepsilon_{ex}^{ul})\rho}{2\rho_0\int f(r)d^3r}\int j_0(k_f r)j_0(kr)f(r)d^3r. \qquad \ldots(3.50)$$

To analyse the momentum and density dependence of isovector part of nuclear mean field $u_\tau(k, \rho)$ more explicitly, we give here the form of $u_\tau(k, \rho)$ given in Eq. (2.46)

$$u_\tau(k,\rho) = 2J_\tau(\rho) - \frac{\hbar^2 k_f^{\,2}}{3M}\left[\left(\frac{M^*(k,\rho)}{M}\right)^2 + \frac{\hbar^2 k^2}{M^2c^2}\right]^{-1/2}_{k=k_f} + u_\tau^{ex}(k,\rho) \qquad ...(3.51)$$

In the above equation the nuclear symmetry energy $J_\tau(\rho)$ is given as

$$J_\tau(\rho) = \frac{\hbar^2 k_f^{\,2}}{6M}\left[\left(\frac{M^*(k,\rho)}{M}\right)^2 + \frac{\hbar^2 k^2}{M^2c^2}\right]^{-1/2}_{k=k_f} + \frac{1}{4}\rho A(\rho) + \frac{(\varepsilon_{ex}^{l} - \varepsilon_{ex}^{ul})\rho}{4\rho_0 \int f(r)d^3r}\int j_0^2(k_f r) f(r) d^3r, \qquad ...(3.52)$$

and the functionals $u_\tau^{ex}(k, \rho)$ defined in Eq. (2.47) is expressed as

$$u_\tau^{ex}(k,\rho) = \frac{(\varepsilon_{ex}^{l} - \varepsilon_{ex}^{ul})\rho}{2\rho_0 \int f(r)d^3r}\int [j_0(kr) - j_0(k_f r)] j_0(k_f r) f(r) d^3r. \qquad ...(3.53)$$

From equations (3.50) to (3.53) it is quite evident that the momentum dependence of isovector part of nuclear mean field $u_\tau(k, \rho)$ at a particular nucleon density ρ comes from the momentum dependence of the functional $u_\tau^{ex}(k, \rho)$. From Eq. (3.53) it can be seen that the behaviour of the functional $u_\tau^{ex}(k, \rho)$ depends upon the value and sign of the exchange strength combination ($\varepsilon_{ex}^{l} - \varepsilon_{ex}^{ul}$) and the range parameter α.

The contradicting behaviour of $u_\tau^{ex}(k, \rho)$ as was seen in chapter 2 for two very popular nonrelativistic effective interactions, i.e. Skyrme and Gogny interactions, is now shown for the finite range interaction considered here in Fig. 3.7 for the two parameter sets, set–A and set–B, at densities $\rho = \rho_0$ and $3\rho_0$. It is seen that for set–A $u_\tau^{ex}(k, \rho)$ increases with increase in momentum k and for set–B it decreases with increase in momentum k. As can be seen the functional $u_\tau^{ex}(k, \rho)$ vanishes at $k = k_f$. At higher density, for set–A, the value of $u_\tau^{ex}(k, \rho)$ is more at low momenta but becomes less at some higher momenta and for set–B, the value of $u_\tau^{ex}(k, \rho)$ is less at low momenta but becomes more at higher momenta.

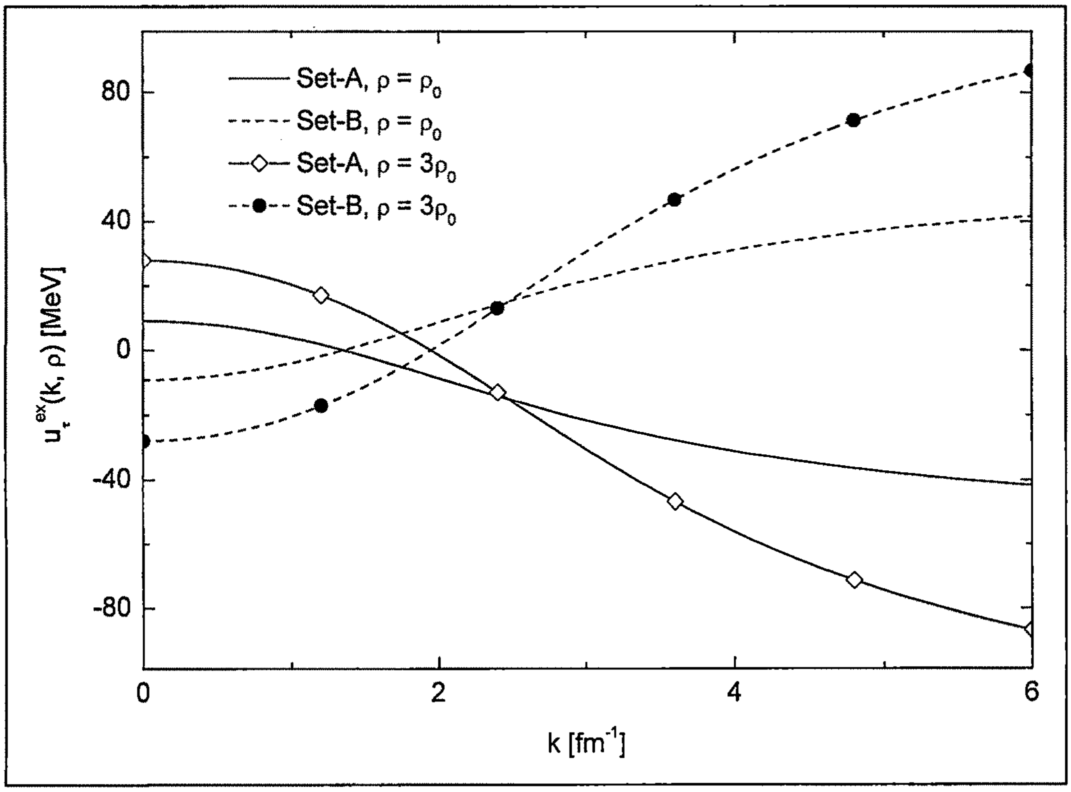

Figure 3.7: Momentum dependence of the functional $u_\tau^{ex}(k,\rho)$ for the two different exchange parameter sets A and B for densities $\rho = \rho_0$ and $3\rho_0$.

Complete description of momentum and density dependence of the isovector part of nuclear mean field $u_\tau(k, \rho)$ given in Eq. (3.50) requires the knowledge of all the parameters of the interaction. However, at normal nuclear matter density, $\rho = \rho_0$, one can make use of standard values of $J_\tau(\rho_0)$ and $M^*(k = k_{f0}, \rho_0)/M$ and examine the momentum dependence of $u_\tau(k, \rho_0)$ from Eq. (3.51) using only two parameters, the exchange strength combination ($\varepsilon_{ex}^{l} - \varepsilon_{ex}^{ul}$) and the range parameter α. This is shown for the Yukawa form of exchange interaction in Fig. 3.8 for the two different sets of the exchange strength parameters A and B by using, $M^*(k = k_{f0}, \rho_0)/M = 0.67$ and $J_\tau(\rho_0) = 30$ MeV. The two different sets of exchange strength parameters A and B exhibit quite contradicting momentum dependence of the isovector part of nuclear mean field. While $u_\tau(k, \rho_0)$ decreases with increase in momentum for set–A, it increases for set–B and the two curves intersect at $k = k_{f0}$. This contradiction in momentum dependence of the isospin part of nuclear mean field will however become

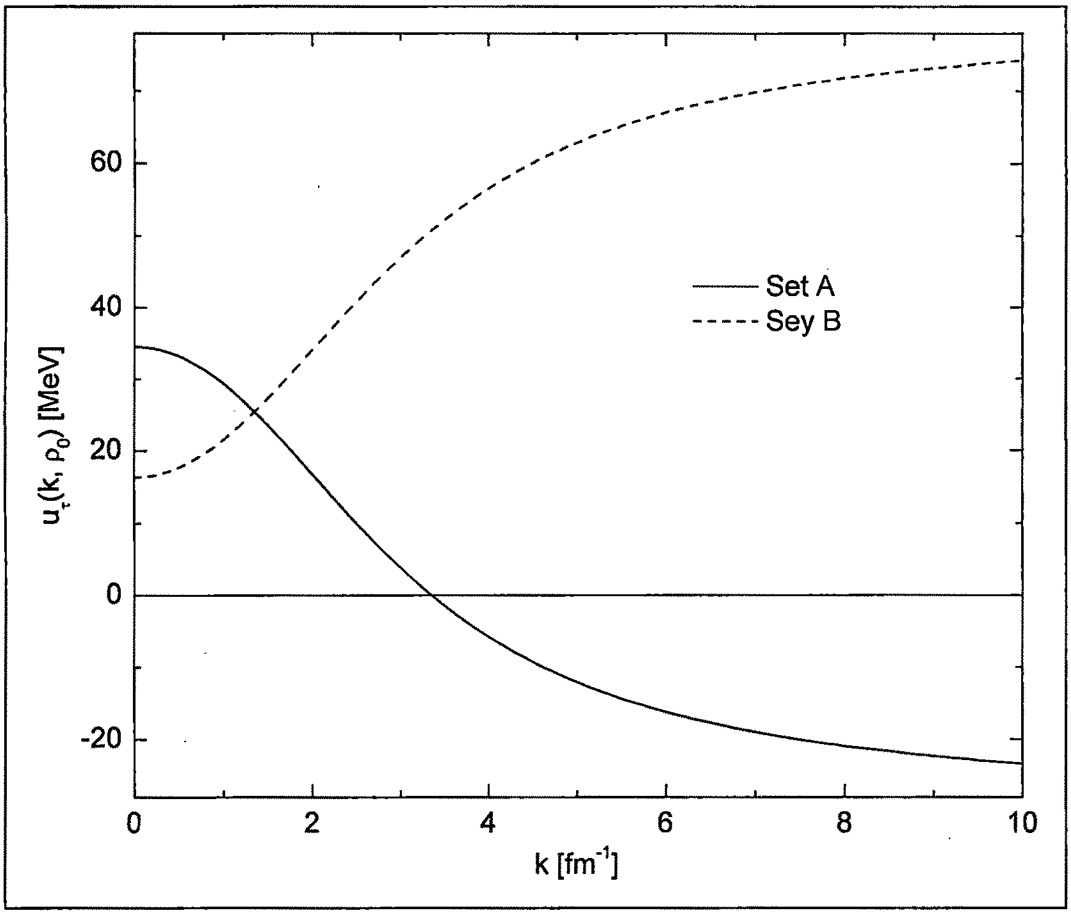

Figure 3.8: Isovector part of nuclear mean field at normal density $u_\tau(k, \rho_0)$ shown as function of momentum k for exchange parameter sets A and B with $J_\tau(\rho_0) = 30\ MeV$ and $M^*(k = k_{f0}, \rho_0)/M = 0.67$.

less and less pronounced with decrease in the absolute value of $(\varepsilon_{ex}^{l} - \varepsilon_{ex}^{ul})$. It is interesting to note that a zero–crossing point occurs in case of $u_\tau(k, \rho_0)$ for set–A at $k = 3.3$ fm^{-1}, where it vanishes and then becomes negative with further increase in k and the isospin effect on the difference between neutron and proton mean fields are inverted. Such inversion of the isospin effect at a crossing point is observed in BHF calculations using realistic nucleon–nucleon interactions [2, 51, 52] and also in the work of Li *et al.* [29] mentioned earlier in this section. However, it is worth noticing that such a crossing point can appear only if $u_\tau(k, \rho)$ vanishes at some value of momentum k and ultimately approaches a negative asymptotic value in the limit of $k \rightarrow \infty$. On the other hand, such a zero–crossing point does not occur in case of set–B and consequently the difference between neutron and proton mean fields becomes more and more repulsive with increase in k and approaches higher and higher asymptotic values in the limit $k \rightarrow \infty$ with decrease in the proton fraction Y_p.

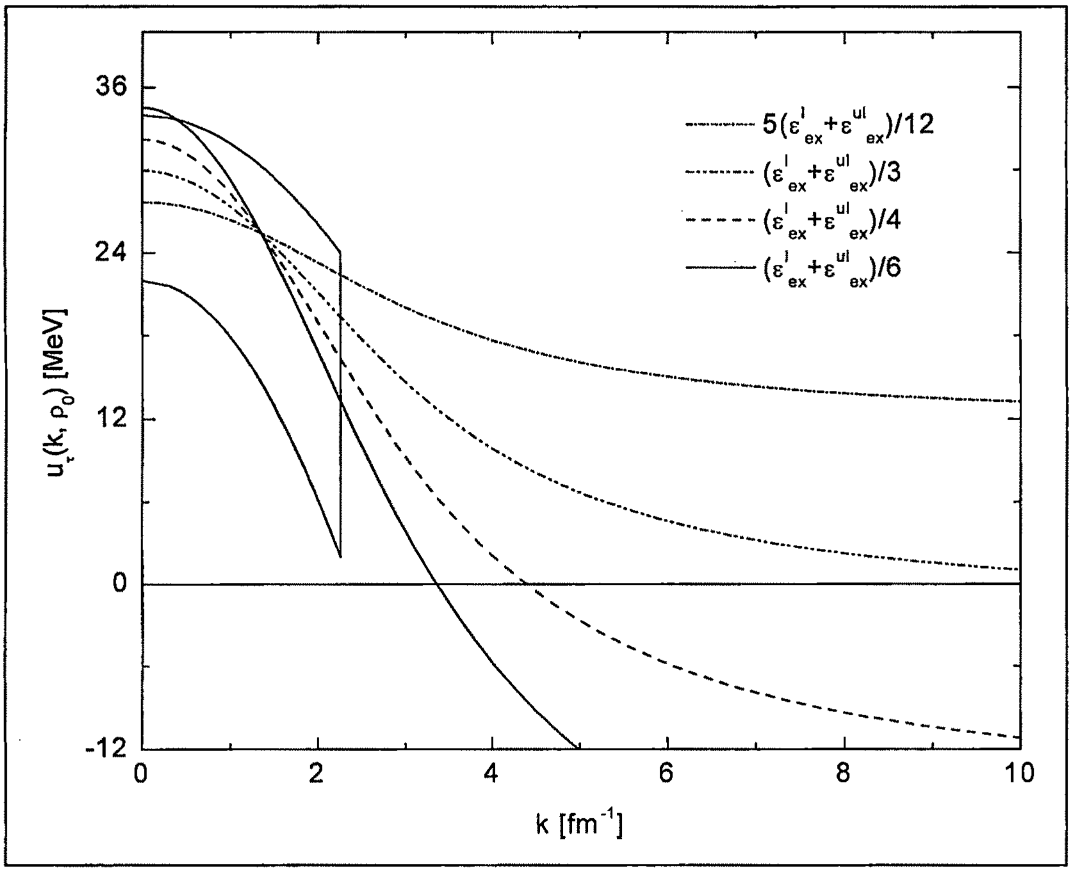

Figure 3.9: Momentum dependence of $u_\tau(k, \rho_0)$ at normal density ρ_0 calculated with different splitting of $\varepsilon_{ex}{}^l$ and $\varepsilon_{ex}{}^{ul}$ and compared with the result extracted from nucleon-nucleus scattering data up to 100 MeV, denoted by the bounded region.

The momentum dependence of Lane potential [143], $v_l = 4u_\tau(k, \rho_0)$ at normal density ρ_0, has been used to constrain the isospin splitting of nuclear mean field in ref [146, 147]. The value of the Lane potential and its momentum dependence has been extracted from nucleon–nucleus scattering data up to 100 MeV [148, 149]. At normal nuclear matter density v_l has a value of about 112 ± 24 MeV at k = 0 and decreases as a function of incident energy with a slope between 0.1 and 0.2 [147]. This is shown in Fig. 3.9 by the bounded region. In the same figure the calculated results of $u_\tau(k, \rho_0)$ for different values of $\varepsilon_{ex}{}^l$ are also shown for comparison. It is observed that all calculated curves of $u_\tau(k, \rho_0)$ for which ε_{ex}^{l} lies within the range $\varepsilon_{ex}^{l}/3$ to $5\varepsilon_{ex}^{l}/6$ pass through the bounded region. It can be seen that parameter set B for which $\varepsilon_{ex}^{l} = 5\varepsilon_{ex}/3$, gives an opposite behaviour of $u_\tau(k, \rho_0)$ in comparison to the behaviour of Lane potential extracted from experimental data. It should be noted that for all the splittings of ε_{ex}^{l} and ε_{ex}^{ul}, for which the curves of $u_\tau(k, \rho_0)$ pass through the experimentally allowed region will give neutron effective mass to be greater than proton effective mass.

The divergent nature of the curves at higher momenta, shown in Fig. 3.9, emphasizes the importance of a more detailed understanding of isovector part of the nuclear mean field $u_\tau(k, \rho)$ over a wide range of momentum and density which can only be achieved through a continuous analysis of nucleon–nucleus scattering data at intermediate energies as well as experimental observables sensitive to the differences between neutron and proton flow data in highly asymmetric dense nuclear matter.

3.6. Nuclear symmetry energy

To study the density dependence of nuclear symmetry energy $J_\tau(\rho)$, we first examine the validity of the approximation given in Eq. (3.24). To do so in Fig. 3.10 we have plotted the functional $[e(\rho_n, \rho_p) - e(\rho)]$ as a function of σ^2 for three different densities $\rho = \rho_0$, $3\rho_0$ and $5\rho_0$ for the parameter set: $\gamma = 1/6$, $\varepsilon_{ex}^{l} = 4\varepsilon_{ex}/3$ and $J_\tau(\rho_0) = 30$ *MeV* given in table 3.2(ii). The linear relation between the functional $[e(\rho_n, \rho_p) - e(\rho)]$ and σ^2 seen from Fig. 3.10, indicates that the empirical parabolic law is valid for neutron–rich matter. We have verified that this holds true for all the parameter sets given in table 3.2.

In Fig. 3.11 we have shown nuclear symmetry energy $J_\tau(\rho)$, calculated from the relations given in Eqs. (3.20), (3.24), (3.25) and (3.41) for the parameter set $\gamma = 1/6$, $\varepsilon_{ex}^{l} = 4\varepsilon_{ex}/3$ and $J_\tau(\rho_0) = 30$ *MeV*, over a wide range of density. We have taken $\sigma = 0.5$ in the calculation where ever necessary. It is seen that all the relations are almost equal to each other. Only at very high densities $\rho > 7\rho_0$ there appears a slight discrepancy. From Fig. 3.11 it is evident that the definition of nuclear symmetry energy $J_\tau(\rho)$ given in Eq. (3.41) is valid.

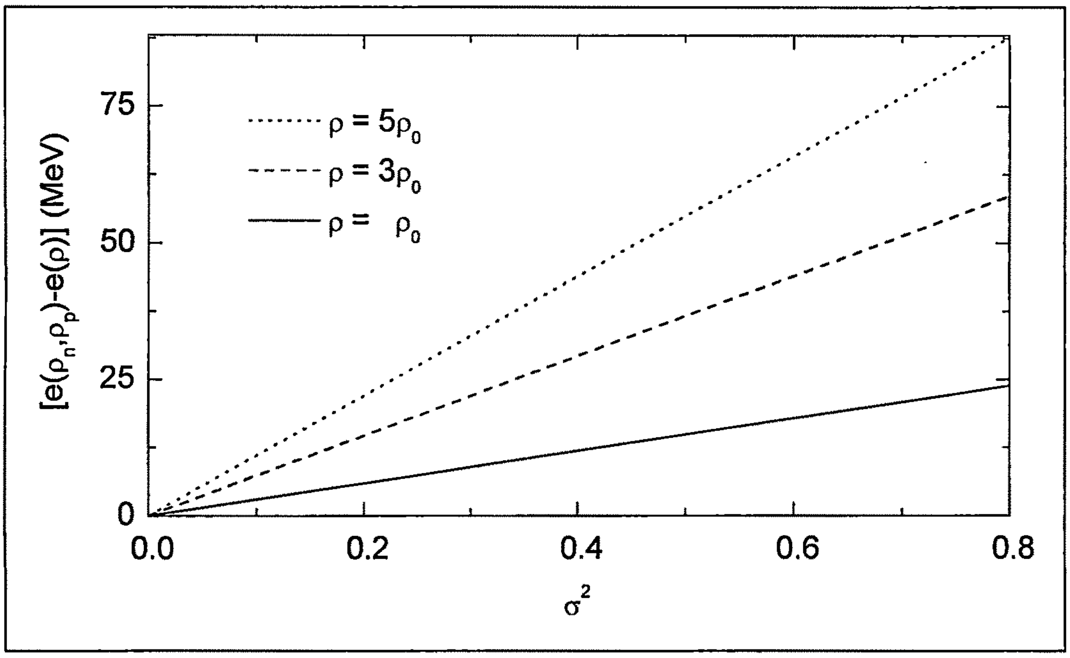

Figure 3.10: The functional $[e(\rho_n, \rho_p) - e(\rho)]$ is shown as function of σ^2 for densities $\rho = \rho_0$, $3\rho_0$ and $5\rho_0$ for the parameter set: $\varepsilon_{ex}^{l} = 4\varepsilon_{ex}/3$, $\gamma = 1/6$ and $J_\tau(\rho_0) = 30$ MeV.

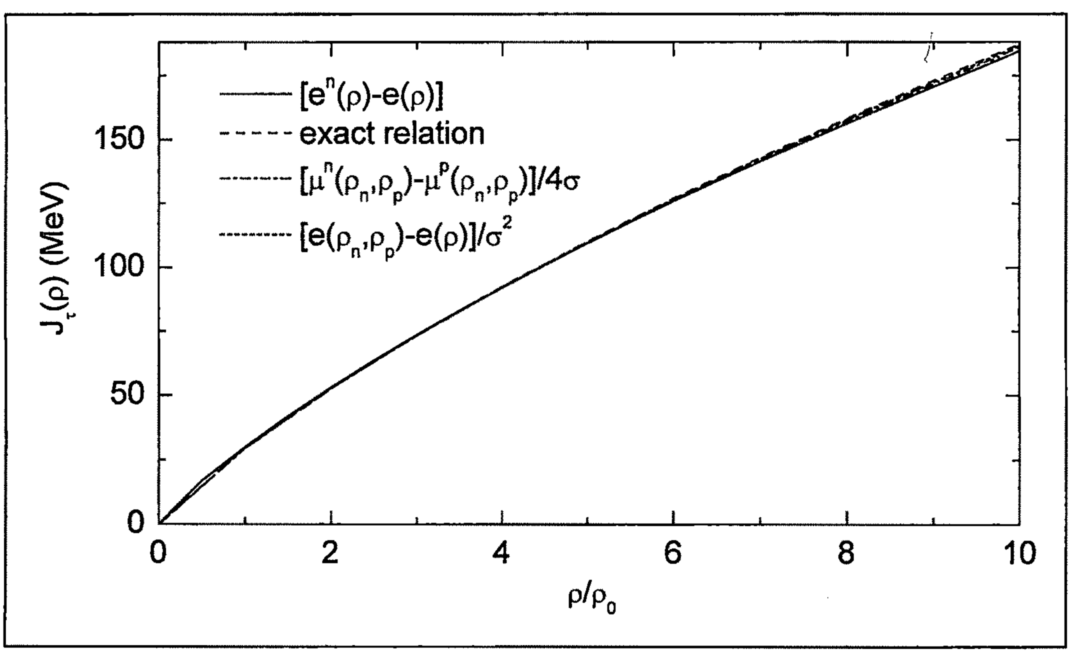

Figure 3.11: Nuclear symmetry energy $J_\tau(\rho)$ calculated from Eqs. (3.20), (3.24), (3.25) and (3.41) shown as function of density for the parameter set $\varepsilon_{ex}^{l} = 4\varepsilon_{ex}/3$, $\gamma = 1/6$ and $J_\tau(\rho_0) = 30$ MeV.

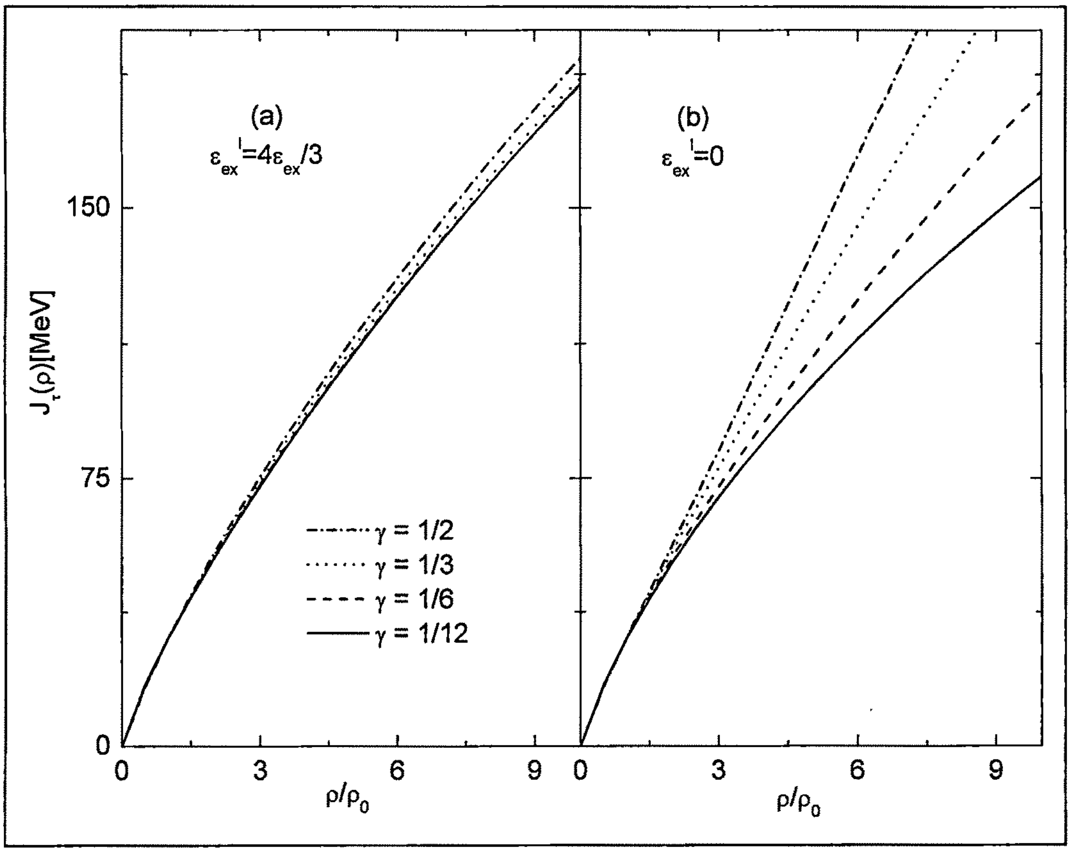

Figure 3.12: Influence of parameter γ on high density behaviour of nuclear symmetry energy $J_\tau(\rho)$ for the stiffest EOS of PNM is shown for two typical values of ε_{ex}^{l} with $J_\tau(\rho_0)$ = 30 MeV. The left panel (ε_{ex}^{l} = $4\varepsilon_{ex}/3$) and right panel (ε_{ex}^{l} = 0) exhibit the minimum and maximum influence of the parameter γ.

The value of $J_\tau(\rho)$ has been calculated from Eq. (3.41) over a wide rage of density for different sets of parameters given in table 3.2 with different values of γ, ε_{ex}^{l} and $J_\tau(\rho_0)$. It is observed that the curves of $J_\tau(\rho)$ are least influenced by different values of the exponent γ when ε_{ex}^{l} is around $4\varepsilon_{ex}/3$, whereas, these curves are most influenced by different values of γ when ε_{ex}^{l} = 0. This is shown in Fig. 3.12 (a) and (b) for γ = 1/12, 1/6, 1/3 and 1/12 with the same value of $J_\tau(\rho_0)$ = 30 MeV. All the four curves of $J_\tau(\rho)$ with ε_{ex}^{l} = $4\varepsilon_{ex}/3$ shown in Fig. 3.12 (a) are nearly same over the entire range of density involved. On the other hand these curves become more and more stiff at higher densities with increase in γ for the case ε_{ex}^{l} = 0 shown in Fig. 3.12 (b).

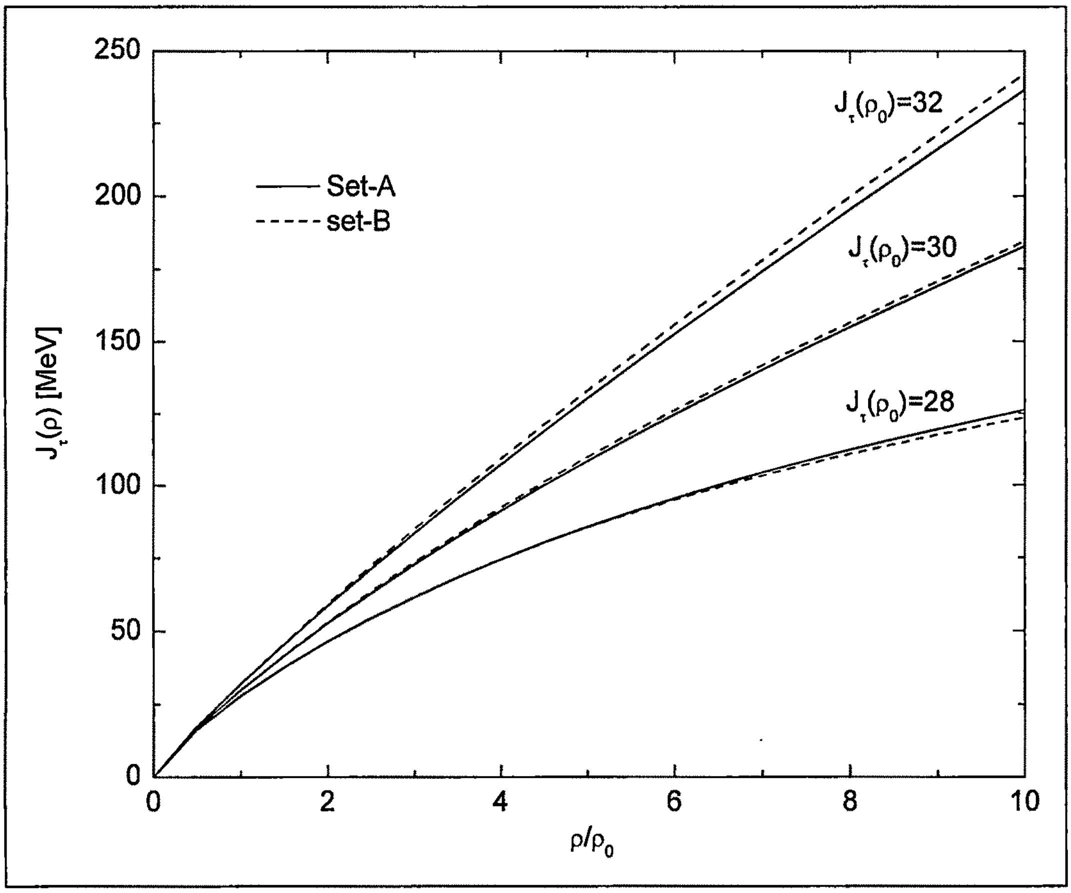

Figure 3.13: High density behaviour of nuclear symmetry energy for the stiffest EOS of PNM is shown for two different exchange parameter sets A and B (see text) with $\gamma = 1/6$ and $J_\tau(\rho_0) = 28$, 30 and 32 MeV.

It is also observed that variation of the parameter ε_{ex}^{l} over its range $0 - 2\varepsilon_{ex}$ has a very little influence on the density dependence of $J_\tau(\rho)$ when γ is around 1/6. This is shown in Fig. 3.13 for the two different sets of exchange strength parameters A and B with three standard values of $J_\tau(\rho_0) = 28$, 30 and 32 MeV. The curves of $J_\tau(\rho)$ are almost same over the entire range of density for the two sets of exchange strength parameters A and B corresponding to a given value of $J_\tau(\rho_0)$. The stiffness of the curves increase steadily with increase in the standard value of $J_\tau(\rho_0)$. Here we have an example of different EOS in ANM which share the same density dependence of nuclear symmetry energy $J_\tau(\rho)$ over a wide range of density but having quite contradicting momentum dependence of the isovector part of nuclear mean filed leading to two opposite types of splitting of neutron and proton effective masses.

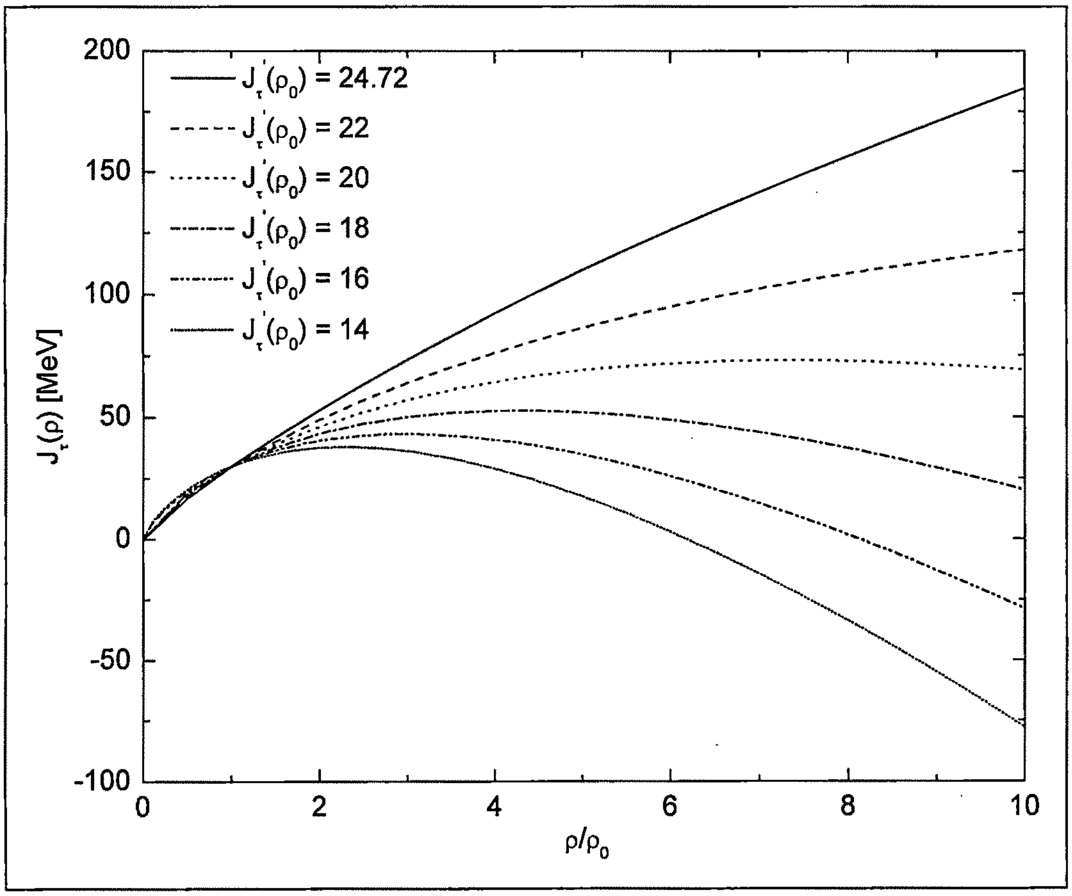

Figure 3.14: High density behaviour of nuclear symmetry energy $J_\tau(\rho)$ for six different EOS of PNM including the stiffest one are shown in decreasing order of stiffness from top to bottom. All the curves correspond to $\varepsilon_{ex}^{l} = 4\varepsilon_{ex}/3$, $\gamma = 1/6$ and $J_\tau(\rho_0) = 30$ MeV but differ in the values of the gradient $J'_\tau(\rho_0)$.

The density dependence of $J_\tau(\rho)$ obtained from several other admissible EOS of PNM under the constraint in Eq. (3.40) but softer than the stiffest one are shown in Fig. 3.14. The six different curves shown in this figure correspond to $\gamma = 1/6$, $\varepsilon_{ex}^{l} = 4\varepsilon_{ex}/3$, $J_\tau(\rho_0) = 30$ MeV and are distinguished from each other by the value of the gradient $J_\tau'(\rho_0)$ at normal density. These curves clearly exhibit the extremely divergent and even contradicting behaviour of $J_\tau(\rho)$ at high densities predicted by different theoretical calculations [1, 27, 28].

In connection with the extremely divergent and even contradicting high density behaviour of nuclear symmetry energy as seen from Fig. 3.14 it may be noted here that Stone *et al.* [19] have recently analysed the high density behaviour of $J_\tau(\rho)$ for 87 different Skyrme interactions. It is observed that only 27 of these interactions give a monotonically increasing behaviour of $J_\tau(\rho)$ over a wide range of density. For the other interactions considered in ref. [19] with increase in density $J_\tau(\rho)$ reaches a maximum value and then decreases until it becomes negative. Microscopic calculations based on realistic nucleon–nucleon interactions as well as RMF calculations predict a monotonically increasing behaviour of $J_\tau(\rho)$.

3.6.1. The slope and curvature parameter

The nuclear symmetry energy $J_\tau(\rho)$ can be expanded into a Taylor series about $\rho = \rho_0$ and is given as

$$J_\tau(\rho) = J_\tau(\rho_0) + \frac{(\rho-\rho_0)}{\rho_0}\left[\frac{\partial J_\tau(\rho)}{\partial \rho}\right]_{\rho=\rho_0} + \frac{(\rho-\rho_0)^2}{2!\,\rho_0^{\,2}}\left[\frac{\partial^2 J_\tau(\rho)}{\partial \rho^2}\right]_{\rho=\rho_0} + \ldots.. \qquad \ldots(3.54)$$

Neglecting higher order terms than second order the symmetry energy is very often written as

$$J_\tau(\rho) = J_\tau(\rho_0) + \frac{L(\rho_0)}{3}\left(\frac{\rho-\rho_0}{\rho_0}\right) + \frac{K_{sym}(\rho_0)}{18}\left(\frac{\rho-\rho_0}{\rho_0}\right)^2, \qquad \ldots(3.55)$$

were $L(\rho_0) = 3\,J_\tau'(\rho_0)$ is the slope parameter and $K_{sym}(\rho_0) = 9\,J_\tau''(\rho_0)$ is the curvature parameter of the nuclear symmetry energy around saturation density ρ_0. The slope parameter $L(\rho_0)$ and the curvature parameter $K_{sym}(\rho_0)$ can provide important information on the density dependence of nuclear symmetry energy $J_\tau(\rho)$ at both high and low densities. The slope parameter is strongly related to the thickness of neutron skin in heavy nuclei. So information on the slope parameter can be found from measurements of neutron skin thickness in heavy nuclei [1, 5, 13]. Unfortunately there is large uncertainty in measured neutron skin thickness values of heavy nuclei. Recently in ref. [10] it has been suggested that the value of slope parameter $L(\rho_0)$ lies in the range 62 $MeV \leq L(\rho_0) \leq 107$ MeV from a combination of analysis of neutron skin thickness in finite nuclei and isospin diffusion in high energy heavy ion collisions.

At normal nuclear matter density ρ_0 and around $\sigma = 1/2$, the incompressibility of ANM can also be expressed as

$$K(\rho_0, \sigma) = K(\rho_0) + (1-2\sigma)^2 K_{asy}(\rho_0), \qquad \ldots(3.56)$$

where we have neglected terms higher than second order. $K(\rho_0)$ is the incompressibility of symmetric nuclear matter at saturation density ρ_0 and $K_{asy}(\rho_0)$ is the isospin dependent part of nuclear incompressibility in ANM. Neglecting higher order terms $K_{asy}(\rho_0)$ is related to the slope and curvature parameters of nuclear symmetry energy by the relation

$$K_{asy}(\rho_0) \approx K_{sym}(\rho_0) - 6L(\rho_0). \qquad \ldots(3.57)$$

The value of $K_{asy}(\rho_0)$ can be extracted from Giant Monopole Resonance (GMR) data of neutron–rich nuclei. Recent measurements from GMR of the even–A Sn isotopes gives the value of $K_{asy}(\rho_0) = -550 \pm 100$ MeV [150]. In ref. [14] the value of $K_{asy}(\rho_0)$ is estimated in the range -500 ± 50 MeV from analysis of isospin diffusion in high energy heavy–ion collisions.

We have calculated the values of slope parameter $L(\rho_0)$ and isospin dependent part of nuclear incompressibility in ANM $K_{asy}(\rho_0)$ for the different parameter sets given in table 3.2(i)–3.2(iii). It was seen that the value of $L(\rho_0)$ lies in the range 62 $MeV \leq L(\rho_0) \leq 110$ MeV which can be compared with neutron skin thickness in finite nuclei and isospin diffusion in high energy heavy ion collisions. The value of $K_{asy}(\rho_0)$ was found to lie in the range $-$ 531.88 MeV to $-$ 424.56 MeV which is within the experimental range found from analysis of isospin diffusion in HI collisions.

3.7. Energy per particle, pressure, incompressibility, chemical potential and speed of sound in ANM

We have also calculated a few properties of ANM at zero temperature such as energy density, pressure, neutron and proton chemical potentials, nuclear matter incompressibility and speed of sound in nuclear matter. These properties of ANM has been calculated for all the parameter sets given in table 3.2. We have shown here the results for the parameter set $\gamma = 1/6$, $\varepsilon_{ex}^{l} = 2\varepsilon_{ex}/3$, $J_\tau(\rho) = 30$ MeV. It has been verified that other parameter sets also show similar type of behaviour for the nuclear matter property as for the parameter set shown here.

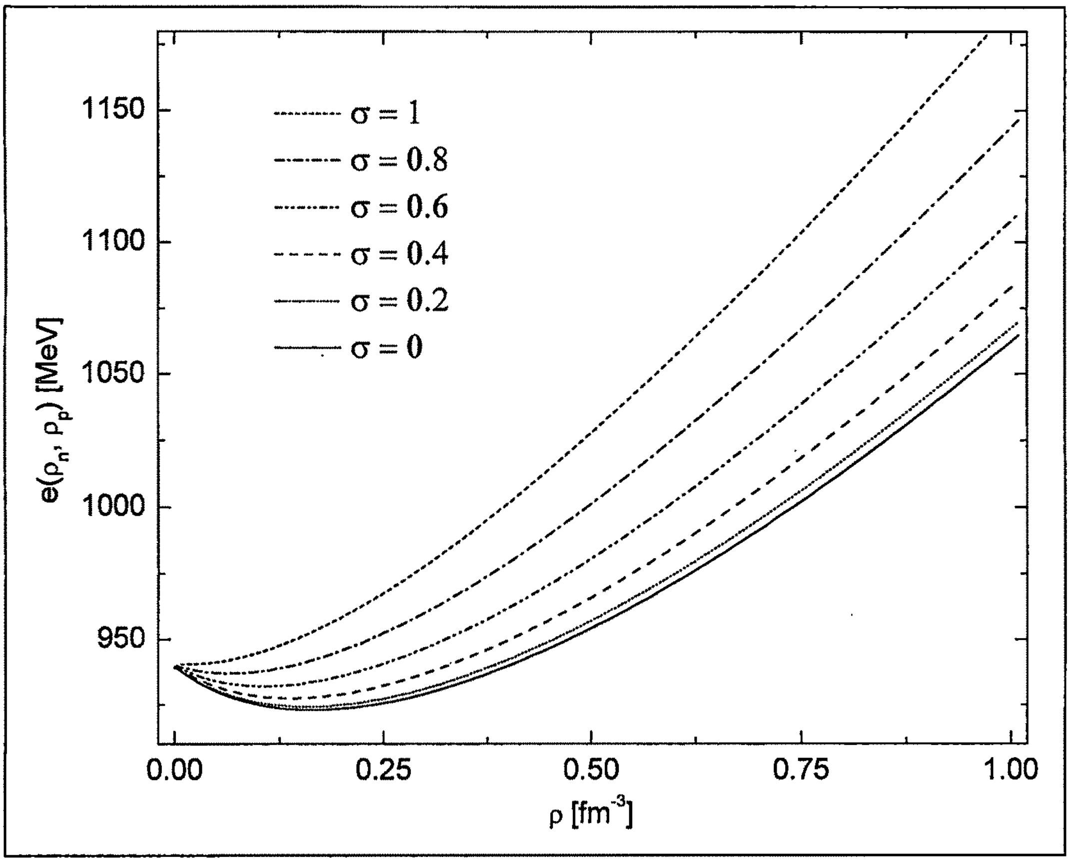

Figure 3.15: Energy per particle $e(\rho_n, \rho_p)$ in ANM is shown as function of density for different values of σ for the parameter set $\varepsilon_{ex}^{\ l} = 4\varepsilon_{ex}/3$, $\gamma = 1/6$ and $J_\tau(\rho_0) = 30\ MeV$.

In fig 3.15 we have shown the energy per particle $e(\rho_n, \rho_p)$ in ANM as a function of total nuclear density ρ for different values of asymmetry parameter σ from 0 (SNM) to 1 (PNM). It is seen that energy per particle $e(\rho_n, \rho_p)$ at first decreases and then increases with increase in density, except for $\sigma = 1$ where it increases monotonically with increase in density, indicating the fact that PNM is not bound. An important property of EOS of ANM is the variation of saturation density with asymmetry parameter σ keeping in mind that saturation must disappear when σ increases, as PNM is not bound. From Fig. 3.15 it can be seen that the saturation density decreases with increase in σ.

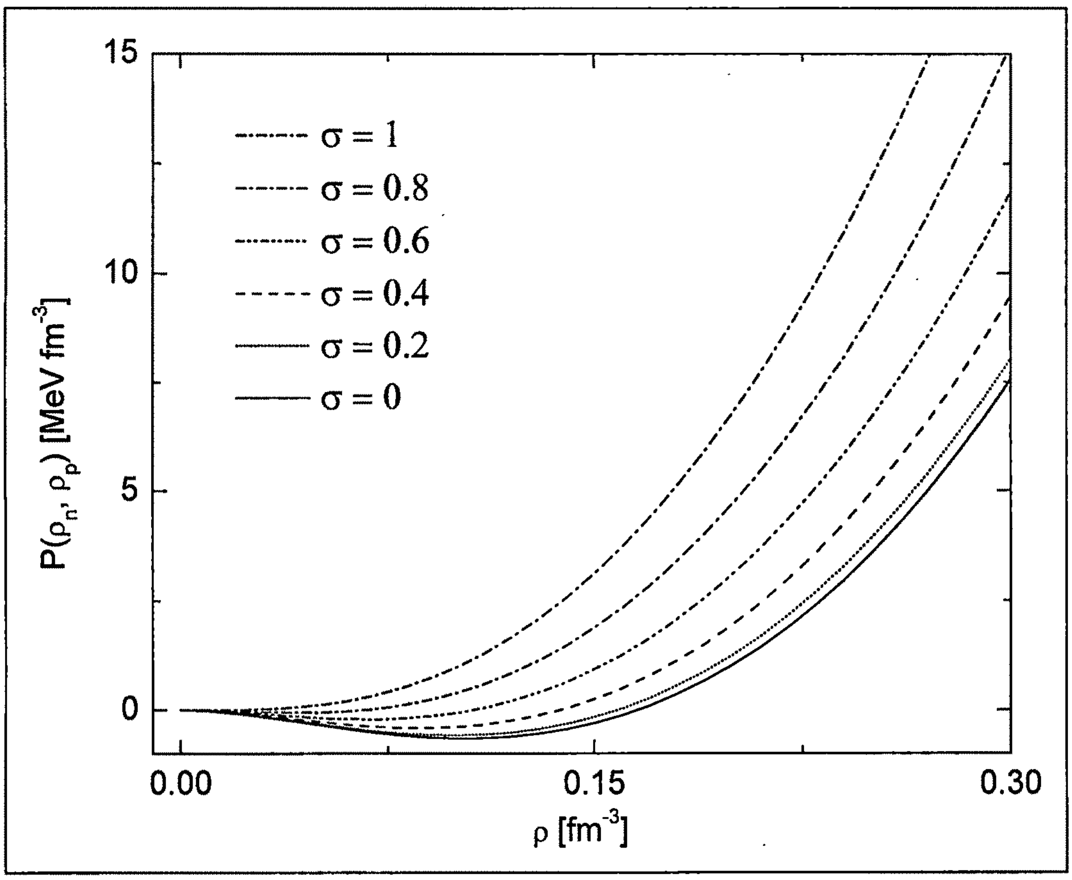

Figure 3.16: Pressure $P(\rho_n, \rho_p)$ in ANM is shown as function of density for different values of σ for the parameter set $\varepsilon_{ex}^{l} = 4\varepsilon_{ex}/3$, $\gamma = 1/6$ and $J_\tau(\rho_0) = 30$ MeV.

In Fig. 3.16 we have shown pressure $P(\rho_n, \rho_p)$ in ANM as a function of total nucleon density ρ for different values of asymmetry parameter σ. It is seen that pressure $P(\rho_n, \rho_p)$ in ANM at first decreases and then increases with increase in density, except for $\sigma = 1$ where it increases monotonically with increase in density. With increase in asymmetry parameter σ the value of pressure $P(\rho_n, \rho_p)$ in ANM increases for a given total nucleon density ρ.

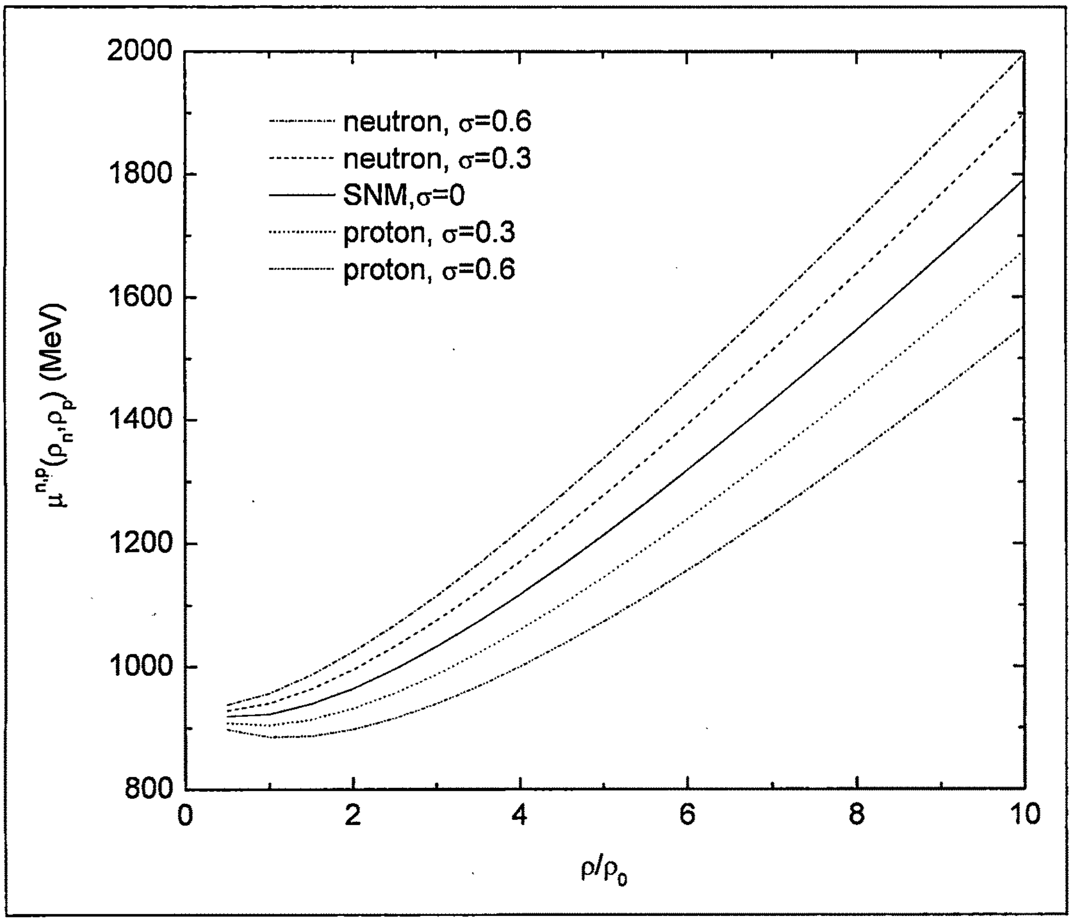

Figure 3.17: Variation of chemical potentials $\mu^{n,p}(\rho_n, \rho_p)$ with density ρ for different asymmetries σ = 0, 0.3 and 0.6 for the parameter set $\varepsilon_{ex}^{l} = 4\varepsilon_{ex}/3$, $\gamma = 1/6$ and $J_\tau(\rho_0)$ = 30 MeV.

In Fig. 3.17 we have shown the variation of neutron and proton chemical potentials $\mu^{n,p}(\rho_n, \rho_p)$ with density ρ for different asymmetries σ = 0, 0.3 and 0.6. It can be seen that both neutron and proton chemical potentials $\mu^{n,p}(\rho_n, \rho_p)$ increase with increase in density ρ. With increase in asymmetry the neutron chemical potential μ^n (ρ_n, ρ_p) increases while $\mu^p(\rho_n, \rho_p)$ decreases.

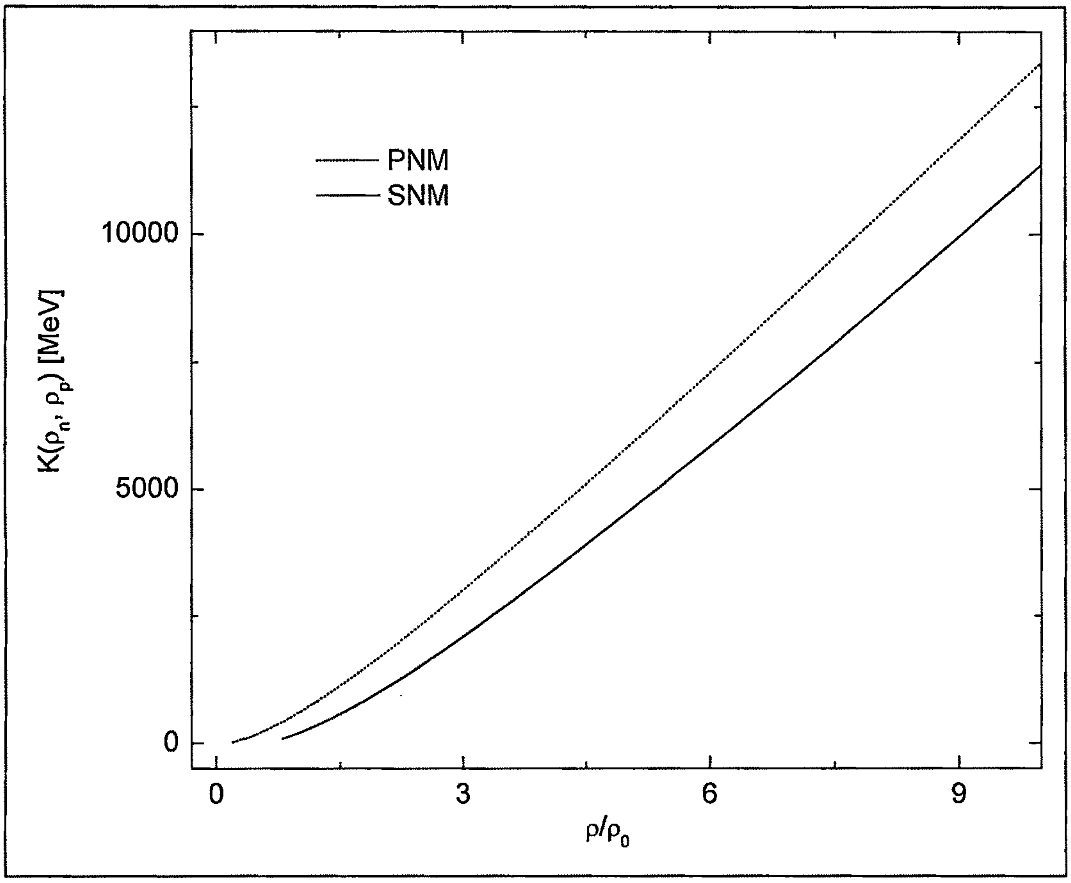

Figure 3.18: Nuclear incompressibility in SNM and PNM is shown as function of density for the parameter set $\varepsilon_{ex}^{l} = 4\varepsilon_{ex}/3$, $\gamma = 1/6$ and $J_\tau(\rho_0) = 30\ MeV$.

The incompressibility of nuclear matter $K(\rho_n, \rho_p)$ is shown as function of ρ/ρ_0 for SNM and PNM in Fig. 3.18. It is seen that with increase in density incompressibility of nuclear matter increases. The incompressibility of PNM is greater than SNM.

The speed of sound in nuclear matter is an important property which has been defined in Eq. (3.22). The widely used Skyrme forces violate causality in extremely dense nuclear matter, when a nonrelativistic treatment for speed of sound is adopted [123]. This phenomena of causal violation is also known as supraluminosity which should be always avoided. The speed of sound in nuclear matter v^2/c^2 as function of density is shown in Fig. 3.19 for SNM and PNM. It is seen that the speed of sound v^2/c^2 increases with increase in density for both the cases. However, it remains below the speed of light at any density. From Fig. 3.19 it can be also observed that at very high density the speed of sound in SNM becomes larger than that in PNM.

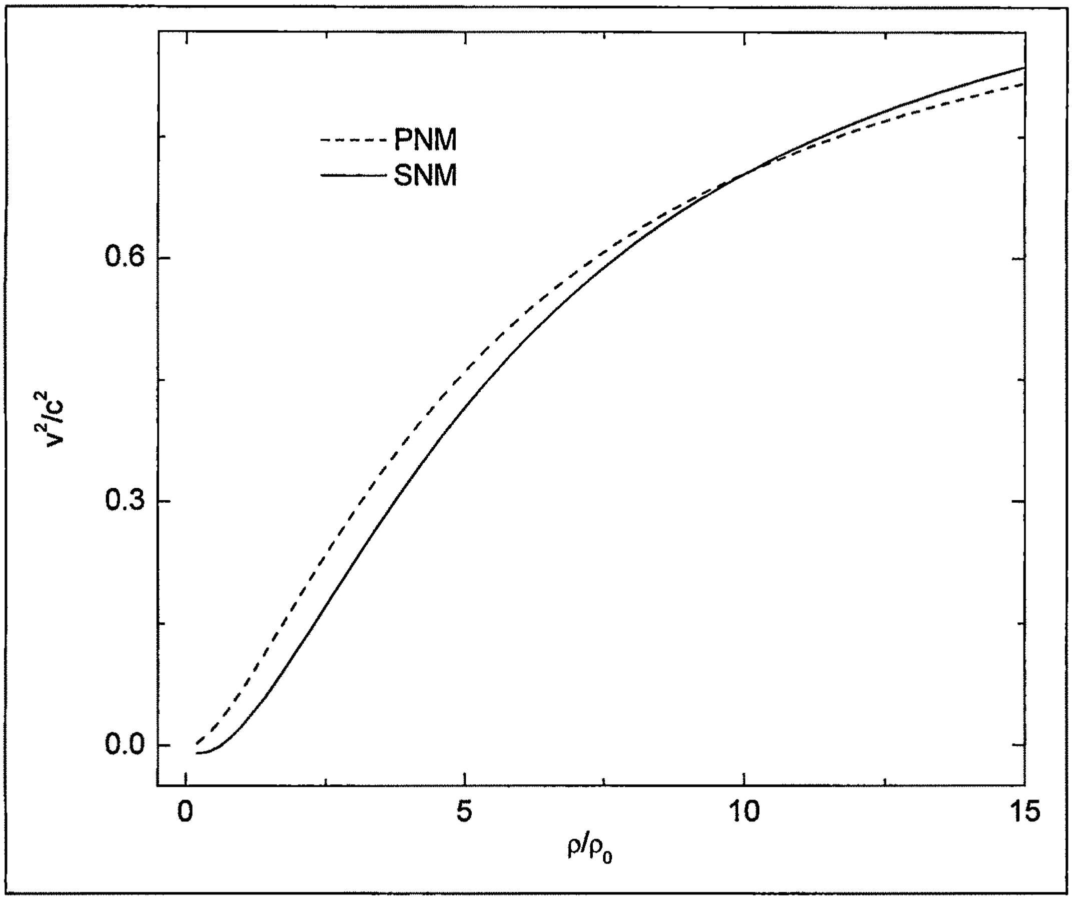

Figure 3.19: Speed of sound in nuclear medium v^2/c^2 in SNM and PNM is shown as function of density for the parameter set $\varepsilon_{ex}^{l} = 4\varepsilon_{ex}/3$, $\gamma = 1/6$ and $J_\tau(\rho_0) = 30\ MeV$.

3.8. Summary

In this chapter a simple density dependent finite range effective interaction, having Yukawa form for the short range exchange interaction part, was chosen to analyse the EOS and properties of nuclear matter. The EOS of asymmetric nuclear matter (ANM) was constructed for this simple short range effective interaction in such a way that a minimum number of parameters were sufficient to describe the EOS of ANM. To explain the EOS of ANM it was observed that nine adjustable interaction parameters were required. Since a complete description of ANM is equivalent to separate description of SNM and PNM, to determine the parameters required to describe ANM, the parameters involved in the EOS of SNM and PNM were fixed from simple physical conditions and existing experimental/empirical data. Some parameters like γ, related to nuclear matter incompressibility and the exchange strength parameters between like nucleons ε_{ex}^{l}, and the value of $J_{\tau}(\rho_0)$ were kept open to analyse their effect on the EOS of ANM. The density dependence of energy per particle and pressure in SNM and pressure in PNM were calculated using these parameters and were compared with experimental results from flow of matter in high energy heavy–ion collisions. Using the parameters the momentum, density and asymmetry dependence of a number of nuclear matter properties were studied.

The parameter dependence of neutron and proton effective mass splitting was examined for two parameter sets A and B having same range but different strengths for interaction between like and unlike nucleons. Two different trends of neutron and proton effective mass splitting were noticed; one where the neutron effective mass is greater than proton effective mass and the other where the proton effective mass is greater than the neutron effective mass. This clearly shows that for non–relativistic effective interaction the sign of the neutron–proton effective mass splitting depends on the value of the parameters involved in the exchange part of the effective interaction.

The extremely divergent and contradicting behaviour of the functional $u_{\tau}^{ex}(k,\rho)$ with momentum was examined for the two parameter sets A and B. The momentum dependence of isovector part of nuclear mean filed $u_{\tau}(k, \rho)$ was also studied for the two parameter sets A and B. Two different trends of momentum dependence were noticed; one in which $u_{\tau}^{ex}(k,\rho)$ and $u_{\tau}(k, \rho)$ increase with increase in momentum and the other where they decrease with increase in momentum. The momentum dependence of Lane potential at normal nuclear matter density ρ_0 extracted from nucleon–nucleus scattering data was used to constrain the momentum dependence of isovector part of nuclear mean field $u_{\tau}(k, \rho_0)$ at normal nuclear matter density ρ_0.

The density dependence of nuclear symmetry energy $J_{\tau}(\rho)$ was studied using a number of parameter sets giving the stiffest EOS of ANM satisfying the stability condition of PNM. It was observed that the exchange strength parameter has little influence on the density dependence of nuclear symmetry energy. It was also shown that EOS satisfying the stability condition but softer than the stiffest one can give rise to different behaviour of nuclear symmetry energy $J_\tau(\rho)$. Here in this chapter we are not constraining the high density behaviour of nuclear symmetry energy $J_\tau(\rho)$.

Properties of nuclear matter such as energy density, pressure, chemical potential, incompressibility and speed of sound were calculated over a wide range of density and asymmetry.

In the next chapter we will study the nuclear EOS at temperature $T \neq 0$ and study the liquid–gas phase transition in ANM using the simple short range effective interaction.

CHAPTER 4

EQUATION OF STATE OF NUCLEAR MATTER AT FINITE TEMPERATURE AND PHASE TRANSITION

4.1. Introduction

In the past few decades significant effort has been given to the study of EOS and properties of ANM at zero temperature. The EOS and properties of ANM at finite temperature ($T \neq 0$), on the other hand, has received very little attention so far [151–154]. During the dynamical evolution of HI collisions at intermediate and high energies a transient state of hot and dense matter can be produced and liquid–gas phase transition may occur depending on the temperatures and densities involved [155, 156]. Besides its role in nuclear physics, EOS of hot ANM plays an important role in understanding astrophysical phenomena involved in supernova explosion and evolution of protoneutron stars formed during the latest stage of type–II supernova collapse [38]. Due to the van der Waals–like behaviour of NN interaction, it has long been expected that a liquid–gas (LG) like phase transition occurs in nuclear matter at low density and moderate temperature [156]. Since the early works, see, e.g., refs. [157–159], many investigations have been carried out to explore the properties of nuclear LG phase transition both experimentally and theoretically over the last three decades [160]. Most of these studies focus on investigating features of the LG phase transition in SNM. In SNM the phase transition studies are relatively easier than that of ANM where one has to deal with separate neutron and proton chemical potentials. The LG phase–transition was suggested to be of second order in ANM in contrast to the first order transition that occurs in SNM [156]. This suggestion together with the need to better understand the properties of hot ANM have recently stimulated much work, see, e.g., refs. [1, 151, 161–167].

The EOS of hot nuclear matter has been studied widely using phenomenological approaches; such as non–relativistic models [108, 109, 159, 163] and RMF theory [156,162]. All of these investigations predict a Van der Waals behaviour for infinite SNM. The critical temperature T_c of the liquid–gas phase transition predicted by these models is in the range from 14 to 20 MeV depending on the adopted models and NN interactions. In ref. [108] the EOS of SNM at finite temperature was studied using a simple density dependent short range interaction of conventional form. The value of T_c was obtained to be 14.9 MeV. In ref. [156] the liquid–gas phase transition in ANM has been studied in detail where the RMF theory has been used to construct the EOS of ANM at finite temperature. Along microscopic approach the EOS of nuclear matter at finite temperature has been studied using various approaches, e.g., see refs. [168–170]. In ref. [168], the liquid–gas phase transition has been predicted for SNM by using the variational method based on the Argonne V14 two–body NN interaction plus a phenomenological three body force and the critical temperature obtained is about 17.5 MeV close to the values from Skyrme forces calculations. Using DB calculation in ref. [169] the critical temperature was predicted to be as low as 10 MeV. Recently Zuo *et al.* [167] have studied the properties of hot ANM and isospin dependence of the liquid–gas phase transition in finite–temperature BHF approach extended to include contribution from a three–body force. They predict T_c around 13 MeV for SNM.

In this chapter we will investigate the EOS of ANM at finite temperature using the simple density dependent finite range interaction which was used in chapter 3 to study the EOS of ANM at zero temperature. In section 4.2 we have constructed the EOS of ANM at finite temperature for the effective interaction given in Eq. (3.1). In section 4.3 the properties of ANM at finite temperature, such as energy density, pressure, chemical potential and nuclear symmetry energy were calculated for a wide range of temperature, density and asymmetry using the parameters given in table–2 from chapter 3. It should be mentioned here that at finite temperature analytical simplification is not possible and the properties of nuclear matter has been calculated self–consistently. The liquid–gas phase transition in ANM has been analysed in section 4.4. Finally a brief summary has been given in section 4.5.

4.2. EOS of ANM at finite temperature

The energy density functional $H_T(\rho_n, \rho_p)$ in ANM at temperature T obtained from the simple effective interaction given in Eq. (3.1) is given as

$$H_T(\rho_n,\rho_p)=\int[f_T^n(\vec{k})+f_T^p(\vec{k})](c^2\hbar^2k^2+M^2c^4)^{1/2}d^3k$$
$$+\frac{1}{2}\left[\frac{\varepsilon_0^l}{\rho_0}+\frac{\varepsilon_\gamma^l}{\rho_0^{\gamma+1}}\left(\frac{\rho}{1+b\rho}\right)^\gamma\right](\rho_n^2+\rho_p^2)+\left[\frac{\varepsilon_0^{ul}}{\rho_0}+\frac{\varepsilon_\gamma^{ul}}{\rho_0^{\gamma+1}}\left(\frac{\rho}{1+b\rho}\right)^\gamma\right]\rho_n\rho_p$$
$$+\frac{\varepsilon_{ex}^l}{2\rho_0}\iint[f_T^n(\vec{k})f_T^n(\vec{k}')+f_T^p(\vec{k})f_T^p(\vec{k}')]g_{ex}(|\vec{k}-\vec{k}'|)d^3kd^3k'$$
$$+\frac{\varepsilon_{ex}^{ul}}{2\rho_0}\iint[f_T^n(\vec{k})f_T^p(\vec{k}')+f_T^p(\vec{k})f_T^n(\vec{k}')]g_{ex}(|\vec{k}-\vec{k}'|)d^3kd^3k'$$

...(4.1)

The neutron and proton mean fields $u_T^n(k, \rho_n, \rho_p)$ and $u_T^p(k, \rho_n, \rho_p)$ at temperature T can be obtained from the respective functional derivative of the energy density $H_T(\rho_n, \rho_p)$ and are given as

$$u_T^n(k,\rho_n,\rho_p)=\varepsilon_0^l\frac{\rho_n}{\rho_0}+\varepsilon_0^{ul}\frac{\rho_p}{\rho_0}+\frac{\varepsilon_\gamma^l}{\rho_0^{\gamma+1}}\left(\frac{\rho}{1+b\rho}\right)^\gamma\rho_n+\frac{\varepsilon_\gamma^{ul}}{\rho_0^{\gamma+1}}\left(\frac{\rho}{1+b\rho}\right)^\gamma\rho_p$$
$$+\frac{1}{2}\frac{\varepsilon_\gamma^l}{\rho_0^{\gamma+1}}\frac{\gamma\rho^{\gamma-1}}{(1+b\rho)^{\gamma+1}}(\rho_n^2+\rho_p^2)+\frac{\varepsilon_\gamma^{ul}}{\rho_0^{\gamma+1}}\frac{\gamma\rho^{\gamma-1}}{(1+b\rho)^{\gamma+1}}\rho_n\rho_p$$
$$+\frac{\varepsilon_{ex}^l}{\rho_0}\int f_T^n(\vec{k}')g_{ex}(|\vec{k}-\vec{k}'|)d^3k'+\frac{\varepsilon_{ex}^{ul}}{\rho_0}\int f_T^p(\vec{k}')g_{ex}(|\vec{k}-\vec{k}'|)d^3k'$$

...(4.2)

and

$$u_T^p(k,\rho_n,\rho_p)=\varepsilon_0^l\frac{\rho_p}{\rho_0}+\varepsilon_0^{ul}\frac{\rho_n}{\rho_0}+\frac{\varepsilon_\gamma^l}{\rho_0^{\gamma+1}}\left(\frac{\rho}{1+b\rho}\right)^\gamma\rho_p+\frac{\varepsilon_\gamma^{ul}}{\rho_0^{\gamma+1}}\left(\frac{\rho}{1+b\rho}\right)^\gamma\rho_n$$
$$+\frac{1}{2}\frac{\varepsilon_\gamma^l}{\rho_0^{\gamma+1}}\frac{\gamma\rho^{\gamma-1}}{(1+b\rho)^{\gamma+1}}(\rho_n^2+\rho_p^2)+\frac{\varepsilon_\gamma^{ul}}{\rho_0^{\gamma+1}}\frac{\gamma\rho^{\gamma-1}}{(1+b\rho)^{\gamma+1}}\rho_n\rho_p$$
$$+\frac{\varepsilon_{ex}^l}{\rho_0}\int f_T^p(\vec{k}')g_{ex}(|\vec{k}-\vec{k}'|)d^3k'+\frac{\varepsilon_{ex}^{ul}}{\rho_0}\int f_T^n(\vec{k}')g_{ex}(|\vec{k}-\vec{k}'|)d^3k'$$

...(4.3)

The functional $g_{ex}(|k-k'|)$ appearing in the above equations is the normalized Fourier transform of the short range interaction $f(r)$ and is given by

$$g_{ex}(k) = \frac{\int e^{i(\vec{k}\cdot\vec{r})} f(r) d^3r}{\int f(r) d^3r}. \qquad ...(4.4)$$

For Yukawa form of $f(r)$ the functional $g_{ex}(k)$ is given as

$$g_{ex}(k) = (1+\alpha^2 k^2)^{-1} \qquad ...(4.5)$$

The pressure $P_T(\rho_n, \rho_p)$ at temperature T in ANM is defined as

$$P_T(\rho_n,\rho_p) = \rho_n \mu_T^n + \rho_p \mu_T^p - H_T(\rho_n,\rho_p) + T\left\{S_T^n(\rho_n,\rho_p) + S_T^P(\rho_n,\rho_p)\right\} \qquad ...(4.6)$$

where $\mu^{n,p}{}_T(\rho_n, \rho_p)$ are the chemical potentials given as

$$\mu_T^{n,p}(\rho_n,\rho_p) = \frac{\partial H_T(\rho_n,\rho_p)}{\partial \rho_{n,p}}, \qquad ...(4.7)$$

and $S_T^{n,P}(\rho_n,\rho_p)$ are the neutron, proton entropy density defined as

$$S_T^{n,P}(\rho_n,\rho_p) = -\frac{g}{(2\pi)^3}\int\left\{n_T^{n,P}(\vec{k})\ \ln\left(n_T^{n,P}(\vec{k})\right) + \left(1-n_T^{n,P}(\vec{k})\right)\ln\left(1-n_T^{n,P}(\vec{k})\right)\right\}d^3k \qquad ...(4.8)$$

In Eq. (4.8) g is the spin–isospin degeneracy factor and $n_T^{n,P}(k)$ are the neutron, proton occupation probability related to neutron, proton momentum distribution functions $f_T^{n,P}(k)$ by the Eqs. (2.13) and (2.14) given in chapter 2.

Similar to the case of zero temperature ANM, the empirical parabolic law for the EOS of ANM at density ρ, temperature T, and isospin asymmetry σ can be written as

$$e_T(\rho,\sigma) = e_T(\rho,\sigma=0) + \sigma^2[J_\tau(\rho)]_T \qquad ...(4.9)$$

Putting $\sigma = 1$ in the above equation we can get the expression for nuclear symmetry energy $[J_\tau(\rho)]_T$ at a finite temperature as

$$[J_\tau(\rho)]_T = e_T(\rho,\sigma=1) - e_T(\rho,\sigma=0) \qquad ...(4.10)$$

From the above equation it is clear that similar to zero temperature case, symmetry energy $[J_\tau(\rho)]_T$ at a finite temperature gives an estimation of the energy required to convert all protons in SNM to neutrons in PNM at fixed temperature T and density ρ.

4.3. Thermal evolution of ANM properties

In this section we analyze the thermal evolution of ANM properties, like energy density, pressure, chemical potential etc., using the simple effective interaction considered in this thesis work. Calculation of the above thermodynamical properties require a self–consistent evaluation of the momentum distribution functions as described in detail in chapter 2. To study the thermal evolution of properties of ANM, we have calculated the properties of ANM at finite temperature relative to their zero temperature results. In doing so it may be observed from Eqs. (4.1) – (4.8) and (3.7) – (3.19) that we require the knowledge of only the range parameter α and exchange strength parameters $\varepsilon_{ex}{}^{l}$ and $\varepsilon_{ex}{}^{ul}$ to study the thermal evolution of ANM properties.

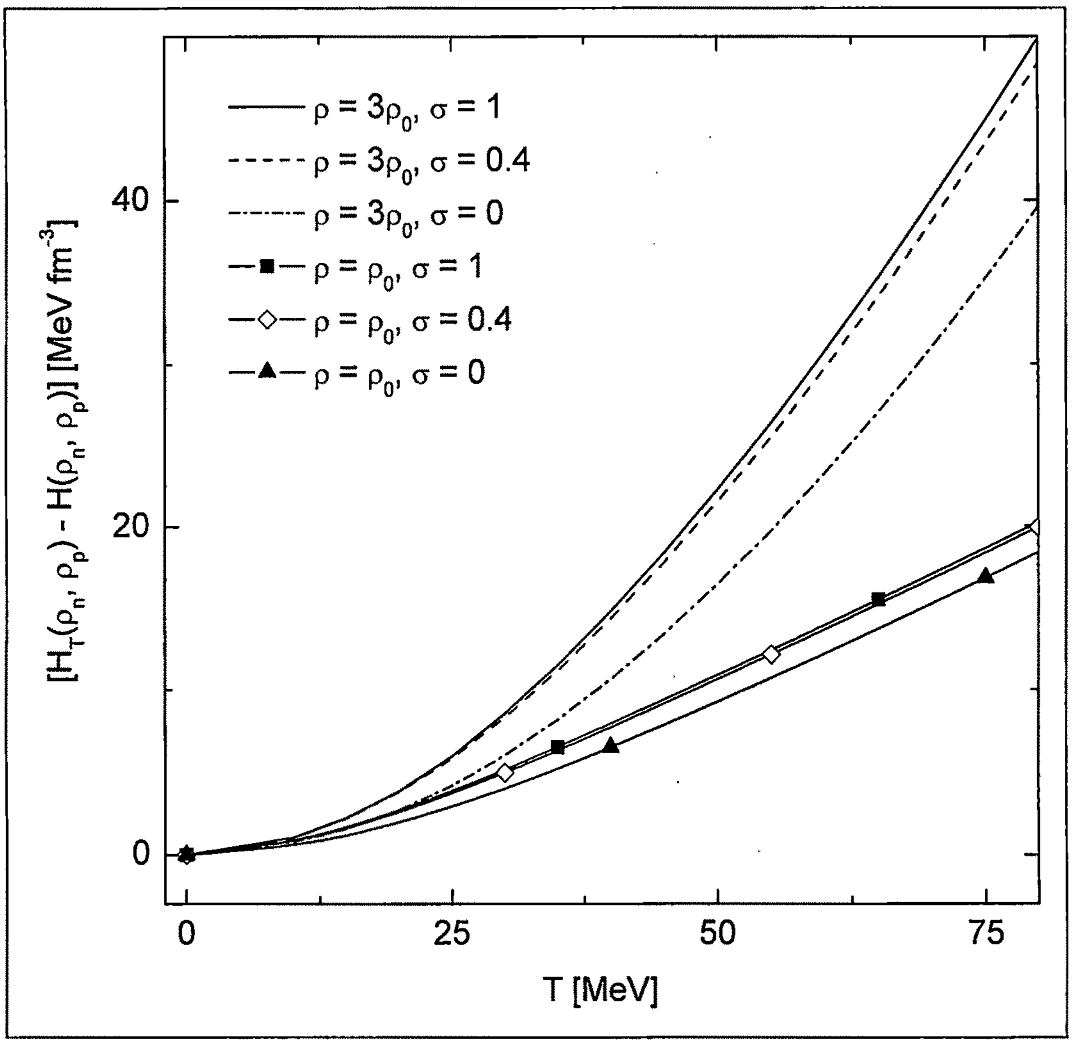

Figure 4.1: The functional $[H_T(\rho_n, \rho_p) - H(\rho_n, \rho_p)]$ as function of temperature T for different asymmetries (σ = 0, 0.4 and 1) and densities ($\rho = \rho_0$ and $3\rho_0$) for the parameter set $\varepsilon_{ex}{}^{l} = 2\varepsilon_{ex}/3$.

In Fig. 4.1 the functional $[H_T(\rho_n, \rho_p) - H(\rho_n, \rho_p)]$ has been plotted as function of temperature T for different asymmetries (σ = 0, 0.4 and 1) and densities ($\rho = \rho_0$ and $3\rho_0$) for the parameter set $\varepsilon_{ex}^{\,l} = 2\varepsilon_{ex}/3$. It can be seen that the functional $[H_T(\rho_n, \rho_p) - H(\rho_n, \rho_p)]$ increases with increase in temperature T. For a fixed temperature, with increase in density the functional $[H_T(\rho_n, \rho_p) - H(\rho_n, \rho_p)]$ increases.

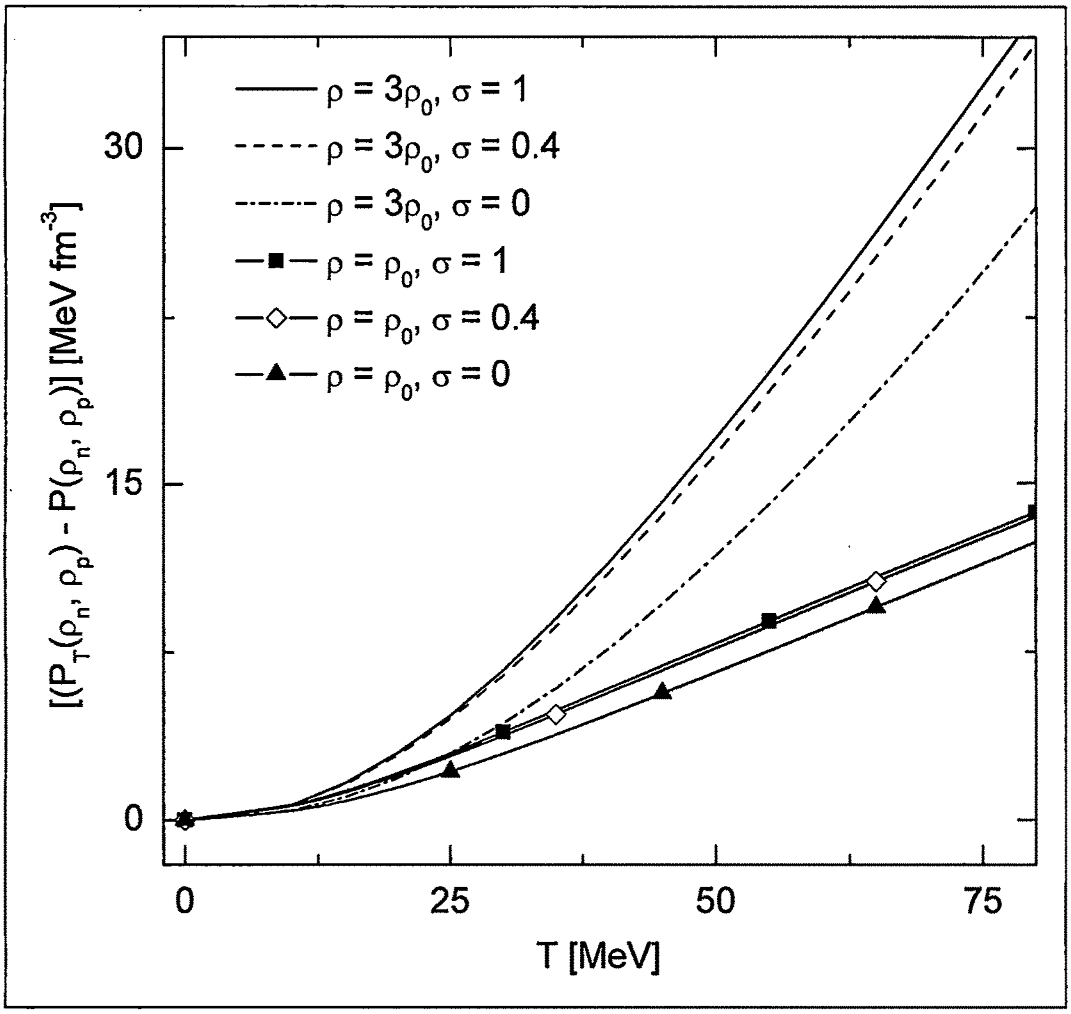

Figure 4.2: The functional $[P_T(\rho_n, \rho_p) - P(\rho_n, \rho_p)]$ as function of temperature T for different asymmetries (σ = 0, 0.4 and 1) and densities ($\rho = \rho_0$ and $3\rho_0$) for the parameter set $\varepsilon_{ex}^{\,l} = 2\varepsilon_{ex}/3$.

In Fig. 4.2 the functional $[P_T(\rho_n, \rho_p) - P(\rho_n, \rho_p)]$ has been plotted as function of temperature T for different asymmetries (σ = 0, 0.4 and 1) and densities ($\rho = \rho_0$ and $3\rho_0$) for the parameter set $\varepsilon_{ex}^{\,l} = 2\varepsilon_{ex}/3$. It can be seen that the functional $[P_T(\rho_n, \rho_p) - P(\rho_n, \rho_p)]$ increases with increase in temperature T.

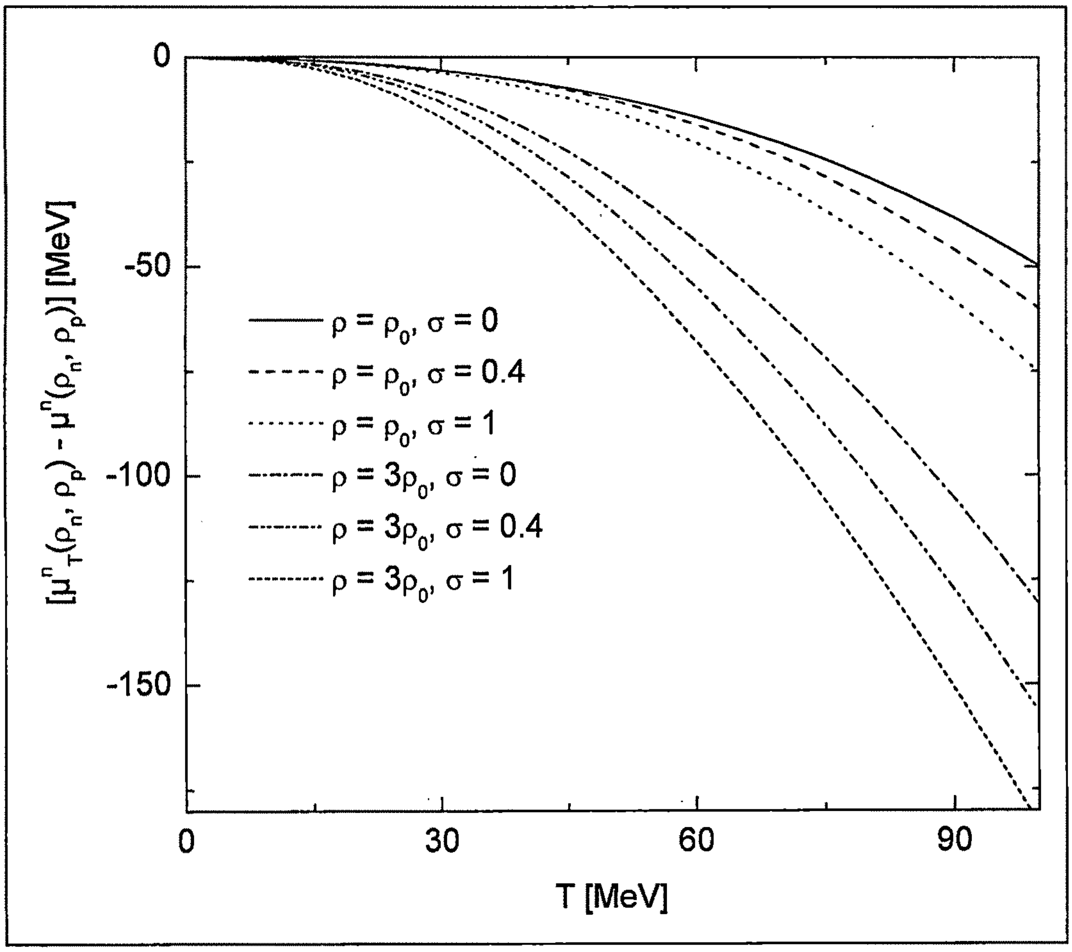

Figure 4.3: The functional $[\mu^n{}_T(\rho_n, \rho_p) - \mu^n(\rho_n, \rho_p)]$ as function of temperature T for different asymmetries (σ = 0, 0.4 and 1) and densities ($\rho = \rho_0$ and $3\rho_0$) for the parameter set $\varepsilon_{ex}{}^l = 2\varepsilon_{ex}/3$.

In Fig. 4.3 the functional $[\mu^n{}_T(\rho_n, \rho_p) - \mu^n(\rho_n, \rho_p)]$ has been plotted as function of temperature T for different asymmetries (σ = 0, 0.4 and 1) and densities ($\rho = \rho_0$ and $3\rho_0$) for the parameter set $\varepsilon_{ex}{}^l = 2\varepsilon_{ex}/3$. It can be seen that the functional $[\mu^n{}_T(\rho_n, \rho_p) - \mu^n(\rho_n, \rho_p)]$ decreases with increase in temperature T. It can be seen from the figure that the functional $[\mu^n{}_T(\rho_n, \rho_p) - \mu^n(\rho_n, \rho_p)]$ has negative sign, i.e. $\mu^n{}_T(\rho_n, \rho_p) < \mu^n(\rho_n, \rho_p)$.

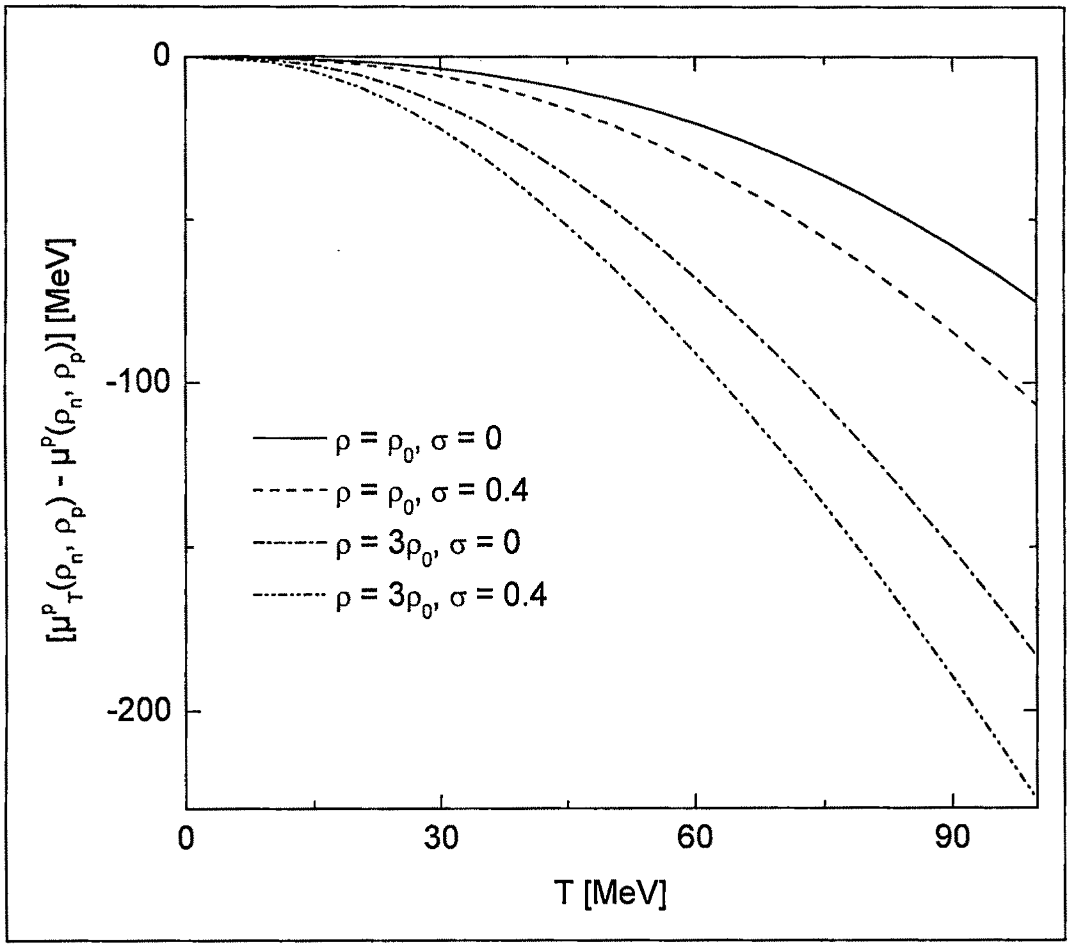

Figure 4.4: The functional $[\mu^p{}_T(\rho_n, \rho_p) - \mu^p(\rho_n, \rho_p)]$ as function of temperature T for different asymmetries (σ = 0 and 0.4) and densities ($\rho = \rho_0$ and $3\rho_0$) for the parameter set $\varepsilon_{ex}{}^l = 2\varepsilon_{ex}/3$.

In Fig. 4.4 the functional $[\mu^p{}_T(\rho_n, \rho_p) - \mu^p(\rho_n, \rho_p)]$ has been plotted as function of temperature T for different asymmetries (σ = 0 and 0.4) and densities ($\rho = \rho_0$ and $3\rho_0$) for the parameter set $\varepsilon_{ex}{}^l = 2\varepsilon_{ex}/3$. It can be seen that the functional $[\mu^p{}_T(\rho_n, \rho_p) - \mu^p(\rho_n, \rho_p)]$ decreases with increase in temperature T. It can be seen from the figure that the functional $[[\mu^p{}_T(\rho_n, \rho_p) - \mu^p(\rho_n, \rho_p)]]$ has negative sign, i.e. $\mu^p{}_T(\rho_n, \rho_p) < \mu^p(\rho_n, \rho_p)$.

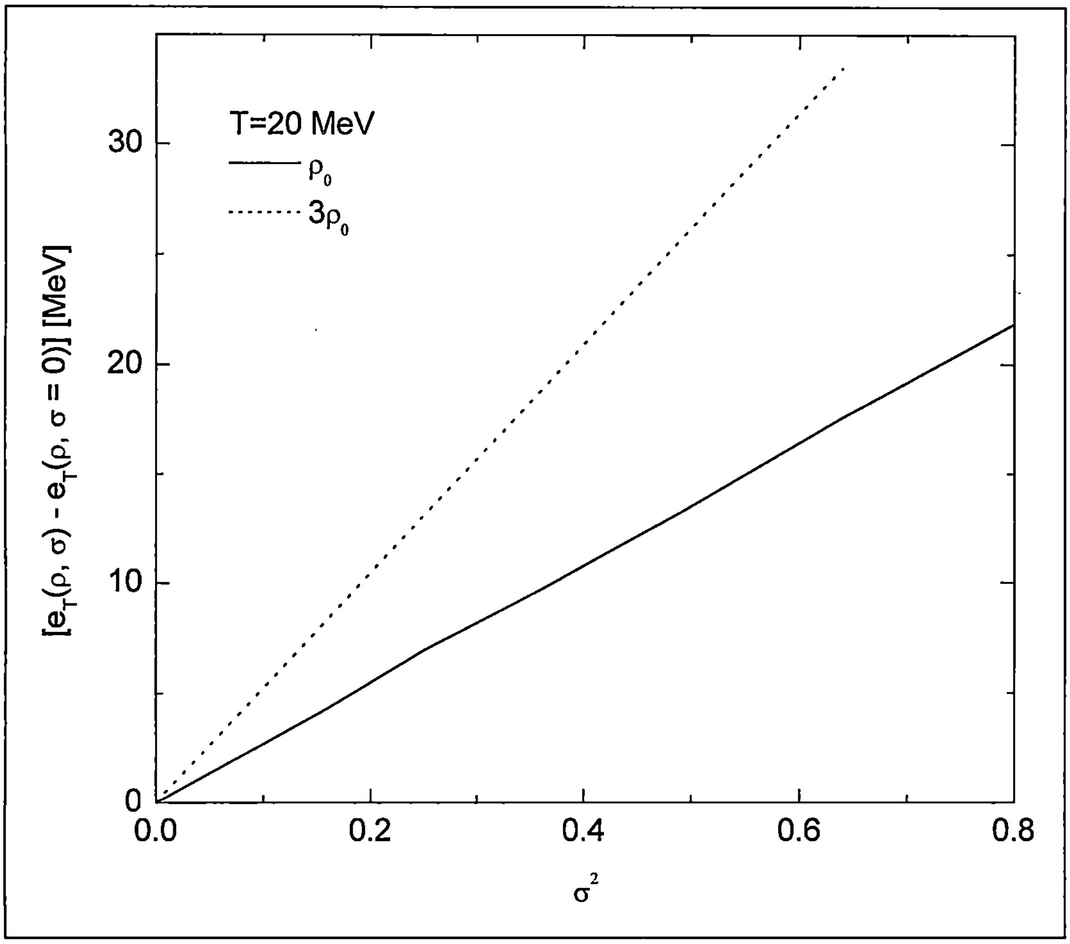

Figure 4.5: The functional $[e_T(\rho, \sigma) - e_T(\rho, \sigma = 0)]$ versus σ^2 at temperature T = 20 *MeV* for two different densities $\rho = \rho_0$ and $3\rho_0$ for the parameter set $\varepsilon_{ex}^l = 2\varepsilon_{ex}/3$, γ = 1/3 and $J_\tau(\rho_0) = 30$ *MeV*.

In Fig. 4.5 we have shown the validity of the approximation given in Eq. (4.9). The functional $[e_T(\rho, \sigma) - e_T(\rho, \sigma = 0)]$ is plotted as a function of σ^2 at temperature T = 20 *MeV* for two different densities $\rho = \rho_0$ and $3\rho_0$ for the parameter set $\varepsilon_{ex}^l = 2\varepsilon_{ex}/3$, γ = 1/3 and $J_\tau(\rho_0) = 30$ *MeV*. The almost linear relation between the functional $[e_T(\rho, \sigma) - e_T(\rho, \sigma = 0)]$ and σ^2, even at high asymmetry, seen from Fig. 4.5 indicates that the empirical parabolic law is also valid for hot neutron–rich matter. Several studies based on both phenomenological and microscopic models [152, 154] have also shown the validity of the parabolic approximation for the EOS of ANM at finite temperature.

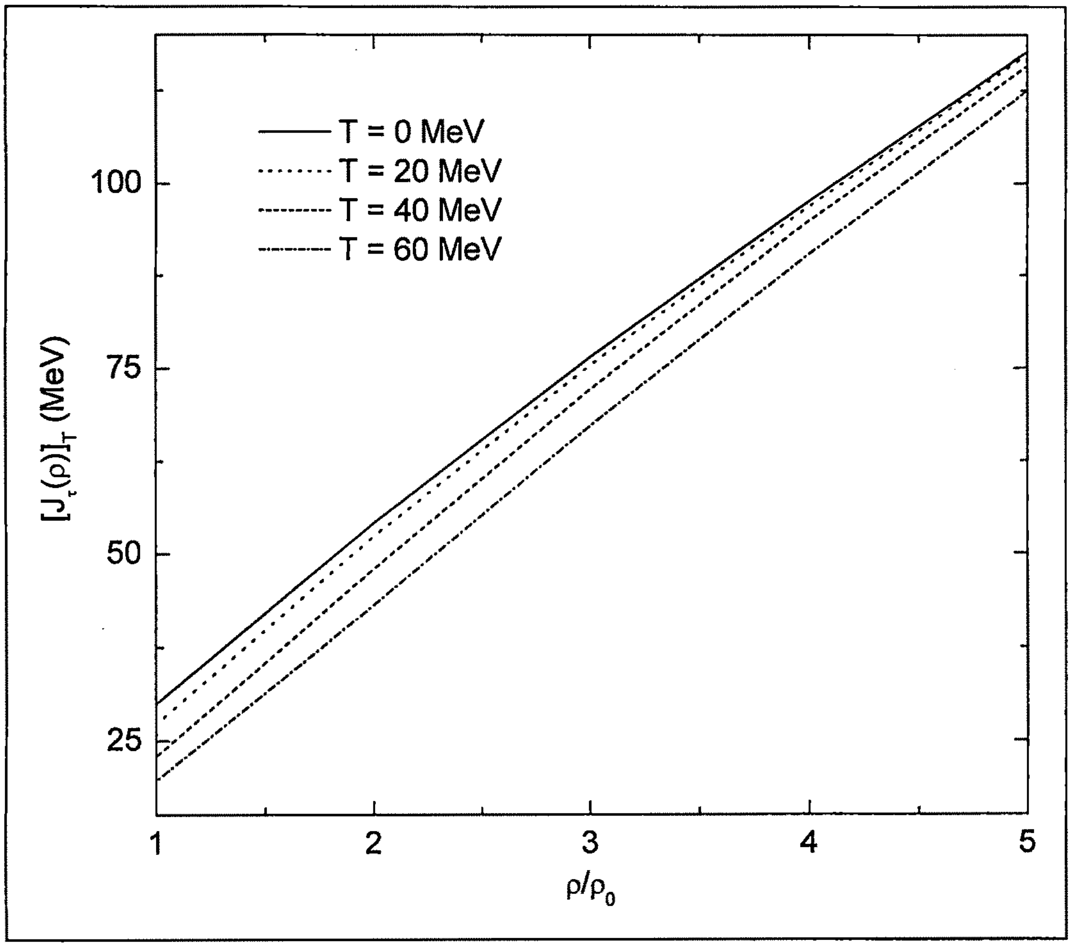

Figure 4.6: Density dependence of nuclear symmetry energy $[J_\tau(\rho_0)]_T$ at temperatures T = 0, 20, 40 and 60 MeV for the parameter set $\varepsilon_{ex}^{\,l} = 2\varepsilon_{ex}/3$, $\gamma = 1/3$ and $J_\tau(\rho_0) = 30$ MeV.

In Fig. 4.6 we have shown the density dependence of nuclear symmetry energy $[J_\tau(\rho_0)]_T$ at temperatures T = 0, 20, 40 and 60 MeV for the parameter set $\varepsilon_{ex}^{\,l} = 2\varepsilon_{ex}/3$, $\gamma = 1/3$ and $J_\tau(\rho_0) = 30$ MeV. It is seen that the symmetry energy $[J_\tau(\rho_0)]_T$ decreases with increase in temperature and at finite temperature it remains a monotonically increasing function of density.

4.4. Liquid–gas phase transition in ANM

The liquid–gas phase transition in ANM is much more complex than that in SNM. We have followed the thermodynamic approach of refs. [156] and [1].

4.4.1. Formalism

The stability conditions for asymmetric nuclear matter require that

$$\left(\frac{\partial P}{\partial \rho}\right)_{T,\sigma} \geq 0 \qquad \text{...(4.11)}$$

$$\left(\frac{\partial \mu_n}{\partial \sigma}\right)_{P,T} > 0 \quad \text{or} \quad \left(\frac{\partial \mu_p}{\partial \sigma}\right)_{P,T} < 0 \qquad \text{...(4.12)}$$

If one of the stability conditions is violated, a system with two phases is energetically favorable. The phase coexistence is governed by Gibbs conditions of equal pressures and chemical potentials. For ANM with different concentrations of protons and neutrons, the two–phase coexistence conditions are

$$P^L(T,\rho^L,\sigma^L) = P^G(T,\rho^G,\sigma^G), \qquad \text{...(4.13)}$$

$$\mu_n{}^L(T,\rho^L,\sigma^L) = \mu_n{}^G(T,\rho^G,\sigma^G) \qquad \text{...(4.14)}$$

$$\mu_p{}^L(T,\rho^L,\sigma^L) = \mu_p{}^G(T,\rho^G,\sigma^G) \qquad \text{...(4.15)}$$

where L and G stand for the liquid phase and the gas phase, respectively.

4.4.2. Mechanical and chemical instability

The condition given in Eq. (4.11) reflects the mechanical stability of ANM at finite temperature. If the condition (4.11) is not satisfied in certain parts of the system, any increase in density would lead to a decrease of pressure. As the pressure of this region will be lower than other parts of the system, the nuclear matter in this region would be compressed, leading to further growth of density. As a result any fluctuation in density would make the system mechanically unstable [1]. In Fig. 4.7 we have plotted pressure $P_T(\rho_n, \rho_p)$ in ANM at finite temperature as function of density ρ for different values of isopsin asymmetry σ at a fixed temperature $T = 10\ MeV$ for the parameter set $\varepsilon_{ex}^{\ l} = 2\varepsilon_{ex}/3$, $\gamma = 1/3$ and $J_t(\rho_0) = 30\ MeV$. It was observed that for $\sigma > \sigma_c$, where σ_c represents critical asymmetry, pressure increases monotonically with increase in density. This means that nuclear matter is stable at all densities for $\sigma > \sigma_c$. In contrast, for $\sigma < \sigma_c$, it was observed that the mechanical stability condition given in Eq. (4.11) is violated. The critical asymmetry σ_c can be determined from the condition

$$\left(\frac{\partial P}{\partial \rho}\right)_{T,\sigma_c} = \left(\frac{\partial^2 P}{\partial \rho^2}\right)_{T,\sigma_c} = 0. \qquad \text{...(4.16)}$$

For the interaction parameter set considered in Fig. 4.5 we obtained the value of σ_c = 0.62. The pressure of the inflection point is 0.1092 *MeV*, above which mechanical instability disappears.

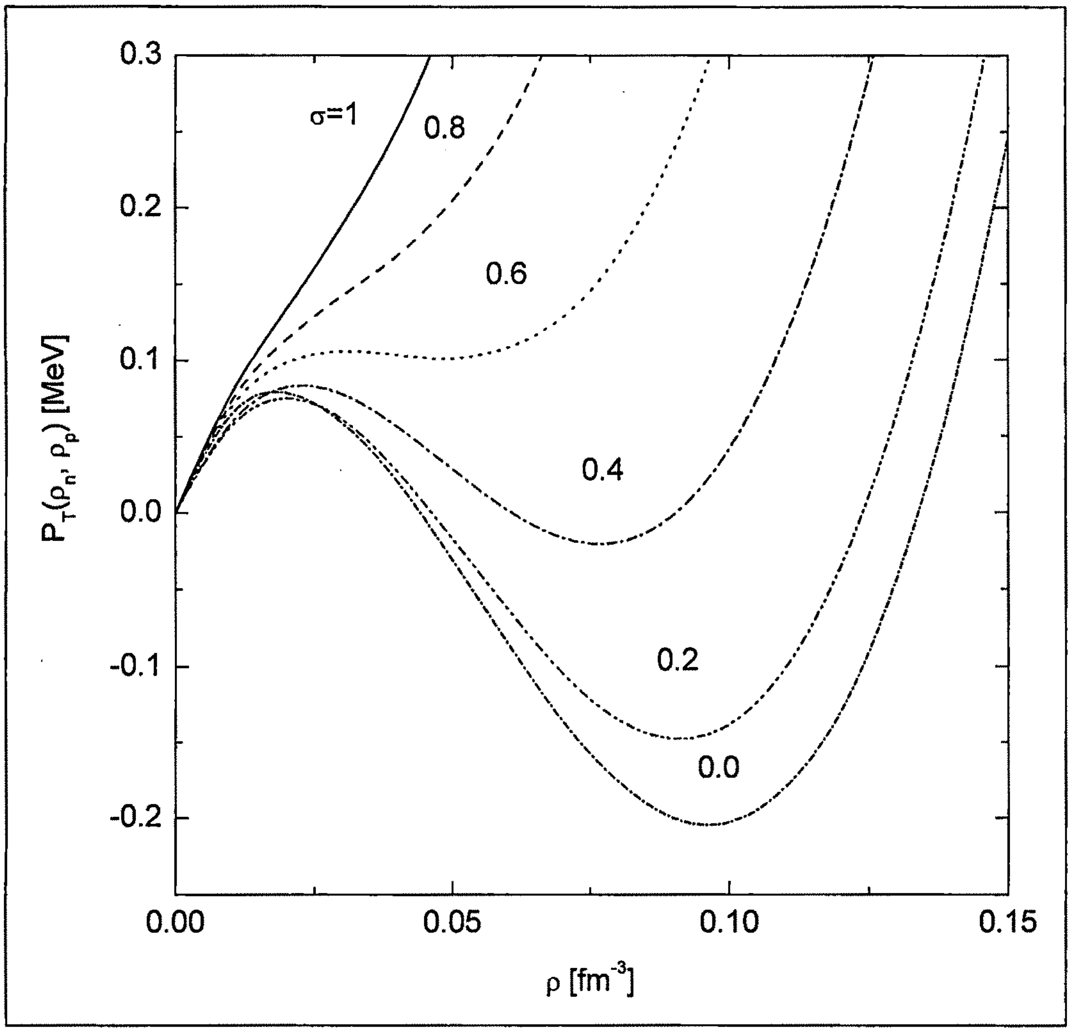

Figure 4.7: Pressure $P_T(\rho, \sigma)$ in ANM as function of density at temperature T = 10 *MeV* for σ = 0, 0.2, 0.4, 0.6, 0.8 and 1 for the parameter set $\varepsilon_{ex}^{l} = 2\varepsilon_{ex}/3$, $\gamma = 1/3$ and $J_\tau(\rho_0) = 30$ *MeV*.

Similar to the above case where the $P_T(\rho_n, \rho_p)$ was calculated for a fixed temperature but different isospin asymmetries we have calculated $P_T(\rho_n, \rho_p)$ as function of density ρ at a fixed isospin asymmetry σ but different values of temperature T. It is seen that there exist a critical temperature T_c beyond which nuclear matter is stable at all densities. In Fig. 4.8 we have plotted critical temperature T_c as function of asymmetry parameter σ for the parameter set $\varepsilon_{ex}^{l} = 2\varepsilon_{ex}/3$, $\gamma = 1/3$ and $J_\tau(\rho_0) = 30\ MeV$. It can be seen that the value of T_c decreases with increase in asymmetry parameter σ. The variation in T_c is small upto $\sigma = 0.4$ and then it decreases rapidly and beyond $\sigma = 0.9$ phase transition disappears.

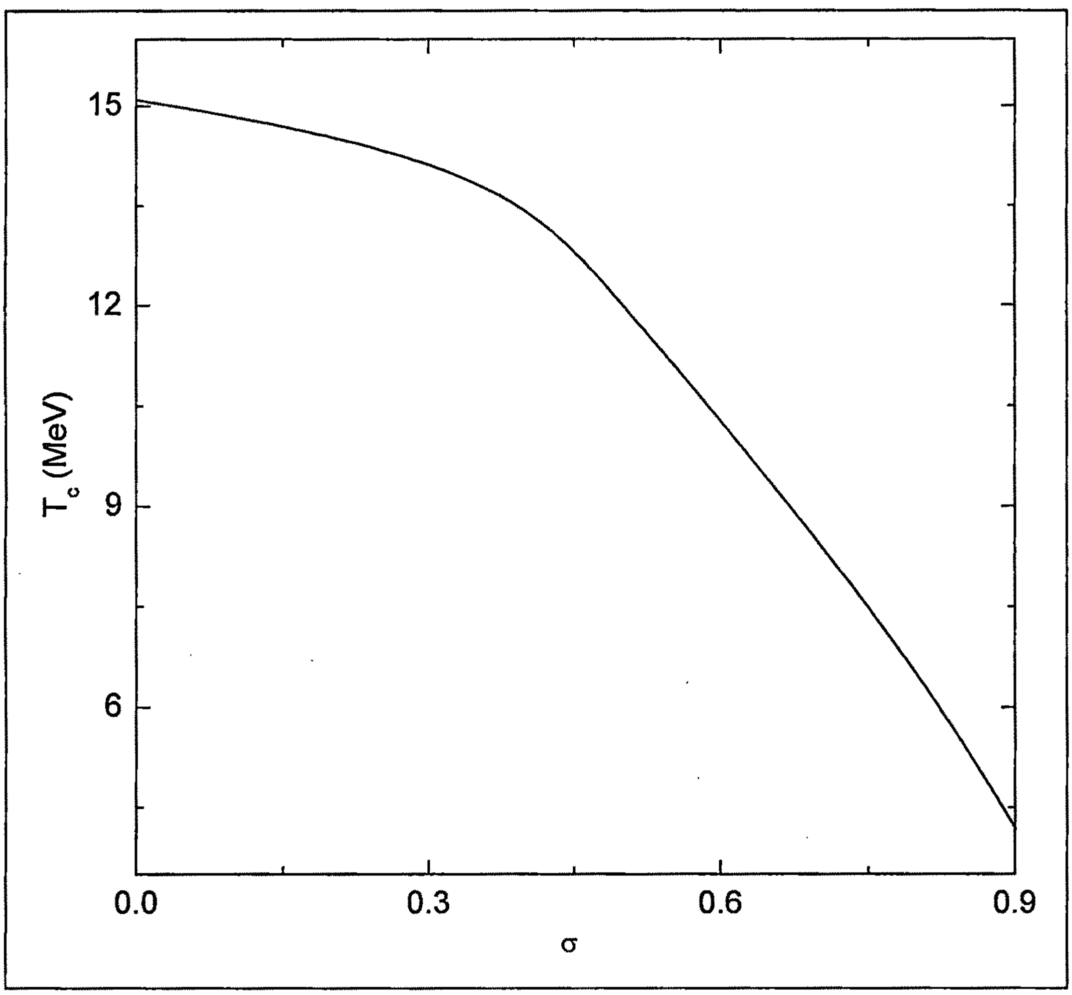

Figure 4.8: Critical temperature T_c versus σ for the parameter set $\varepsilon_{ex}^{l} = 2\varepsilon_{ex}/3$, $\gamma = 1/3$ and $J_\tau(\rho_0) = 30\ MeV$.

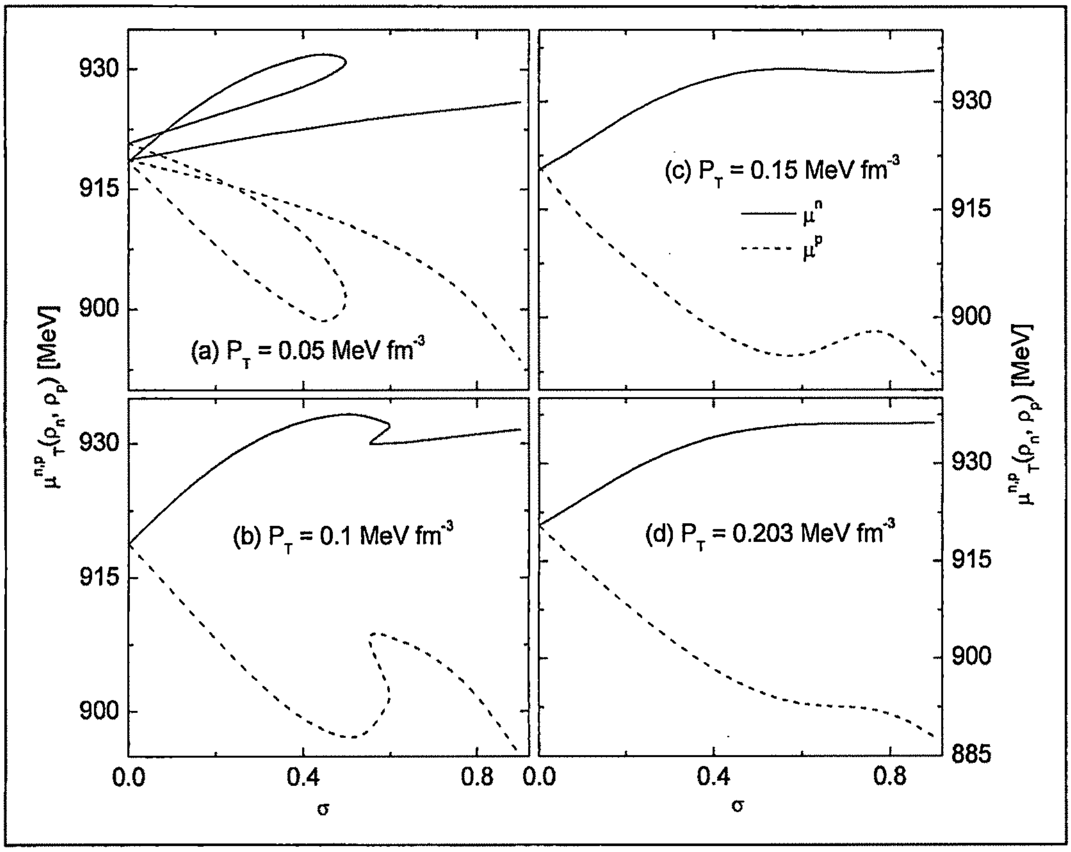

Figure 4.9: Chemical potential isobars for neutrons and protons as function of σ at fixed temperature $T = 10$ *MeV*. The panels (a), (b), (c) and (d) have pressure ($P_T(\rho,\ \sigma)$ = 0.05, 0.1, 0.15 and 0.203 $MeV\,fm^{-3}$) respectively. All the curves have been plotted for the parameter set $\varepsilon_{ex}^{\ l} = 2\varepsilon_{ex}/3$, $\gamma = 1/3$ and $J_\tau(\rho_0) = 30$ *MeV*.

ANM at finite temperature becomes chemically unstable if either of the inequality condition given in Eq. (4.12) is violated. To analyze chemical instability in nuclear matter, we need information on the chemical potential isobar for neutrons and protons at fixed temperature and pressure. In Fig. 4.9 we have shown the chemical potential isobars for neutron and protons as function of asymmetry σ corresponding to temperature $T = 10$ *MeV* and pressures (P_T = 0.05, 0.1, 0.15 and 0.203 MeV/fm^3) for the parameter set $\varepsilon_{ex}^{\ l} = 2\varepsilon_{ex}/3$, $\gamma = 1/3$ and $J_\tau(\rho_0) = 30$ *MeV*. From Fig. 4.9 we can see that the shapes of the chemical potential isobar curves are different for different pressures. The critical isospin asymmetry for mechanical instability is 0.62 and the pressure of the inflection point is 0.109 MeV/fm^3. Above the inflection point mechanical instability disappears and only chemical instability exists. The chemical potential isobars above this pressure at inflection point have only one branch for all values of σ. The one for P_T = 0.203 MeV/fm^3 corresponds to the critical pressure P_c for the interaction at T = 10 MeV, above which the chemical potential of neutrons (protons) increases (decreases) monotonically with σ and the chemical instability disappears. The chemical potential isobar corresponding to P_c marks the upper boundary of instability with respect to pressure and defines a critical point (P_c, σ_c). The critical pressure P_c is determined from the inflection point which satisfies the relation

$$\left(\frac{\partial\mu}{\partial\sigma}\right)_{P_c,T}=\left(\frac{\partial^2\mu}{\partial\sigma^2}\right)_{P_c,T}=0 \quad . \qquad \ldots(4.17)$$

4.4.3. Liquid–gas phase transition

The Gibbs conditions given in Eqs. (4.13), (4.14) and (4.15) for phase equilibrium demand equal pressure and chemical potentials for two phases with different concentrations. For a fixed pressure, the solutions thus form the edges of a rectangle in proton and neutron chemical potential isobars as functions of isospin asymmetry and can be found by means of the geometrical construction method [1, 156].

In order to investigate the LG phase transition, in Fig. 4.10 the chemical potentials of neutron and proton as function of asymmetry σ at fixed pressure P_T = 0.1 MeV/fm^3 and T = 10 MeV has been plotted for the parameter set mentioned. In the same figure the resulting rectangle from geometrical construction is shown. The two different values of σ obtained from the geometrical construction correspond to two different phases with different densities, with the lower density phase (with larger σ value) being a gas phase while the higher density phase (with smaller σ value) being a liquid phase. Collecting all such pairs of $\sigma(T, P)$ and $\sigma'(T, P)$ forms the binodal surface. Fig. 4.11 displays the binodal surface for interaction at T = 10 MeV. Above the critical pressure or below the pressure of equal concentration (EC) point, no phase–coexistence region can exist. The EC point (the rectangle shrinks to a point at this particular pressure) indicates the special case that SNM with equal density coexists. The left side of the bimodal surface is the region of liquid phase and the right side of the region of gas phase, and within the surface is the liquid–gas phase–coexistence region.

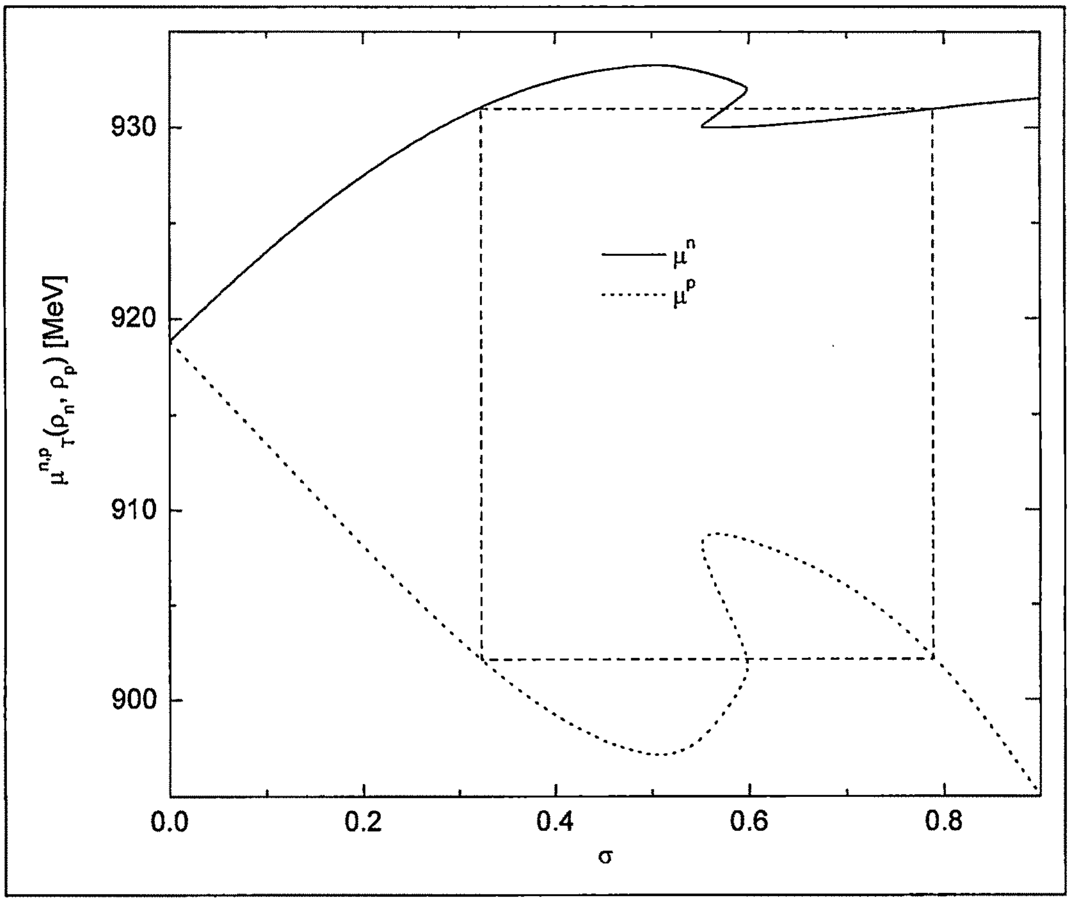

Figure 4.10: Geometrical construction used to obtain σ and chemical potentials in the two coexisting phase at fixed T = 10 MeV and pressure P_T = 0.1 $MeV\,fm^{-3}$ for the parameter set $\varepsilon_{ex}^{\,l} = 2\varepsilon_{ex}/3$, $\gamma = 1/3$ and $J_\tau(\rho_0)$ = 30 MeV.

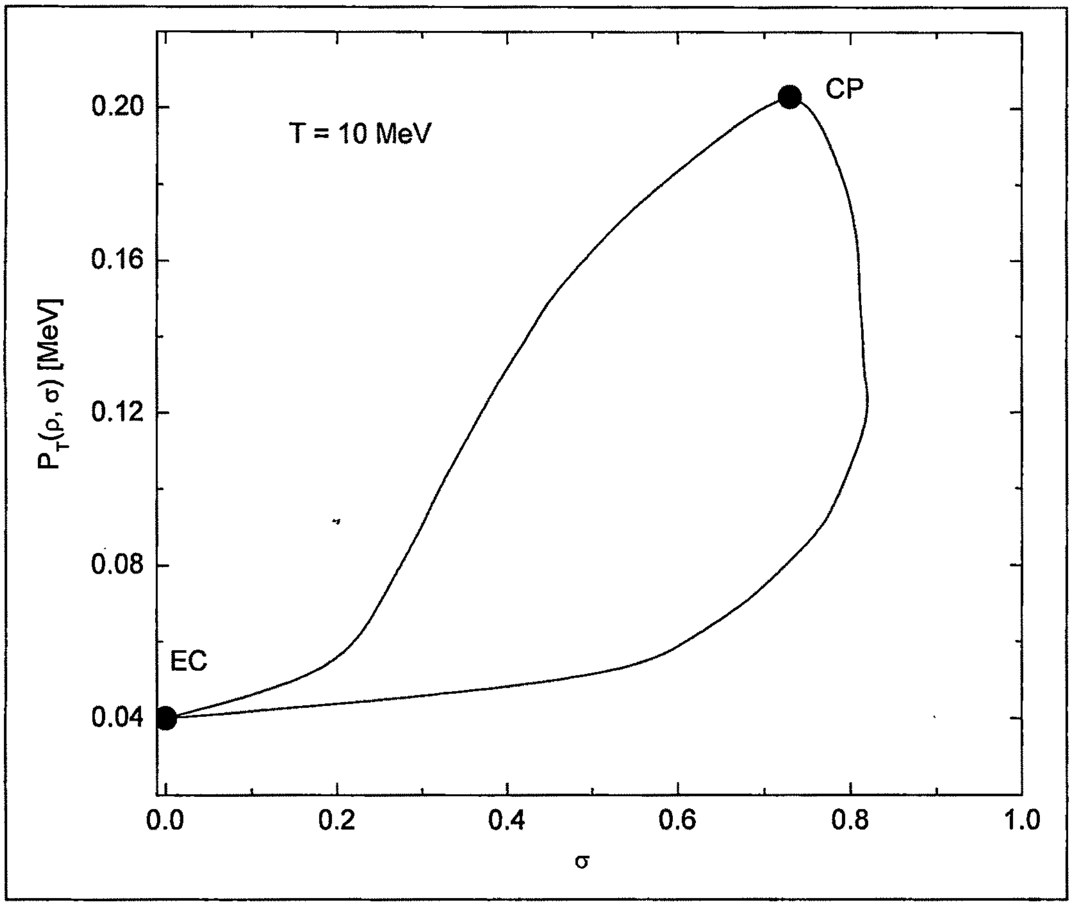

Figure 4.11: Binodal curve at $T = 10$ MeV for the parameter set $\varepsilon_{ex}^{l} = 2\varepsilon_{ex}/3$, $\gamma = 1/3$ and $J_{\tau}(\rho_0) = 30$ MeV. The critical point (CP) and the points of equal concentration (EC) are also indicated.

4.5. Summary

In this chapter the EOS and other properties of ANM was studied at finite temperature by using the simple density dependent short range effective interaction given in chapter 3. Energy density, pressure, neutron and proton chemical potentials and nuclear symmetry energy in ANM at finite temperature with respect to their zero–temperature values were calculated for a wide range of density, temperature and asymmetry. To study the thermal evolution of these properties of hot ANM relative to their zero temperature values it was observed that knowledge of only exchange strength parameter is required. The empirical parabolic law for EOS of ANM was found to be valid at finite temperature also. Further we studied the mechanical and chemical instability in ANM and the role of neutron–proton asymmetry in liquid–gas phase transition was also analysed. It was observed that in ANM the liquid–gas phase transition is of second order.

To conclude this chapter we would like to say that given the present scenario of EOS of ANM at zero temperature it seems ambitious to study the EOS of hot ANM and extend to study of phase transition in ANM. Nevertheless, in this thesis work we have done only a brief study on phase transition in ANM. Much more effort will be given in this direction in future works.

CHAPTER 5

EQUATION OF STATE OF BETA STABLE MATTER AND PROPERTIES OF NEUTRON STAR

5.1. Introduction

To understand the evolution and structure of neutron stars it is very important to understand the EOS of nuclear matter. Unfortunately the equation of state of highly dense asymmetric nuclear matter, which plays the most crucial role in calculation of neutron star properties, is still very uncertain. On the other hand, theoretical study of neutron star properties is very important since comparison of theoretical predictions with experimental observations can lead to effective constraints on the EOS of dense asymmetric nuclear matter [171].

Neutron stars are one of the densest forms of matter known in the observable universe having density as high as 5 to 10 times normal nuclear matter density ρ_0 [7]. They have a typical mass of the order of 1.5 times solar mass M_{solar} and a radius of the order of about 12 *km*. A neutron star is born when the core of a massive star (mass greater than 8 times solar mass) at the end of its life collapses, triggering a supernova explosion. It has three major regions: crust, outer core or nuclear matter core and an inner core. The crust primarily contains nuclei from ^{56}Fe to nuclei with mass number ~ 200 (near the core-crust interface). When density reaches the neutron drip density $\sim 4.3 \times 10^{11}$ g/cm^3 nuclei are so neutron rich that neutron states in the continuum begin to be filled. Above the neutron drip density free neutrons appear and the crust consists of lattice of neutron rich nuclei embedded in an ultra-relativistic neutron gas. With increase in density a series of transition takes place and ultimately a phase transition to nucleonic matter takes place at density ~ 2×10^{14} g/cm^3. Neutron star matter in the outer core consists mostly of neutrons, a few protons, electrons and muons in beta-equilibrium. As density increases further in the inner core of the star exotic particles such as heavier mesons and strange baryons become abundant and ultimately a quark matter phase may develop in the center of the star.

Since a neutron star contains nucleonic matter at density about 8-10 times ρ_0 in its core and matter at such high density has not been reproduced in the laboratory, neutron stars can serve as a laboratory to study the high density behaviour of highly asymmetric nuclear matter. Properties of neutron star such as mass, radius, baryon mass etc. which are related to the EOS of neutron star matter can provide constrains on the EOS of dense ANM. Maximum mass can provide constraint on the stiffness of EOS at high densities while radius measurements can constrain the EOS at densities about saturation density. Hence accurate measurement of neutron star properties is very important for nuclear physicists also. New advance probes and observatories are enabling astrophysicists to discover a large number of neutron stars, in the form of radio pulsars, x-ray binaries, x-ray bursters and thermally emitting isolated stars, and measure more accurate data from them.

Theoretically the properties of neutron star can be calculated by solving the Tolman-Oppenheimer-Volkoff (TOV) equation [172] which requires the knowledge of EOS of nuclear matter. Both relativistic and non relativistic models of nuclear matter EOS have been used to solve the TOV equation and calculate the properties of neutron stars. A number of early calculations on properties of neutron star were done within the non relativistic Skyrme framework. For a review see ref. [173]. Chabanat *et al.* [17] constructed a Skyrme parameterization using microscopic constraints to study the EOS of nuclear matter over a wide range of density and calculate the properties of neutron star. Recently Rikovska-Stone *et al.* [19] have studied 87 different Skyrme parameterization and have calculated their neutron star properties. The RMF approach has been widely used to calculate neutron star masses and radii [174, 175]. In the variational framework Wiringa *et al.* [15] have studied the EOS of beta-stable neutron star matter and neutron star structure using different microscopic NN interactions. In ref. [176] the conventional Brueckner theory with a continuous choice for the single particle potential and three body forces was used to calculate the properties of neutron star. The BHF scheme was extended in ref. [177] to include the contribution from hyperons along with nucleons and leptons in beta-stable neutron star matter. The DBHF approach has been widely used to compute neutron star properties [178-180].

In chapter 3 we saw that the extremely divergent nature of the nuclear symmetry energy at high densities is a consequence of the choice of interaction parameters. In this chapter we will constrain the high density behaviour of nuclear symmetry energy further on the basis of an approximate universal high density behaviour of asymmetric contribution to the nucleonic part of energy density of neutron star matter [6]. In this chapter we have studied the high density behaviour of infinite n+p+e+μ matter in beta equilibrium, which can be found in the core of neutron stars, using the simple finite range effective interaction considered in the previous chapter. In section 5.2 we have given the formalism required to calculate the EOS of beta-stable matter and properties of neutron star. In section 5.3 we have tried to constrain the high density behaviour of nuclear symmetry energy using the EOS of beta-stable neutron star matter. In section 5.4 results of properties of neutron star have been discussed for the different EOSs and a brief summary is given in section 5.5.

5.2. Formalism

5.2.1. EOS of beta stable neutron star matter

The core of a neutron star is expected to be formed by an uncharged mixture of neutrons, protons, electrons and muons in equilibrium with respect to the weak interaction (beta-stable neutron star matter (NSM)). Since muons would contribute much less to the effects of chemical equilibrium compared to electrons, we first consider NSM with neutrons and small fractions of protons and electrons only. Equilibrium for the reaction

$$n \Leftrightarrow p + e^{-}$$

requires that

$$[\mu^n(\rho, Y_p) - \mu^p(\rho, Y_p)] = \mu^e(\rho, Y_e)\,, \qquad \ldots(5.1)$$

where, μ^i ($i = n, p, e$) are the chemical potentials of the respective particles and $Y_e = \rho_e/\rho$ is the electron fraction, ρ_e being the electron density.

As density increases above normal nuclear matter density ρ_0, the electron chemical potential $\mu^e(\rho, Y_e)$ exceeds the muon rest mass energy $m_\mu c^2$ and the reaction

$$n \Leftrightarrow p + \mu^-$$

is energetically allowed. This changes the equilibrium condition in Eq. (5.1) to

$$[\mu^n(\rho, Y_p) - \mu^p(\rho, Y_p)] = \mu^e(\rho, Y_e) = \mu^\mu(\rho, Y_\mu) \qquad \ldots(5.2)$$

In the above equation $\mu^\mu(\rho, Y_\mu)$ is the chemical potential of muons and $Y_\mu = \rho_\mu/\rho$ is the muon fraction, ρ_μ being the muon density.

Local charge neutrality requires that total electric charge inside the star should vanish. This means that

$Y_p = Y_e$ in first condition given in Eq. (5.1)

and $Y_p = Y_e + Y_\mu$ in second condition given in Eq. (5.2).

In this work, we have calculated the difference between neutron and proton chemical potentials $[\mu^n(\rho, Y_p) - \mu^p(\rho, Y_p)]$ from the EOS of asymmetric nuclear matter (ANM) as described in chapter 3. The electron and muon chemical potentials as functions of total density ρ and respective particle fractions Y_i have been approximated by their relativistic Fermi-gas expressions,

$$\mu^i(\rho, Y_i) = [m_i^2 c^4 + c^2\hbar^2\{3\pi^2\rho Y_i\}^{2/3}]^{1/2} \qquad \ldots(5.3)$$

Using these relations we have numerically calculated the proton fraction Y_p and other particle fractions for each given and fixed value of total nucleon density ρ.

The crucial dependence of proton fraction $Y_p(\rho)$ in beta-stable matter on the high density behaviour of nuclear symmetry energy $J_\tau(\rho)$ can be examined by considering the approximate relation for energy density $H(\rho, Y_p)$ in ANM given in Eq. (3.24) in chapter 3. For this form of $H(\rho, Y_p)$, the difference between neutron and proton chemical potentials was obtained in the simple form,

$$[\mu^n(\rho, Y_p) - \mu^p(\rho, Y_p)] = 4(1\text{-}2Y_p)\, J_\tau(\rho). \qquad \ldots(5.4)$$

With this result of $[\mu^n(\rho, Y_p) - \mu^p(\rho, Y_p)]$ and for ultra relativistic electrons satisfying the relation $\mu^i \approx c\hbar(3\pi^2\rho Y_i)^{1/3}$, the equilibrium condition in Eq.(5.1) for the case of electrons only can be exactly solved to give

$$Y_p(\rho) = \left[(2/\sqrt{3})q^{1/2}\sinh(\phi/3)\right]^3, \qquad \ldots(5.5)$$

with $\quad sinh(\varphi) = (3/q)^{3/2}/4$ and $q = c\hbar(3\pi^2\rho)^{1/3}/[8\, J_\tau(\rho)]$. $\qquad \ldots(5.6)$

This result clearly shows that density dependence of the equilibrium proton fraction $Y_p(\rho)$ is entirely determined by $J_\tau(\rho)$ and would follow a trend quite similar to the density dependence of nuclear symmetry energy $J_\tau(\rho)$.

The total energy density of beta-stable $n+p+e+\mu$ neutron star matter (NSM) is given as

$$H^{NSM}(\rho, Y_p) = H^N(\rho, Y_p) + H^e(\rho, Y_e) + H^\mu(\rho, Y_\mu) \qquad \ldots(5.7)$$

where the first term represents the nucleonic part and the last two terms represent the leptonic contribution towards total energy density of beta-stable matter. We have used the EOS of ANM described in chapter 3 to calculate the nuclear part of the total energy density $H^N(\rho, Y_p)$, while the corresponding leptonic parts, $H^e(\rho, Y_e)$ and $H^\mu(\rho, Y_\mu)$ have been approximated in terms of their relativistic Fermi gas expressions given as

$$H^i(\rho, Y_i) = \frac{3m_i c^2 \rho_i}{8x_i^3}\left[2x_i u_i^3 - x_i u_i - \ln(x_i + u_i)\right] \qquad \ldots(5.8)$$

with $\quad x_i = \dfrac{\hbar k_i}{m_i c}$; $u_i = (1 + x_i^2)^{1/2}$ and $k_i = (3\pi^2\rho_i)^{1/3}$; $i = e, \mu$ $\qquad \ldots(5.9)$

The total pressure in beta-stable $n+p+e+\mu$ matter is given by

$$P^{NSM}(\rho, Y_p) = P^N(\rho, Y_p) + P^e(\rho, Y_e) + P^\mu(\rho, Y_\mu) \qquad \ldots(5.10)$$

Similar to total energy density the nuclear part of total pressure has been calculated from the EOS of ANM as discussed in chapter 3 while the leptonic parts have been calculated from the relation

$$P^i(\rho, Y_i) = \mu^i \rho_i - H^i(\rho, Y_i) \quad , i = e, \mu \qquad \ldots(5.11)$$

where μ^i ($i = e, \mu$) are the electron (muon) chemical potentials.

5.2.2. URCA cooling

Newborn neutron stars are very hot, with interior temperature in the range of tens of MeV. But they cool very rapidly to temperature below 1 MeV in few seconds by neutrino emission and continue to cool further to temperature of few eV in a few million years by further neutrino emission, X-ray emission and photon emission. It is believed that neutrino emission takes place chiefly through the reactions

$$n \rightarrow p + e^- + \nu^-_e, \qquad p \rightarrow n + e^+ + \nu_e,$$

and $n + (n, p) \rightarrow p + (n, p) + e^- + \nu^-_e, \qquad p + (n, p) \rightarrow n + (n, p) + e^+ + \nu^-_e.$

These reactions are called Urca process where thermally excited nucleons undergo beta and inverse beta decay producing an antineutrino or a neutrino. The former reactions are called the direct Urca (DU) process while the latter are called the modified Urca process where an additional nucleon participates. The DU process is the most efficient in cooling among the two since modified Urca process rate is slower than DU process and hence neutron star cooling is correspondingly slower in the modified Urca process.

The DU process is permitted only when energy and momentum can be simultaneously conserved. The relative fractions of the components of the beta-stable matter are crucial for the rate of neutrino cooling of neutron stars. Whenever, the neutron fraction $Y_n = \rho_n/\rho$ satisfies the condition

$$Y_n^{1/3} \leq Y_p^{1/3} + Y_e^{1/3}$$

and/or $\quad Y_n^{1/3} \leq Y_p^{1/3} + Y_\mu^{1/3}$

the DU process is allowed, leading to a very rapid cooling of neutron stars [6-9, 15, 16]. However, the question of whether DU process occurs or not is controversial since the neutrino emissivity in DU process is so large that it can lead to unacceptably fast cooling of neutron stars in contradiction to modern observational data. On the other hand, the DU process can be used to constrain the EOS of nuclear matter. Since proton fraction Y_p depends on the symmetry energy $J_\tau(\rho)$ as seen from Eq. (5.5) the threshold density at which the DU process occurs will depend on the density dependence of nuclear symmetry energy $J_\tau(\rho)$. Analysis of threshold density at which direct process will occur can provide a constraint on the density dependence of symmetry energy.

5.2.3. Properties of neutron star

The mass and radius of a neutron star can be calculated by solving the Tolman-Oppenheimer-Volkov (TOV) equation which is derived from the Einstein's field equations in general relativity. For a spherically symmetric non-rotating star the Tolman-Oppenheimer-Volkov (TOV) equation [172] can be written as

$$\frac{dP(r)}{dr}=-\frac{G\left[H(r)+\frac{P(r)}{c^2}\right]\left[m(r)+\frac{4\pi r^3 P(r)}{c^2}\right]}{r^2\left[1-\frac{2Gm(r)}{rc^2}\right]} \qquad ...(5.12)$$

with
$$\frac{dm(r)}{dr}=4\pi r^2 H(r) \qquad ...(5.13)$$

In the above equations $P(r)$ is the pressure, $H(r)$ is the energy density of matter, $m(r)$ is the gravitational mass enclosed within a radius r, G is the gravitational constant and c is the velocity of light.

To solve the TOV equation the EOS of NSM has to be provided in the form $P(H(r))$ starting from some central energy density $H_c = H(0)$ at the center of the star (r = 0) and with the initial condition $m(0) = 0$, the above equations are integrated until pressure vanishes i.e. $P(R) = P_{surf} = 0$. The point $r = R$ where pressure vanishes gives the radius of the neutron star and $M = m(R)$ gives the gravitational mass M of the star. The TOV equation can be solved when the relation between pressure $P(r)$ and energy density $H(r)$ is known at each point. This means that the properties of the star depend on the EOS of the NSM matter. In this work the TOV equations given in Eqs. (5.12) and (5.13) have been integrated numerically using a tabulated form of EOS of beta-stable $n+p+e+\mu$ NSM calculated using Eqs. (5.7) and (5.10).

We have also calculated some other important properties concerning neutron stars. The binding energy liberated in a supernova core collapse, resulting in the formation of a neutron star, is approximated as

$$E_{bind} = (M_A - M)\, c^2 \qquad ...(5.14)$$

where M is the gravitational mass of the neutron star and M_A is the baryon mass given as

$$M_A = m_0 A \qquad ...(5.15)$$

In Eq. (5.15) $m_0 = 1.66 \times 10^{-24}$ gm is the mass of atom ^{56}Fe and A is the total baryon no. defined as

$$A = \int_0^R \frac{4\pi r^2 \rho(r)}{\left[1 - \frac{2Gm(r)}{rc^2}\right]^{1/2}} dr \qquad \text{...(5.16)}$$

5.3. High density behaviour of nuclear symmetry energy

In chapter 3 we observed that for a given splitting of the exchange strength parameter ($\varepsilon_{ex}^{l} + \varepsilon_{ex}^{ul}$) into ε_{ex}^{l} and ε_{ex}^{ul} and given values of the parameters γ and $J_\tau(\rho_0)$ the behaviour of nuclear symmetry energy $J_\tau(\rho)$ shows very diverse result with variation in the value of $J_\tau'(\rho_0)$ (as seen from Fig. 3.14)). The stiffest EOS gives rise to 'very stiff' behaviour of nuclear symmetry energy at high density while very small values of $J_\tau'(\rho_0)$ give 'very soft' behaviour of nuclear symmetry energy at high density. This shows that the divergent behaviour of nuclear symmetry energy as predicted by different theoretical calculations is due to the choice of interaction parameter.

For a given splitting of ($\varepsilon_{ex}^{l} + \varepsilon_{ex}^{ul}$) into ε_{ex}^{l} and ε_{ex}^{ul}, we will again vary $J_\tau'(\rho_0)$ to examine how the density dependence of nuclear symmetry energy $J_\tau(\rho)$ can be constrained by the high density behaviour of asymmetric contribution to the nucleonic part of the energy density in NSM. The asymmetric contribution to the nucleonic part of the energy density in NSM can be defined as

$$S^{NSM}(\rho, Y_p) = [H^N(\rho, Y_p) - H(\rho, Y_p = 1/2)], \qquad \text{...(5.17)}$$

where $H^N(\rho, Y_p)$ is the nucleonic part of the energy density of beta-stable matter and $H(\rho, Y_p = 1/2)$ is the energy density of SNM. It should be mentioned here that while analyzing the EOS of NSM in this way we have assured that the stability condition of PNM given in Eq. (3.40) is not violated.

We take $\varepsilon_{ex}^{l} = (\varepsilon_{ex}^{l} + \varepsilon_{ex}^{ul})/4$ and assume a standard value of $J_\tau(\rho_0) = 30$ MeV and calculate the functional $S^{NSM}(\rho, Y_p)$ by varying the value of $J_\tau'(\rho_0)$. The high density behaviour of the functional $S^{NSM}(\rho, Y_p)$ obtained in this way from several admissible EOSs in accordance with conditions in Eq. (3.40) are shown in Fig. 5.1. All these curves

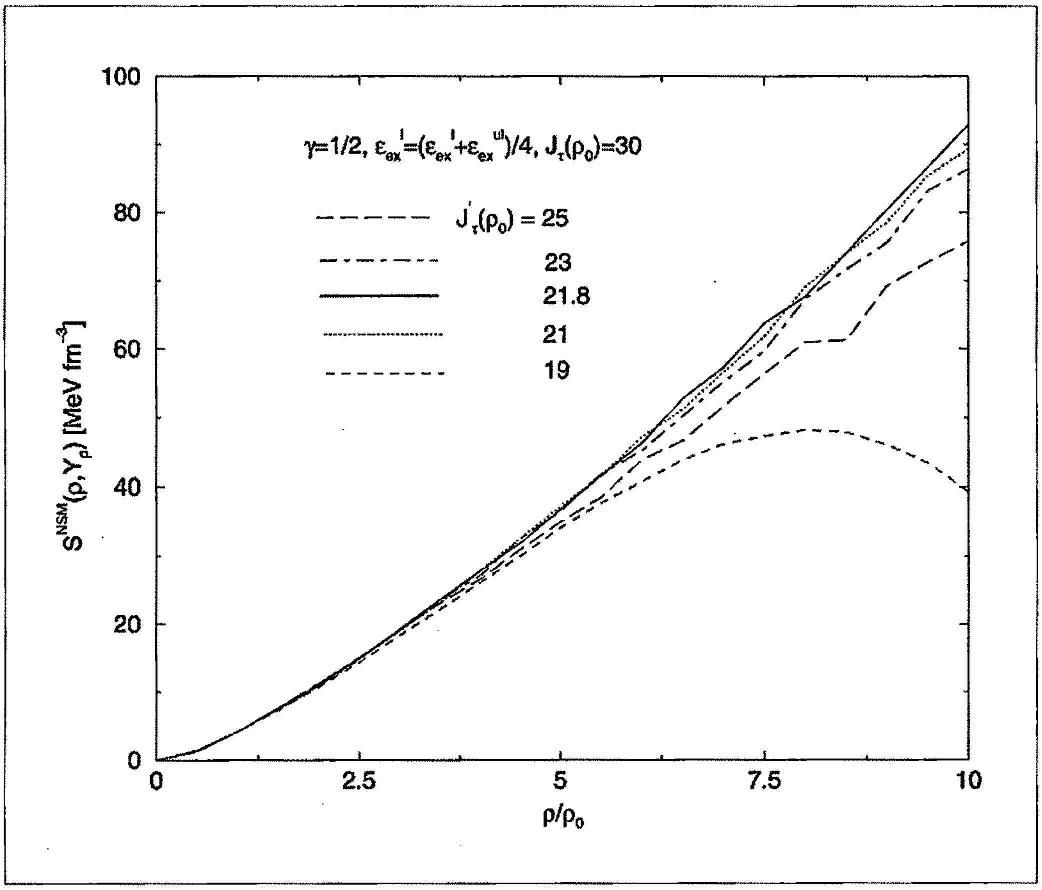

Figure 5.1: High density behaviour of the functional $S^{NSM}(\rho,\ Y_p)$ obtained from several EOS of ANM. All these EOS correspond to same value of $J_\tau(\rho_0)$, $\varepsilon_{ex}^{\ l}$ and γ but differ in the values of $J_\tau'(\rho_0)$.

of $S^{NSM}(\rho,\ Y_p)$ in this figure correspond to $\gamma = 1/2$, and $\varepsilon_{ex}^{\ l} = (\varepsilon_{ex}^{\ l} + \varepsilon_{ex}^{\ ul})/4$ and $J_\tau(\rho_0) = 30\ MeV$ but differ from each other in values of $J_\tau'(\rho_0)$. The high density behaviour of nuclear symmetry energy $J_\tau(\rho)$ and equilibrium proton fraction $Y_p(\rho)$ in NSM obtained from these different EOS are also shown in Figs. 5.2(a) and 5.2(b), respectively. Different EOS considered in Figs. 5.2(a) and 5.2(b) give almost same results for $J_\tau(\rho)$ and $Y_p(\rho)$ up to normal density ρ_0, but differ considerably from each other when extrapolated to high densities. This exhibits the extremely divergent and contradicting behaviour of $J_\tau(\rho)$ and $Y_p(\rho)$ at high densities predicted by different theoretical calculations [27, 28]. However,

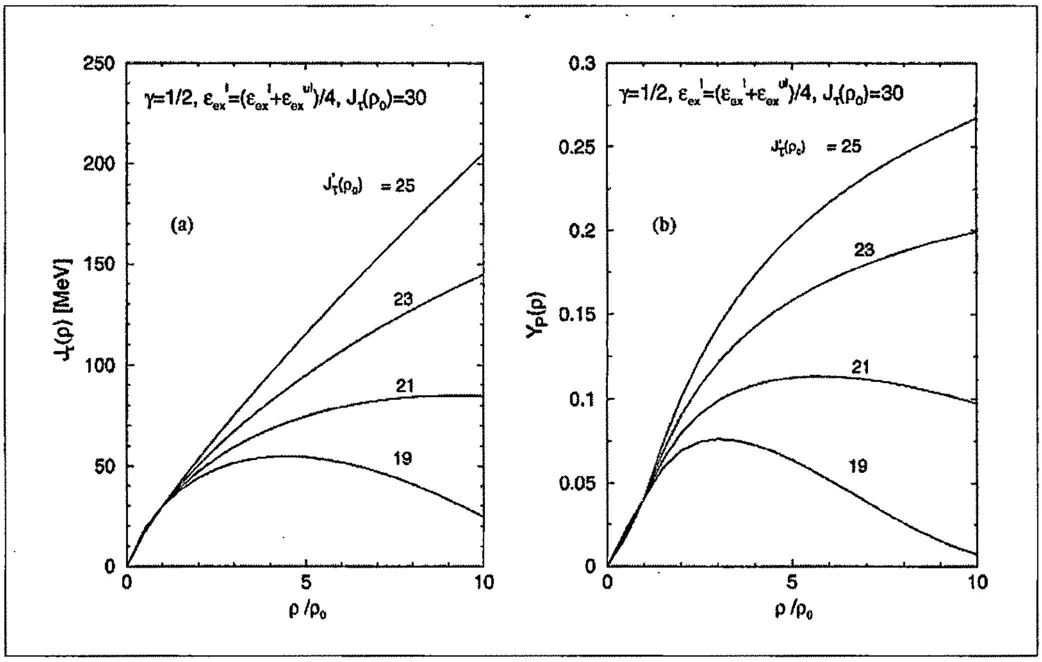

Figure 5.2: High density behaviour of nuclear symmetry energy $J_\tau(\rho)$ (panel (a)) and equilibrium proton fraction $Y_p(\rho)$ (panel (b)) in NSM for different EOS.

under the condition of beta-equilibrium the range of functional $S^{NSM}(\rho,\ Y_p)$ for different EOS considered in Fig. 5.1 shows a much smaller variation over a wide range of density than exhibited by $J_\tau(\rho)$ and $Y_p(\rho)$ for these EOS in Figs. 5.2(a) and 5.2(b). The stiffest behaviour of the functional $S^{NSM}(\rho,\ Y_p)$ at high densities is obtained around the value $J_\tau'(\rho_0) = 21.8\ MeV$. Moreover, this stiffest high density behaviour of $S^{NSM}(\rho,\ Y_p)$ remains almost the same with respect to a variation of $J_\tau'(\rho_0)$ within a narrow range around this critical value although the two extreme EOS in this narrow range can differ significantly in their high density behaviour of symmetry energies $J_\tau(\rho)$ and equilibrium proton fractions $Y_p(\rho)$ in NSM. This is illustrated in Figs. 5.1, 5.2(a) and 5.2(b) for EOS with $J_\tau'(\rho_0)$ in the range $21\ MeV \leq J_\tau'(\rho_0) \leq 23\ MeV$. It should be noted that stiffest behaviour of the functional $S^{NSM}(\rho,\ Y_p)$ at high densities leads to a density dependence of $J_\tau(\rho)$ which is neither very stiff nor soft. The variation in the critical values of $J_\tau'(\rho_0)$ with respect to changes in the assumed standard values of $J_\tau(\rho_0)$ and the parameter γ are listed in Table 5.1. The critical value of $J_\tau'(\rho_0)$ for which the functional $S^{NSM}(\rho,\ Y_p)$ has the stiffest high density behaviour is found to increase with increase in the value of $J_\tau(\rho_0)$. On the other hand, the critical value of $J_\tau^{'}(\rho_0)$ increases rather slowly with the increase in γ for relatively higher values of symmetry energy $J_\tau(\rho_0)$.

Table 5.1: Critical values of $J_\tau^{'}(\rho_0)$ along with those of isospin-dependant part of isobaric incompressibility, $K_{asy}(\rho_0)$, for the stiffest behaviour of the functional $S^{NSM}(\rho, Y_p)$ at high densities obtained from EOSs with different values of $J_\tau(\rho_0)$ and γ. The nuclear matter incompressibility $K(\rho_0)$ at normal density ρ_0 which increases with increase in γ is also listed. The threshold densities ρ_{DU} for direct URCA processes and corresponding neutron star masses M_{DU} are also given for those EOSs where these limits are reached (see text).

EOSs	$J_\tau(\rho_0)$ [*MeV*]	γ	$K(\rho_0)$ [*MeV*]	$J_\tau^{'}(\rho_0)$ [*MeV*]	$K_{asy}(\rho_0)$ [*MeV*]	ρ_{DU} [fm^{-3}]	M_{DU} [M_{solar}]
I(A)	*28*	*1/12*	*190*	*20.6*	*−435.5*	*1.19*	*1.673*
I(B)	*28*	*1/2*	*240*	*20.6*	*−435.5*	*1.19*	*1.888*
I(C)	*28*	*1*	*287*	*20.6*	*−435.5*	*1.19**	–
II(A)	*30*	*1/12*	*190*	*21.6*	*−462.9*	*1.18*	*1.659*
II(B)	*30*	*1/2*	*240*	*21.8*	*−467.0*	*1.26*	*1.885*
II(C)	*30*	*1*	*287*	*21.9*	*−469.5*	–	–
III(A)	*32*	*1/12*	*190*	*22.6*	*−490.3*	*1.10*	*1.629*
III(B)	*32*	*1/2*	*240*	*23.0*	*−498.4*	–	–
III(C)	*32*	*1*	*287*	*23.3*	*−503.8*	–	–

The high density behaviour of the functional $S^{NSM}(\rho, Y_p)$ calculated with critical values of $J_\tau^{'}(\rho_0)$ for the four EOS having extreme values of $J_\tau(\rho_0)$ and γ in Table 5.1, namely, I(A), I(C), III(A) and III(C) is given in Fig. 5.3. All curves of $S^{NSM}(\rho, Y_p)$ are almost the same over the entire range of density shown in the figure. In view of this, curves of $S^{NSM}(\rho, Y_p)$ obtained from all EOSs with $1/12 \le \gamma \le 1$, 28 $MeV \le J_\tau(\rho_0) \le 32$ MeV and within a narrow range around their respective critical values of $J_\tau^{'}(\rho_0)$ in Table 5.1 would constitute a very narrow band over a wide range of density. We have also

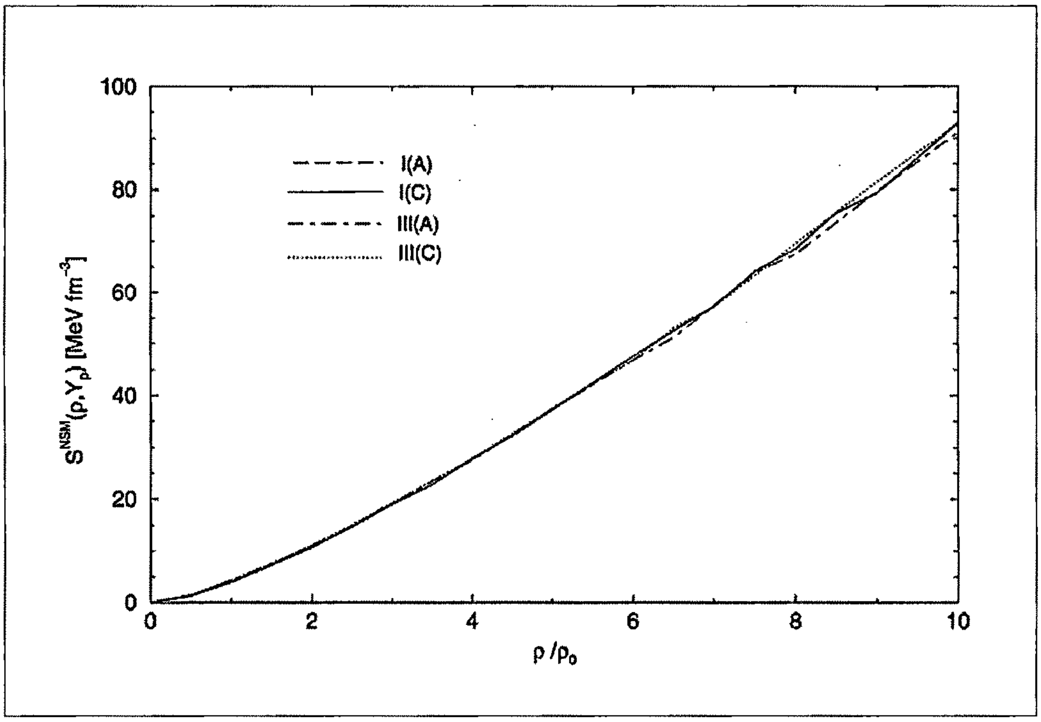

Figure 5.3: Stiffest behaviour of the functional $S^{NSM}(\rho,\ Y_p)$ for four different EOS with extreme values of $J_\tau(\rho_0)$ and γ in Table 5.1.

verified that this narrow band characterizing the stiffest high density behaviour of the functional $S^{NSM}(\rho,\ Y_p)$ remains almost the same when splitting of the asymmetric contribution to the nucleonic part of energy density in NSM, $S^{NSM}(\rho,\ Y_p)$, is found to be universal to a good approximation for nuclear EOSs which are asymmetrical neither very stiff nor soft at high densities. This point is illustrated in Figs. 5.1, 5.2(a) and 5.2(b) for EOS with $J_\tau'(\rho_0)$ in the range 21-23 *MeV* and excludes those with $J_\tau'(\rho_0) > 23$ *MeV*/ $J_\tau'(\rho_0)$ < 21 *MeV* as asymmetrically very stiff/soft EOSs. This universal behaviour of the functional $S^{NSM}(\rho,\ Y_p)$ has also been observed by Klahn *et al.* [6] for many EOS obtained from relativistic description of nuclear matter which fulfill the direct URCA (DU) constraint discussed in next section.

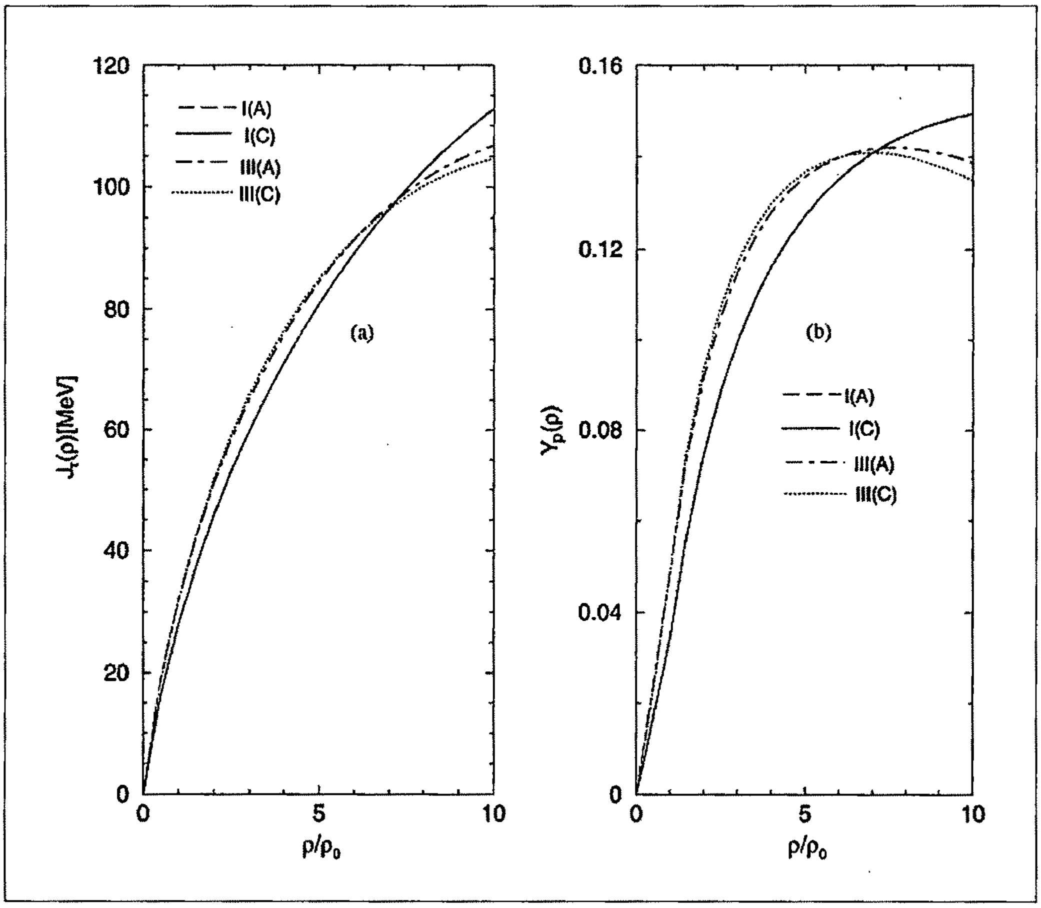

Figure 5.4: Density dependence of nuclear symmetry energy $J_\tau(\rho)$ (panel (a)) and equilibrium proton fraction $Y_p(\rho)$ (panel (b)) in NSM obtained from four different EOS in Table 5.1 with extreme values of $J_\tau(\rho_0)$ and γ.

It should be noted that all EOS in table 5.1 have almost the same high density behaviour of the functional $S^{NSM}(\rho,\ Y_p)$. However, these EOS can differ significantly in their asymmetric stiffness. As discussed in chapter 3 the asymmetric stiffness of nuclear EOS are often characterized by three parameters, namely, the symmetry energy $J_\tau(\rho_0)$, slope parameter $L(\rho_0)$ and $K_{asy}(\rho_0)$ at normal density. The universal behaviour of the functional $S^{NSM}(\rho,\ Y_p)$ at high densities for all EOS in table 5.1 constrains $L(\rho_0)$ and $K_{asy}(\rho_0)$ in the range 62 $MeV \leq L(\rho_0) \leq 70$ MeV and -504 $MeV \leq K_{asy}(\rho_0) \leq -436$ MeV respectively which can be compared with the estimated ranges of these two parameters. As discussed in chapter 3, a combination of analysis of neutron skin thickness in finite nuclei and isospin diffusion in high energy heavy ion collisions [10] suggest that the value of slope parameter $L(\rho_0)$ lies in the range 62 $MeV \leq L(\rho_0) \leq 107$ MeV and the value of $K_{asy}(\rho_0)$ is estimated in the range -500 ± 50 MeV from analysis of isospin diffusion in high energy heavy-ion collisions [14]. The values of $L(\rho_0)$ obtained here also agree well with the recent results obtained by Agrawal *et al.* [21, 22] using generalized Skyrme-effective forces (GSEF) whose parameters are determined from a fit to several properties of normal and isospin-rich nuclei as well as a realistic EOS of pure neutron matter (PNM).

The density dependence of nuclear symmetry energy $J_\tau(\rho)$ and equilibrium proton fraction, $Y_p(\rho)$ in NSM obtained from the four different EOS with extreme values of $J_\tau(\rho_0)$ and γ in table 5.1 are given in Figs. 5.4(a) and 5.4(b), respectively. These figures clearly show that high density behaviour of $J_\tau(\rho)$ and $Y_p(\rho)$ should not be too 'stiff' nor too 'soft'. It is also seen that different curves of $J_\tau(\rho)$ as well as $Y_p(\rho)$ cross over at a density around $\rho = 7\,\rho_0$ which is a consequence of the universal high density behaviour of the functional $S^{NSM}(\rho,\, Y_p)$. As a result of this, the asymmetric stiffness of the EOS in table 5.1 increase with increase in the standard value of $J_\tau(\rho_0)$ in the region $\rho < 7\rho_0$. On the other hand, for a given value of $J_\tau(\rho_0)$ the asymmetric stiffness of these EOS are almost independent of the parameter γ in the region $\rho < 7\rho_0$ but slowly decreases with increase in γ for relatively higher values of $J_\tau(\rho_0)$ when $\rho > 7\rho_0$.

5.4. Neutron star properties

We now calculate the threshold density at which DU process starts for the different EOS given in table 5.1. The DU threshold for a given EOS occurs at a corresponding critical nucleon density ρ_{DU}. The DU-critical densities ρ_{DU} are also listed in table 5.1 for those EOS where the limit is reached. Depending on the EOS this threshold can be reached for a wide range of densities as in the cases of I(A), I(B), I(C), II(A) and II(B) of table 5.1. On the other hand, the DU process does not take place at all for EOS II(C), III(B) and III(C). However, in case of III(A) the DU process takes place within a small range of densities, $\rho = 1.10 - 1.32\ fm^{-3}$. These results show the model dependence of the DU threshold.

In ref. [6] Klahn *et al.*, have discussed that the DU process should not occur in typical neutron stars which have masses in the range $M = 1.0$ to $1.5\ M_{solar}$. All the EOSs considered in their work which fulfill this constraint exhibit a universal high density behaviour of the functional $S^{NSM}(\rho,\ Y_p)$ to a good approximation. Setting ρ_{DU} as a neutron star's central density, results in a DU-critical neutron star mass M_{DU}. The DU-critical densities ρ_{DU} and the corresponding neutron star masses M_{DU} are also listed in table 5.1. Every neutron star with a mass only slightly above M_{DU} will be efficiently cooled by DU-processes and very quickly becomes almost invisible for thermal detection [181]. In this connection it is important to note that M_{DU} is meaningless for those EOS for which ρ_{DU} is greater than the central density ρ_c of the corresponding maximum mass neutron star. It is found from table 5.1 that M_{DU} is significantly larger than $1.5\ M_{solar}$ in all cases. Thus the universal behaviour of the functional $S^{NSM}(\rho,\ Y_p)$ at high densities constrains the density dependence of nuclear symmetry energy $J_\tau(\rho)$ and equilibrium proton fraction, $Y_p(\rho)$ in NSM, in conformity of the DU constraint discussed in the work of Klahn *et al.* [6].

We now examine the influence of parameter γ and the value of $J_\tau(\rho_0)$ on neutron star properties calculated for different EOS in table 5.1. For this purpose, in this work we have compared results of neutron star properties for the four different EOS, namely, I(A), I(C), III(A) and III(C) having extreme values of γ and $J_\tau(\rho_0)$. This brings out the influence of γ and $J_\tau(\rho_0)$ on neutron star properties in a more clear manner. The resulting neutron star masses $M(\rho_c)$ as a function of their central densities ρ_c for different EOS are given in Fig. 5.5. With increase in parameter γ, the $M(\rho_c) \sim \rho_c$ curves are shifted towards the lower density region. Moreover, the $M(\rho_c) \sim \rho_c$ curves for EOSs with same γ but different values of $J_\tau(\rho_0)$ are almost same which is a consequence of the fact that these EOS have the same contribution to the nucleonic part of energy density in NSM. The stiffness of these curves and the values of maximum mass of neutron stars which increase with γ are, therefore, essentially determined by the high density behaviour of the respective EOS in SNM. In connection with the maximum mass neutron star we note that any reliable nuclear EOS should be able to reproduce the recently reported high pulsar mass of $2.1 \pm 0.2\ M_{solar}$ ($1\sigma-$ confidence level) and $2.1 \begin{pmatrix} +0.4 \\ -0.5 \end{pmatrix} M_{solar}$ ($2\sigma-$confidence level) for PSR J0751 + 1807 [182] as well as the mass of 2.1 ± 0.2 M_{solar} estimated from the innermost stable circular orbit for 4U 1636–536 [183]. As can be seen from Fig. 5.5 none of these values for all EOS in table 5.1 falls below the 2σ mass limit of 1.6 M_{solar} for PSR J0751 + 1807. On the other hand, the 1σ lower mass limit of 1.9 M_{solar} for PSR J0751 + 1807 which is also the lower mass limit for 4U 1636– 536 would

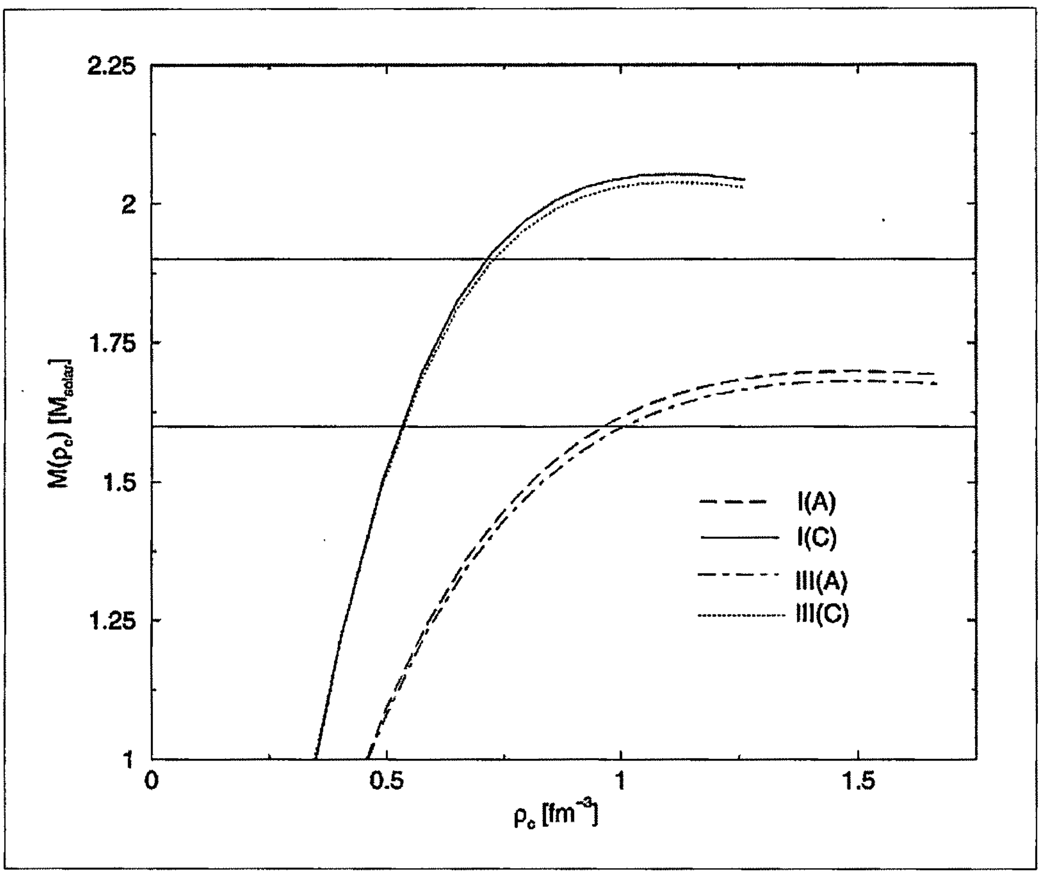

Figure 5.5: Neutron star masses $M(\rho_c)$ as a function of their central densities ρ_c, obtained from four different EOS with extreme values of $J_\tau(\rho_0)$ and γ in Table 5.1. The 1σ – and 2σ – lower mass limits of 1.9 M_{solar} and 1.6 M_{solar} respectively for PSR J0751 + 1807 [182] are also shown by horizontal lines (see text).

exclude all EOS for which $\gamma < 1/2$. In this context we note that while the flow data constraint [3] discussed in connection with Fig. 3.1 would limit the maximum mass of neutron star in the range 1.68 $M_{solar} \leq M_{max} \leq 2.05$ M_{solar} for EOSs considered in this work, the constraint on nuclear matter incompressibility $K(\rho_0)$ at normal density ρ_0 coming from studies on giant monopole resonances in finite nuclei would restrict M_{max} to 1.73 $M_{solar} \leq M_{max} \leq 1.9$ M_{solar}.

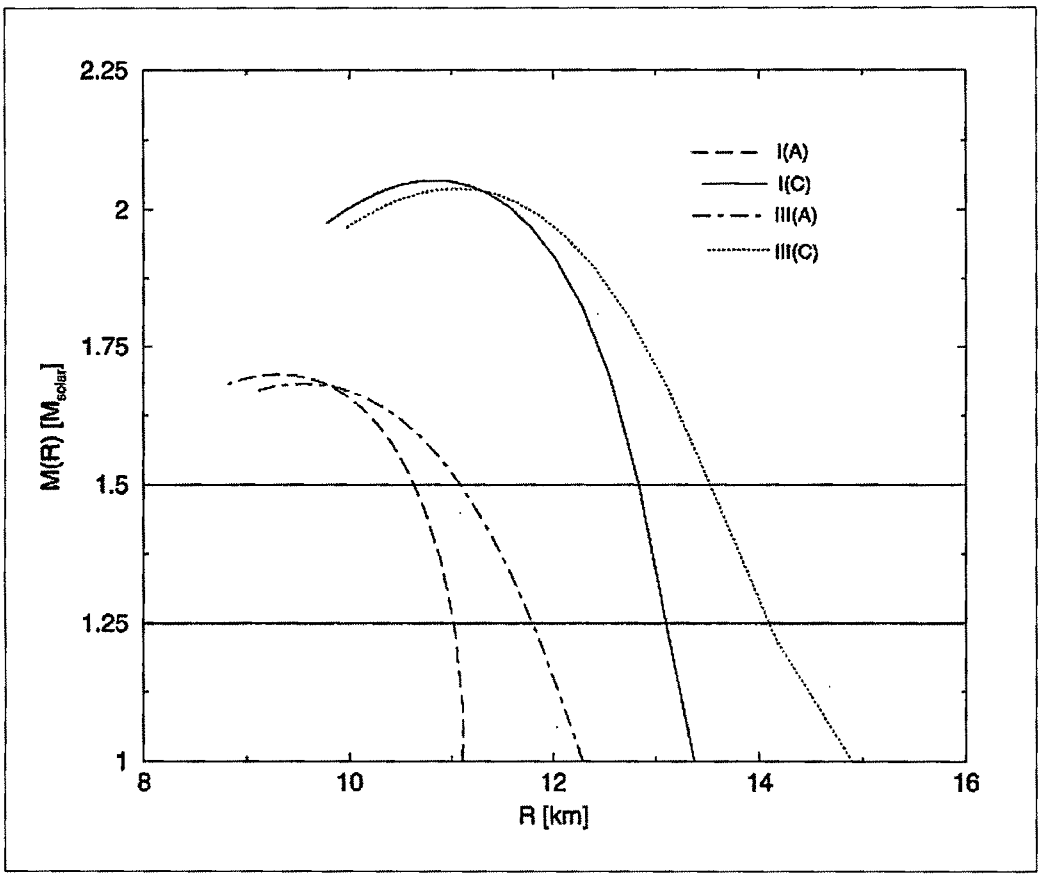

Figure 5.6: Neutron star masses $M(R)$ as a function of their radii R obtained from four different EOS with extreme values of $J_\tau(\rho_0)$ and γ in Table 5.1. The mass of typical neutron stars in the range $M \sim 1.0 - 1.5$ M_{solar} as well as the mass of Pulsar B in the double pulsar J0737–3039 [185] are also shown by horizontal lines.

The neutron star masses $M(R)$ as a function of their radii R obtained from different EOS are given in Fig 5.6. It is found that for typical neutron stars which have masses in the range $M \sim 1.0$ $M_{solar} - 1.5$ M_{solar}, the radius R increases with increase in γ as well as $J_\tau(\rho_0)$. However, for a given value of γ, the rate of increase in R with increase in the value of $J_\tau(\rho_0)$ is slowed down when we move towards higher mass region and curves with same γ but different $J_\tau(\rho_0)$ cross over in the maximum mass region and differ only marginally from each other. This is due to the fact that asymmetric stiffness of the EOS, shown in Figs. 5.4 (a) and 5.4(b), increase with increase in $J_\tau(\rho_0)$ in the region $\rho < 7\rho_0$ and conversely for $\rho > 7\rho_0$. As a result of this the maximum mass of a neutron star is dominantly determined by the parameter γ, a result already observed in connection with $M(\rho_c) \sim \rho_c$ curves in Fig. 5.5.

Recently it has been suggested in ref. [184] that pulsar B in the double pulsar system J0737–3039 can provide an important test for EOS of very dense nuclear matter. This has the lowest reliably measured mass for a neutron star to date, namely, $M = 1.249 \pm 0.001\ M_{solar}$ [185]. The free baryon mass M_A of this neutron star has been inferred theoretically in the range $1.366\ M_{solar} \leq M_A \leq 1.375\ M_{solar}$ on the basis that it originates from the collapse of an ONeMg white dwarf and the loss of matter during its formation is negligible [184]. Any EOS of dense nuclear matter must, therefore, predict a free baryon mass M_A in the range $1.366\ M_{solar} \leq M_A \leq 1.375\ M_{solar}$ for a neutron star whose gravitational mass is in the range $M = 1.249 \pm 0.001\ M_{solar}$. The relation between gravitational mass M and baryon mass M_A of neutron stars for different EOS is given in Fig. 5.7. The rectangle in the figure denotes the constraint derived from pulsar B in the double pulsar J0737–3039. The M-M_A line for ant EOS proposed for NSM must pass through the depicted rectangle. It can be seen from Fig. 5.7 that the M - M_A lines of all EOS listed in table 5.1 pass through the depicted rectangle except those having very low (high) values of both γ and $J_\tau(\rho_0)$. As can be seen from Fig. 5.5 the central densities of typical neutron stars having masses in the range $1\ M_{solar} \leq M \leq 1.5\ M_{solar}$ for all EOSs in table 5.1 approximately varies from $2\rho_0$ to $5\rho_0$. Because of the universal behaviour of the functional $S^{NSM}(\rho, Y_p)$ at high densities, the asymmetric stiffness of the EOS shown in Figs. 5.4(a) and 5.4(b) increases with increase in the value of $J_\tau(\rho_0)$ and remains almost independent of the value of γ in this range of density. Thus EOS with very low (high) value of γ and $J_\tau(\rho_0)$ are very soft (stiff) both symmetrically as well as asymmetrically.

Comparing Figs. 5.6 and 5.7 we see that EOS which are very soft (stiff) both symmetrically as well as asymmetrically predict smaller (larger) radius and an over binding (underbinding) of a neutron star. In view of this symmetrically very soft EOS have to be asymmetrically stiff and conversely so that they can better accommodate the $M(R) - R$ and $M - M_A$ relations. In this context it may be mentioned here that none of the $M - M_A$ lines obtained from relativistic EOS in ref. [6] pass through the depicted rectangle in Fig. 5.7.

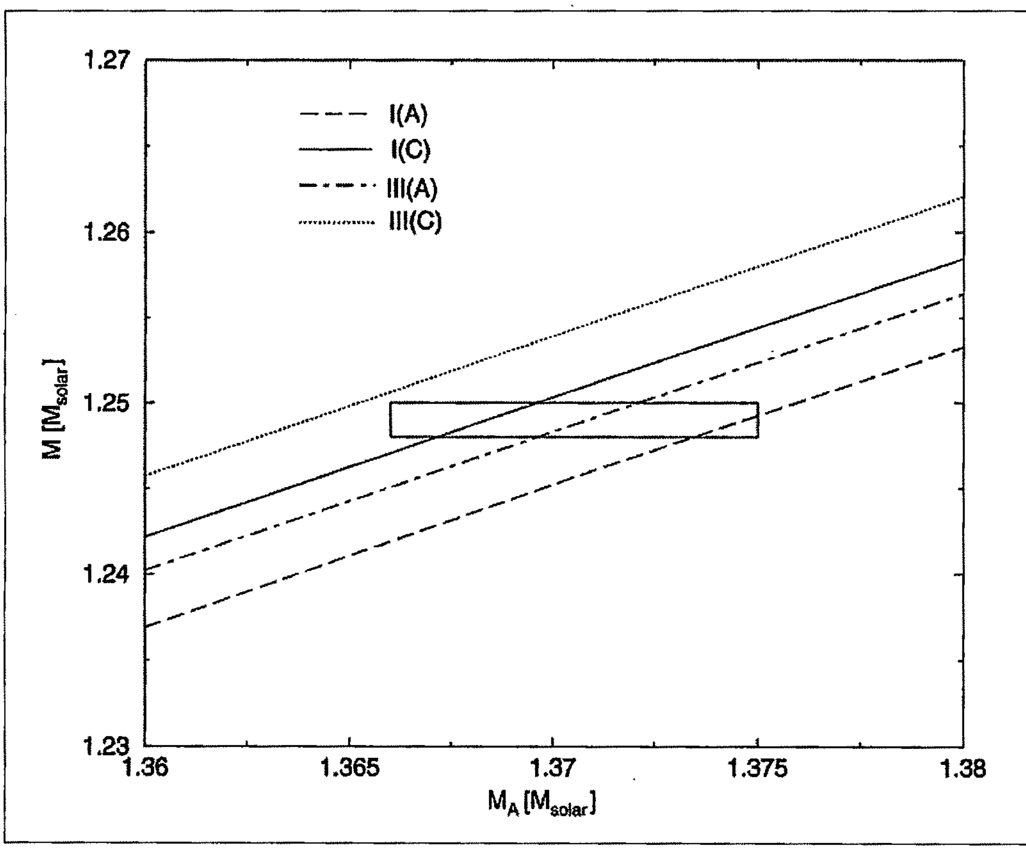

Figure 5.7: Relation between gravitational mass M and baryon mass M_A of neutron stars for four different EOS with extreme values of $J_\tau(\rho_0)$ and γ in Table 5.1. The rectangle denotes the constrain derived from Pulsar B in the double pulsar J0737–3039 [184, 185].

5.5. Summary

In this chapter we studied the EOS of beta-stable n+p+e+μ matter, i.e. NSM, using simple parametrisations of finite range effective interaction which was constructed in chapter 3 to study the EOS of ANM. Information coming from recent findings on neutron star cooling phenomenology as well as mass measurements were applied to constrain the additional parameters involved.

The high density behaviour of asymmetric contribution to nucleonic part of energy density $S^{NSM}(\rho,\ Y_p)$ in NSM was found to exhibit an approximate universal character for nuclear EOS which are neither too stiff nor too soft at high densities. The density dependence of nuclear symmetry energy was constrained on the basis of this universal high density behaviour of the functional $S^{NSM}(\rho,\ Y_p)$. The equilibrium proton fraction $Y_p(\rho)$ in NSM obtained as a function of density ρ with these EOS are found to be in conformity with the DU constraint discussed by Klahn *et al.* [6]. According to this constraint , the DU process would cool neutron stars much faster so that it should not occur for typical stars with masses in the range $M = 1 - 1.5\ M_{solar}$, otherwise it would affect most of the neutron star population.

Because of the universal behaviour of the functional $S^{NSM}(\rho,\ Y_p)$ at high densities, the $M(\rho_c) \sim \rho_c$ curves of neutron stars essentially determined by the high density behaviour of the respective EOS in SNM. Then it appears that the flow data constraint would limit the maximum mass of neutron stars in range $1.68\ M_{solar} \leq M_{max} \leq 2.05\ M_{solar}$ for EOS considered in the present chapter. On the other hand, the constraint on nuclear incompressibility $K(\rho_0)$ at normal density coming from studies on monopole vibrations in finite nuclei would restrict the maximum mass of neutron stars to $1.73\ M_{solar} \leq M_{max} \leq 1.90\ M_{solar}$. These results can be compared with the recently reported high pulsar mass of $2.1 \pm 0.2\ M_{solar}$ (1 σ confidence level) and $2.1 \begin{pmatrix} +0.4 \\ -0.5 \end{pmatrix} M_{solar}$ (2 σ confidence level) for PSR J0752 + 1807 as well as the mass of $2.0 \pm 0.1\ M_{solar}$ estimated from innermost stable circular orbit for 4U 1636-536.

The $M - M_A$ as well as $M(R) - R$ relations of typical neutron stars with masses in the range $M = 1 - 1.5\ M_{solar}$ tend to exclude EOS which are stiff (soft) both symmetrically as well as asymmetrically since such EOS predict larger (smaller) radius and an underbinding (overbinding) of a neutron star. In view of this symmetrically stiff EOS has to be asymmetrically soft and conversely, so that they can better accommodate the $M - M_A$ as well as $M(R) - R$ relations.

To conclude this chapter, we emphasize on the need of more theoretical and experimental efforts for a better understanding of high density behaviour of nuclear matter EOS.

CHAPTER 6

SUMMARY AND CONCLUSION

In the present work we have mainly focused on the study of EOS of isospin asymmetric nuclear matter (ANM) using a simple density dependent finite range effective interaction over a wide range of density, asymmetry and temperature. Particular emphasis has been given to the existing controversy on the density dependence of nuclear symmetry energy, momentum dependence of isovector part of nuclear mean fields and nucleon effective mass splitting. A brief study on thermal evolution of EOS of nuclear matter and phase transition has been done. The EOS of beta-stable matter found in the interior of neutron stars and properties of nuclear matter has also been studied.

From this thesis it was seen that:

- There exists a controversy regarding the high density behaviour of nuclear symmetry energy $J_\tau(\rho)$ as predicted by different theoretical calculations. Based on the behaviour of nuclear symmetry energy at high density all theoretical calculations can be divided into two groups, one where $J_\tau(\rho)$ increases monotonically and the other where it decreases after reaching a maximum value and then ultimately becomes negative with increasing density.
- All theoretical predictions on the momentum dependence of isovector part of nuclear mean field can be classified into two distinct and opposite groups depending on whether it decreases or increases with momentum.
- The sign of neutron and proton effective mass splitting is still controversial.
- The momentum and density dependence of isoscalar and isovector parts of nuclear mean field can be simulated for a general finite range effective interaction.

- The sign of the splitting of neutron and proton effective masses depends on the choice of interaction parameters connected with the exchange part of the effective interaction.
- Density dependence of nuclear matter properties like energy per particle, chemical potentials, pressure, incompressibility and speed of sound in both SNM and ANM are determined by the behaviour of isoscalar and isovector parts of nuclear mean field at the Fermi momentum $k = k_f$ and follow in a trivial way once the density dependence of nuclear symmetry energy $J_\tau(\rho)$ and energy per particle $e(\rho)$ in SNM are fixed.
- Different EOS of ANM sharing the same density dependence of $e(\rho)$ and $J_\tau(\rho)$ but having quite different momentum dependence of isovector part of nuclear mean field will lead to almost the same results for properties like energy per particle, chemical potentials, pressure and incompressibility in both SNM and ANM. However, these different EOS can give rise to significantly different predictions on experimental observables sensitive to the differences between neutron and proton flow data in highly asymmetric dense nuclear matter.
- A simple density dependent finite range effective interaction of Yukawa form can be used to construct the EOS of ANM and the properties of nuclear matter can be studied using this interaction.
- A number of parameter sets of the interaction can be determined from existing experimental/empirical data and simple physical conditions. Information coming from optical model analysis of nucleon-nucleus scattering data, transport model analysis of flow data in HI collisions, monopole mode of vibration in finite nuclei and simple physical conditions were used to constrain the interaction parameters.
- The existing controversies regarding the high density behaviour of symmetry energy and neutron proton effective mass splitting can be analysed using the different parameter sets.
- A liquid-gas (LG) like phase transition occurs in nuclear matter at low density and moderate temperature. The LG phase-transition is found to be of second order in ANM.
- The EOS of beta-stable matter found in the interior of a neutron star can be studied using the simple effective interaction. The high density behaviour of

asymmetric contribution to nucleonic part of energy density $S^{NSM}(\rho)$ in NSM is found to exhibit an approximate universal character for nuclear EOS which are asymmetrically neither too stiff nor soft at high densities.

- The density dependence of the nuclear symmetry energy $J_\tau(\rho)$ can be constrained on the basis of this universal high density behaviour of the functional $S^{NSM}(\rho)$.
- Symmetrically stiff EOS has to be asymmetrically soft and conversely to better accommodate the M - M_A and M(R) – R relations of typical neutron stars.

To conclude, we emphasize on the need of more theoretical and experimental efforts for a better understanding of the EOS of dense ANM. The existing controversies in the prediction of high density behaviour of nuclear symmetry energy and the two opposite types of splitting of neutron and proton effective masses by different theoretical calculations can only be resolved through continuous analysis of experimental observables sensitive to the differences between neutron and proton flow data in highly asymmetric dense nuclear matter. A combined interpretation of experimental data from nucleon-nucleus scattering at intermediate energies, flow data in heavy-ion collisions, centroid energies of giant monopole resonances in finite nuclei as well as astrophysical measurements and cooling phenomenology of neutron stars can put constrain on the high density behaviour of nuclear EOS. The simple form of finite range effective interaction considered in this thesis work appears to be very useful in these investigations.

Finally in future we plan to put more stringent constraints on the interaction parameters and extend the present analysis on EOS of hot ANM and study the phase-transition in nuclear matter using this simple finite range effective interaction.

BIBLIOGRAPHY

1. B.A. Li, L.W. Chen, C.M. Ko, Phys. Rep. **464** (2008) 113.
2. B.A. Li, W. Udo Schroder (Eds.), *Isospin Physics in Heavy-Ion Collisions at Intermediate Energies*, Nova Science Publishers, Inc., New York, 2001.
3. P.Danielewicz, R.Lacey, W.G.Lynch, Science **298** (2002)1592.
4. A.W.Steiner, M. Prakash, J.M. Lattimer, P.J. Ellis, Phys. Rep. **411** (2005) 325.
5. B.G. Todd-Rutel, J. Piekarewicz, Phys. Rev. Lett. **95** (2005) 122501.
6. T. Klahn, et al., Physc. Rev. **C 74** (2006) 035802.
7. J.M. Lattimer, M. Prakash, Science **304** (2004) 536.
8. J.M. Lattimer, M. Prakash, Phys. Rep. **333** (2000) 121.
9. J.M. Lattimer, M. Prakash, Astrophys. J. **550** (2001)426.
10. B.A. Li, A.W. Steiner, Phys. Lett. **B 642** (2006) 436.
11. V. Baran, M. Colonna, V. Grecco, M. Di Toro, Phys. Rep. **410** (2005) 335.
12. M.B. Tsang, et al., Phys. Rev. Lett. **92** (2004) 062701.
13. L.W. Chen, C.M. Ko, B.A. Li, Phys. Rev. Lett. **94** (2005) 032701.
14. B.A. Li, L.W. Chen, Phys. Rev. **C 72** (2005) 064611.
15. R. B. Wiringa, V. Ficks, A. Fabrocini, Phys. Rev. **C 38** (1988) 1010.
16. A. Akmal, V. R. Pandharipande, D.G. Ravenhall, Phys. Rev. **C 58** (1998) 1804.
17. E. Chabanat, P. Bonche, P. Haensel, J. Mayer, R. Schaeffer, Nucl. Phys. **A 627** (1997) 710.
18. E. Chabanat, P. Bonche, P. Haensel, J. Mayer, R. Schaeffer, Nucl. Phys. **A 635** (1998) 231.
19. J.R. Stone, J.C. Miller, R. Koncewicz, P.D. Stevenson, M.R. Strayer, Phys. Rev. **C 68** (2003) 034324.
20. S. Goriely, M. Samyn, P.-H. Heenen, J.M. Pearson, M. Onsi, Nucl. Phys. **A 750** (2005) 425.
21. B.K. Agrawal, S.Shlomo, V.K. Au, Phys. Rev. **C 72** (2005) 014310.
22. B.K. Agrawal, S.K. Dhiman, R.Kumar, Phys. Rev. **C 73** (2006) 034319
23. H.A. Bethe, Rev. Mod. Phys. **62** (1990) 801.

24. C. Fuchs, Prog. Part. Nucl. Phys. **56** (2006) 1.
25. M. Colonna, M. Di Toro, G. Fabri, S. Maccarone, Phys. Rev. **C 57** (1998)1410.
26. B.A. Li, C.M. Ko, W. Bauer, Topical review, Int. J. Mod. Phys. **E** 7 (1998)147.
27. B.A .Li, Phys. Rev. Lett. **88** (2002) 192701.
28. B.A. Li, Nucl. Phys. **A 708** (2003) 365.
29. The DOE/NSF Nuclear Science Advisory Committee Opportunities in Nuclear Science, April, 2002.
30. C.B. Das, S. Das Gupta, C. Gale, B.A. Li, Phys. Rev. **C 67** (2003) 034611.
31. B.A. Li, C.B. Das, S. Das Gupta, C. Gale, Nucl. Phys. **A 735** (2004) 563.
32. B.A. Li, C.B. Das, S. Das Gupta, C. Gale, Phys. Rev. **C 69** (2004) 011603(R).
33. J. Rizzo, M. Colonna, M. Di Toro, V. Greco, Nucl. Phys. **A 732** (2004) 202.
34. W.D. Myers, W.J. Swiatecki, Nucl. Phys. **A 81** (1966) 1.
35. K. Pomorski, J. Dudek, Phys. Rev. **C 67** (2003) 044316.
36. I. Bombaci, in ref. [2], p.35.
37. A.E.L. Dieperink, Y. Dewulf, D. Van Neck, M. Waroquier, V. Rodin, Phys. Rev. **C 68** (2003) 064307.
38. M. Prakash, et al., Phys. Rep. **280** (1997) 1.
39. B. Friedman, V.R. Pandharipande, Phys. Lett. **B 100** (1981) 205.
40. R.B. Wiringa, Phys. Rev. **C 38** (1988) 2967.
41. A. Akmal, V. R. Pandharipande, Phys. Rev. **C 56** (1997) 2261.
42. A. Mukherjee, V.R. Pandharipande, Phys. Rev. **C 75** (2007) 035802.
43. V.R. Pandharipande, R.B. Wiringa, Rev. Mod. Phys., **51** (1979) 821.
44. J. Navarro, R. Guardiola, I.Moliner, *Introduction To Modern Methods Of Quantum Many-Body Theory And Their Applications*, in: A. Fabrocini, S. Fantoni, E. Krotscheck (Eds.) Series on Advances in Many-body theory, Vol.7, World Scientific, Singapore, 2002.
45. A. Bohnet, N. Ohtsuka, J. Aichelin, R. Linden and A. Faessler, Nucl. Phys. **A 494** (1989) 349.
46. J. Jaenicke, J. Aichelin, N. Ohtsuka, R. Linden and A. Faessler, Nucl. Phys. **A 536** (1992) 201.
47. G. Q. Li, Y. Lotfy, S.W. Huang, A. Faessler, J. Phys. **G 18** (1992) 291
48. D.T. Khoa, N. Ohtsuka, M.A. Matin, A. Faessler, S. W. Huang, E. Lehmann, R.K. Puri, Nucl. Phys. **A 548** (1992)102

49. M. Baldo, I. Bombaci, G. Giansiracusa, U. Lombardo, Phys. Rev. **C 40** (19890 R491
50. A. Insolia, U. Lombardo, N.G. Sandulescu, A. Bonasera, Phys. Lett. **B 334** (1994) 12.
51. I. Bombaci, U. Lombardo, Phys. Rev. **C 44** (1991) 1892
52. W. Zuo, I. Bombaci, U. Lombardo, Phys. Rev. **C 60** (1999) 024605
53. M. Baldo, L.S. Ferreira, Phys. Rev. **C 59** (1999) 682
54. W. Zuo, A. Lejeune, U. Lombardo, J.F. Mathiot, Eur. Phys. J. **A 14** (2002) 469.
55. M. Baldo, *Nuclear Methods and The Nuclear Equation of State*, in: M. Baldo (Ed.), International Review of nuclear Physics, vol.8 World Scientific, Singapore, (1999), p1.
56. M. Baldo, C.Maieron, J. Phys. **G 34** (2007) R243.
57. B. ter Haar, R. Malfliet, Phys. Rev. Lett. **56** (1986)1237.
58. B. ter Haar, R. Malfliet, Phys. Rep. **149** (1987)207.
59. R. Brockmann, R. Machleidt, Phys. Lett. **149B** (1984)283.
60. R. Brockmann, R. Machleidt, Phys. Rev. **C 42** (1990)1965.
61. G.Q. Li, R. Machleidt, Phys. Rev. **C 45** (1992)2782.
62. G.Q. Li, R. Machleidt, Phys. Rev. **C 48** (1993)2707.
63. H. Muther, M. Prakash, T.L. Ainsworth, Phys. Lett. **B 199** (1987) 469.
64. B. ter Haar, R. Malfliet, Phys. Rev. Lett. **59** (1987) 1652.
65. R. Malfliet, Nucl. Phys. **A 488** (1988) 721c.
66. L. Engivik, M. Hjorth-Jensen, E. Osnes, G. Bao, E. Ostgaard, Phys. Rev. Lett. **73** (1994) 2650.
67. H. Huber, F. Weber, M.K. Wiegel, Phys. Rev. **C 51**(1995) 1790.
68. C.H. Lee, T.T.S. Kuo, G. Q. Li, G.E. Brown Phys. Rev. **C 57**(1998) 3488.
69. N. Frolich, H. Baier, W. Bentz, Phys. Rev. **C 57**(1998) 3447.
70. F. de Jong, H. Lenske, Phys. Rev. **C 57**(1998) 3099.
71. F. Hofmann, C.M. Keil, H. Lenske, Phys. Rev. **C 64** (2001) 034314.
72. Z.Y. Ma, J. Rong, B.Q. Chen, Z.Y. Zhu, H.Q. Song, Phys. Lett. **B 604** (2004) 170.
73. F. Sammarruca, W. Barredo, P. Krastev, Phys. Rev. **C 71** (2005) 064306.
74. J.P. Jeukenne, A. Lejeune, C. Mahaux, Phys. Rep. **25** (1976) 83.
75. B.D. Day, R.B. Wiringa, Phys. Rev. **C 32** (1985) 1057.

76. H.Q. Song, M. Baldo, G. Giansiracusa, U. Lombardo, Phys. Lett. **B 411** (1997) 237; *ibid*, Phys. Rev. Lett. **81** (1998) 1584.
77. M. Baldo, A. Fiasconaro, H.Q. Song, G. Giansiracusa, U. Lombardo, Phys. Rev. **C 65** (2001) 017303.
78. Z. H. Li, U. Lombardo, H.-J. Schulze, W. Zuo, L.W. Chen. Ma, Phys. Rev. **C 74** (2006) 047304.
79. R. Machleidt, Adv. Nucl. Phys. **19** (1989) 189.
80. E.E. Salpeter, H. A. Bethe, Phys. Rev. **84** (1951) 1232.
81. R. Brockmann, R. Machleidt, *Nuclear Methods and The Nuclear Equation of State*, in: M. Baldo (Ed.), International Review of nuclear Physics, vol.8 World Scientific, Singapore, (1999), p121.
82. M.R. Anastasio, L.S. Celenza, W.S. Pong and C.M. Shakin, Phys. Rep. **100** (1983) 327.
83. C.J. Horowitz, B.D. Serot, Nucl. Phys. **A 464** (1987) 613.
84. N.K. Glendenning, *Compact Stars*, 2nd edition (Springer, New York) 2000.
85. M.Onsi, H. Przysiezniak and J.M. Pearson, Phys. Rev. **C 50** (1994) 460; 55 (1997) 3139.
86. D. Vautherin, D.M. Brink, Phy. Rev. **C 5** (1972) 626.
87. J. Decharge, D. Gogny, Phys. Rev. **C 21** (1980) 1568.
88. J. Heyer, T.T.S. Kuo, J.P. Shen and S.S. Wu, Phys. Lett. **B 202** (1988) 465.
89. M.F. Jiang, S.D.Yang and T.T.S. Kuo, Phys. Lett. **B 223** (1989) 5.
90. J. ventura, A. polls, X. Vinas, S. Hernandez, nd M. Pi Nucl. Phys. **A 545** (1992) 247.
91. P.D. Stevenson, M.R. Strayer and J. Rikovska Stone, Phys. Rev. **C 63** (2001) 054309.
92. J. Rikovska Stone, P.D. Stevenson, J.C. Miller, and M.R. Strayer, Phys. Rev. **C 65** (2002) 064312.
93. J.D. Walecka, Ann. Phys. (NY) **83** (1974) 491.
94. J. Boguta and A.R. Bodmer, Nucl. Phys. **A 292** (1977) 413.
95. Y. Sugahara and H. Toki , Nucl. Phys. **A 579** (1994) 557.
96. H. Toki et al., J. Phys. **G 24** (1998) 1479.
97. B. Liu, V. Greco, V. Baran, M. Colonna, M. Di Toro, Phys. Rev. **C 65** (2002) 045201

98. B. Liu, M. Di Toro, V. Greco, C. W. Shen, E. G. Zhao and B.X. Sun, Phys. Rev. **C 75** (2007) 048801.

99. C. Fuchs, H. Lenske and H.H. Wolter, Phys. Rev. **C 52** (1995) 3043.

100. H. Shen, Y. Sugahara, H. Toki, Phys. Rev. **C 55** (1997) 1211.

101. S. Typel and H.H. Wolter, Nucl. Phys. **A 656** (1999) 331.

102. F. Hofmann, C.M. Keil, H. Lenske, Phys. Rev. **C 64**(2001) 034314.

103. T. Niksic, D. Vretenar, P. Finelli and P. Ring, Phys. Rev. **C 66** (2002) 024306.

104. G.A. Lalazissis, T. Niksic, D. Vretenar and P. ring, Phys. Rev. **C 71** (2005) 024312.

105. L.W. Chen, C.M. Ko, B.A. Li, Phys. Rev. **C 76** (2007) 054316.

106. S. Goriely, M. Samyn, M. Bender and J.M. Pearson, Phys. Rev. **C 68** (2003) 054325.

107. B. Behera , T.R. Routray and R.K. Satpathy, J. Phys. **G 24** (1998)2073.

108. B. Behera , T.R. Routray, B. Sahoo and R.K. Satpathy, Nucl. Phys. **A 699** (2002) 770.

109. J.M. Lattimer, C.J. Pethick, D.G. Ravenhall, D.Q. Lamb, Nucl. Phys. **A 432** (1985) 646.

110. C.J. Pethick, D.G. Ravenhall, C.P. Lorenz, Nucl. Phys. **A 585** (1995) 675.

111. L.G. Cao, U. Lombardo, C. W. Shen, N. Van Giai, Phys. Rev. **C 73** (2006) 014313.

112. Bertsch, S. Das Gupta, Phys. Rep. **160** (1988) 189.

113. J. Aichelin, Phys. Rep. **202** (1991) 233.

114. P. Danielewicz, Nucl. Phys. **A 673** (2000) 375.

115. B.A. Li, S.J. Yennello, Phys. Rev. **C 52** (1995) 1746 (R).

116. B.A. Li, Z.Z. Ren, C.M. Ko, S.J. Yennello, Phys. Rev. Lett. **76** (1996) 4492.

117. B.A. Li, C.M. Ko, Z.Z. Ren, Phys. Rev. Lett. **78** (1997) 1644.

118. L.W. Chen, F.S. Zhang, G.M. Jin, Phys. Rev. **C 58** (1998) 2283.

119. V. Baran, M. Colonna, M. Di Toro, A.B. Larionov, Nucl. Phys. **A 632** (1998) 287.

120. J. Rizzo, M. Colonna, M. Di Toro, V. Greco, Nucl. Phys. **A 732** (2004) 202.

121. B.A. Li, L.W. Chen, Phys. Rev. **C 72** (2005) 064611.

122. Y. Zhang, Z. Li, Phys. Rev. **C 71** (2005) 024604.

123. H. Heiselberg, M. Hjorth-Jensen, Phys. Rep. **328** (2000) 237.

124. C. Mahaux and R. Sartor, in *Nuclear Matter and Heavy Ion Collisions* , Edited by M. Soyeur (Plenum, New York, 1989) Vol. **205**, p.1.
125. F. Coester, S. Cohen, B. Day, C.M. Vincent, Phys. Rev. **C 1** (1970) 769.
126. D.H. Youngblood, H.L. Clark, Y.-W. Lui, Phys. Rev. Lett. **82** (1999) 691.
127. S. Shlomo, B.K. Agrawal, K.V. Au, Nucl. Phys. **A 734** (2004) 589.
128. Z.Y. Ma, et al., Nucl. Phys. **A 686** (2001) 173.
129. H.L. Clark, Y.W. Lui, D.H. Youngblood, Phys. Rev. **C 63** (2001) 03130.
130. C.F. Von Weizsacker, Z. Phys. **96** (1935) 431.
131. P. Moller, W.D. Meyers, W.J. Swiatecki, and J. Treiner, At. Data Nucl. Data Tables **59** (1995) 225.
132. F. Tondeur, S. Goriely, J.M. Pearson, and M.Onsi, Phys. Rev. **C 62** (2000) 024308.
133. J. Aichelin, A. Rosenhauer, G. Peilert, H. Stocker, W. Greiner, Phys. Rev. Lett. **58** (1987) 1926.
134. Q. pan, P. Danielewicz, Phys. Rev. Lett. **70** (193) 2062.
135. V. de la Mota, F. Sebille, B. Remaud, P. Schuck, Phys. Rev. **C 46** (1992) 667.
136. J. Zhang, S. Das Gupta, C. Gale, Phys. Rev. **C 50** (1994) 1617.
137. F. Haddad, et al., Phys. Rev. **C 52** (1995) 2013.
138. G.M. Welke, et al., Phys. Rev. **C 38** (1988) 2101.
139. L.P. Csernai, et al., Phys. Rev. **C 46** (1992) 736.
140. C. Gale, et al., Phys. Rev. **C 41** (1990) 1545.
141. J.P. Blaizot, et al., Nucl. Phys. **A 591** (1995) 435.
142. V. Greco, et al., Phys. Rev. **C 64** (2001) 045203.
143. A.M. Lane, Nucl. Phys. **35** (1962) 676.
144. B. Behera, T.R. Routray, R.K. Satpathy, J. Phys. **G 23** (1997) 445.
145. B.Behera, A. Pradhan, B. Sahoo, T.R. Routray, in Proc. of DAE-BRNS Symp. In Nuclear Physics B47, eds. P. Singh and L.M. Pant (Board of Research in Nuclear Sciences, India, 2004), p.452.
146. B.A. Li, Phys. Rev. **C 69** (2004) 064602.
147. W. Zuo, L.G. Cao, B. A. Li, U. Lombardo, C. W. Shen, Phys. Rev. **C 72** (2005) 014005.
148. P.E. Hodgson, *The Nucleon Optical Model*, World Scientific, Singapore, 1994, p.613.

149. G. W. Hoffmann, W.R. Coker, Phys. Rev. Lett. **29** (1972) 227.
150. T. Li, et al., Phys. Rev. Lett. **99** (2007) 162503.
151. J.Xu, L.W. Chen, B. A. Li, H.R. Ma, Phys. Rev. **C 75** (2007) 014607.
152. W. Zuo, et. al. Phys. Rev. **C. 73** (2006) 035208.
153. B.A. Li, L.W. Chen, Phys. Rev. **C 74** (2006) 034610.
154. Ch. C. Moustakidis, Phys. Rev. **C 76** (2007) 025805.
155. P. Bonche, S. Levit, D. Vautherin, Nucl. Phys. **A 427** (1984) 278.
156. H. Muller, B.D. Serot, Phys. Rev. **C 52** (1995) 2072.
157. G. Bertsch, P.J. Siemens, Phys. Lett. **B 126** (1983) 9.
158. D.Q. Lamb, et al., Phys. Rev. Lett. **41** (1978)1623.
159. H. Jaqaman, A.Z. Mekjian, L. Zamick, Phys. Rev. **C 27** (1983) 2782.
160. Ph. Chomaz, et al., S.J. Yennello (Eds.), *Dynamics and Thermodynamics with Nucleonic Degrees of Freedom*, Springer, 2006.
161. W.L. Qian, R.K. Su, P. Wang, Phys. Lett. **B 491** (2000) 90.
162. P.Wang, Phys. Rev. **C 61** (2000) 054904.
163. S.J. Lee, A.Z. Mekjian, Phys. Rev. **C 63** (2001) 044605.
164. P. Chomaz, J. Margueron, Nucl. Phys. **A 722** (2003) 315c.
165. T. Sil, S.K. Sammadar, J.N. De, S. Shlomo, Phys. Rev. **C 69** (2004) 014602.
166. A.Z. Mekjian, S.J. Lee, L. Zamick, Phys. Rev. **C 72** (2005) 044305.
167. W.Zuo, Z.H. Li, A. Li, U. Lombardo, Nucl. Phys. **A 745** (2004) 34.
168. B. Friedman, V.R. Pandharipande, Nucl. Phys. **A 361** (1981) 502.
169. H. Huber, F. Weber, M.K. Weigel, Phys. Rev. **C 57** (1998) 3484.
170. I. Bombaci, T.T.S. Kuo, U. Lombardo, Phys. Rep. **242** (1994) 165.
171. Baldo, Burgio, *Physics of Neutron Star Interiors*, Edts: Blaschke, N.K. Glendenning, Sedrakian, Springer (2001) p1.
172. J. Oppenheimer, G. Volkoff, Phys. Rev. **55** (1939) 374;
R.C. Tolman, Phys. Rev. **55** (1939) 364.
173. F. Douchin and P. Haensel, Astron. Astrophys. **380** (2001) 151.
174. S. F. Ban, J. Li, S. Q. Zhang, H.Y. Jia, J.P. Sang, J. Meng, Phys. Rev. **C 69** (2004) 045805 .
175. S. Lawley, W. Bentz, A.W. Thomas, Nucl. Phys. Proc. Suppl. **141** (2005) 29.

176. M. Baldo, G.F. Burgio and H.Q. Song and F. Weber, in Proceeding International Workshop XXVI on Gross Properties of Nuclei and Nuclear Excitations, Hirshegg, Austria,1998.

177. M. Baldo, G.F. Burgio and H.-J. Schulze, Phys. Rev. **C 61** (2000) 55801.

178. G. Bao, L. Engvik, M. Hjorth-Jensen, E. Osnes and E. Ostgaard, Nucl. Phys. **A 575** (1994) 707.

179. K. Sumiyoshi, K. Oyamatsu and H. Toki, Nucl. Phys. **A 595** (1995) 327.

180. P.G. Krastev, F. Sammarruca, Phys. Rev. **C 74** (2006) 025808.

181. S. Popov , et al., Astron. Astrophys. **448** (2006) 327.

182. D.J. Nice, et al., Astrophys. J **634** (2005) 1242.

183. D. Barret, J.F. Olive, M. C. Miller, Mon. Not. R. Astron. Soc. **361** (2005) 855.

184. P. Podsiadlowski, et al., Mon. Not. R. Astron. Soc. **361** (2005) 1243.

185. M. Kramer, et al., eConf C041213 (2004) 0038.